Analysis of exported proteins and parasite-induced host cell rigidity changes during the *Plasmodium falciparum* intraerythrocytic life cycle

INAUGURALDISSERTATION

zur

Erlangung der Würde eines Doktors der Philosophie

vorgelegt der

Philosophisch-Naturwissenschaftlichen Fakultät

der Universität Basel

von

Beatrice Schibler

aus

Basel (BS)

Basel, 2018

Genehmigt von der Philosophisch-Naturwissenschaftlichen Fakultät auf Antrag von Prof. Dr. Hans-Peter Beck und Prof. Dr. Volker Heussler

Basel, den 24. April 2018

Prof. Dr. Martin Spiess
Dekan der Philosophisch-
Naturwissenschaftlichen Fakultät

Summary

Malaria is an infectious disease of global public health importance. Despite a number of successful efforts to fight the disease, there are still over 200 million cases and 445,000 deaths each year. *Plasmodium falciparum*, a protozoan parasite, is the causative agent of severe malaria. The parasite is transmitted by female *Anopheles* mosquitos form human to human and has different life stages inside both hosts. However, the only stages that are accountable for clinical symptoms of the disease are asexually replicating stages in the red blood cells. Red blood cells are highly specialized cells lacking a nucleus, organelles and certain cellular mechanisms. Therefore, the parasite has to extensively remodel the erythrocyte to ensure survival. The remodeling is achieved by exporting a large number of proteins that have various functions. Those functions include nutrient update and host immune response evasion. A crucial part of the refurbishment process is the establishment of a protein trafficking system that ensures correct delivery of exported proteins to their final destination. Maurer's clefts are new organelles established by the parasite in the cytosol of infected red blood cells. They are presumably involved in protein trafficking acting as sorting stations. A number of parasite exported proteins have been shown to localize permanently or transiently at Maurer's clefts. Among the latter is PfEMP1, the major virulence factor of *P. falciparum*. PfEMP1 is exported from the parasite, transported to Maurer's clefts and finally inserted in the infected erythrocyte membrane. The surface exposed domain of the protein is able to confer binding to endothelial receptors. Thus, infected red blood cells can sequester in the vasculature and avoid passage through the spleen where they would potentially be removed from circulation and eliminated.

The aim of this project was to expand our knowledge of *P. falciparum* exported proteins, their function and interactions. In this thesis I have characterized three exported proteins, namely PF3D7_0702500, MESA, and STARP. In order to investigate these proteins transgenic parasite lines were generated and analyzed. By establishing cell lines expressing tagged proteins, expression and localization studies as well as co-immunoprecipitation experiments for the identification of protein interaction partners could be performed.

Protein functional analysis was achieved by phenotypical characterization of knock out cell lines. Thereby the main readouts were growth, transport, surface presentation and anchoring of PfEMP1, and infected red blood cell deformability. We propose a function of PF3D7_0702500 in correct PfEMP1 display at the infected red blood cell surface, while the functions of STARP and MESA remain elusive.

Upon *P. falciparum* infection, the physical properties, e.g. cell deformability and membrane flexibility of an erythrocyte change dramatically. These changes are controlled by the parasite and are important for the adaptation to the host environment. Those biomechanical changes can be potentially exploited as a drug target, e.g. with drugs that reduce iRBC deformability, especially in circulating ring stages, enhancing the filtering function of the spleen to remove those iRBCs. Using microsphiltration to assess infected red blood cell deformability, we performed a study on the effect of the spiroindolone drug KAF246 on the rigidity of *P. falciparum* infected red blood cells. We were able to correlate these results with in vivo experiments where we observed *P. berghei* parasites accumulating in the mouse spleen rapidly after KAF246 treatment.

In summary, this thesis contributes to a better understanding of the protagonists of erythrocyte remodeling upon *P. falciparum* infection and gives new insights into parasite induced host cell changes during the pathology relevant stages. The findings of this thesis facilitate further studies and may eventually lead to the identification of potential new malaria intervention strategies.

Acknowledgements

First, I would like to thank Hans-Peter Beck for giving me the opportunity to do my PhD in his research group. I enjoyed working together, discussing science and non-science related topics. Then I am thankful to Tobias Spielmann and Volker Heussler for joining my PhD thesis committee and travelling to the yearly committee meetings being important “islands” during the project. Till Voss and Pascal Mäser helped me at the start of the PhD by reviewing my PhD research proposal – thank you very much! I am also grateful to Freddy Frischknecht for being interested in my research and killing the AFM project (prematurely). For the help with the AFM project during the first year of my PhD I would like to thank Philipp Oertle and Marija Plodinec. A big thank you goes to Catherine Lavazec, Florian Dupuy, and Bernina Naissant in Paris where I spent two extremely well organized weeks and learnt microsphiltration from the experts.

I would also like to thank Sebastian Rusch who taught me a lot about malaria parasites, culturing them and general useful tips for the lab and outside. I am thankful to Eva Hitz, Stephan Wichers, and Eron Rushiti, ‘my’ 3 Master students challenging me continuously and motivating me to learn even more about molecular biology. I would also like to thank Jan Warncke, Armin Passecker, Françoise Brand and Clara Antunes Moniz for being nice lab companions. Then I thank the former lab members Alexander Oberli for excellent lab books, and Esther Mundwiler-Pachlatko for paving the way for this project. I would like to thank Jemma Day and John Vakonakis from Oxford for the collaboration on exported co-chaperones. Matthias Rottmann and Anja Schäfer for taking me to more applied (rocket) science. Thomas Lavstsen and Falk Butter were instrumental for PfEMP1 variant typing and mass spectrometry analyses. Moreover the technical service, Fabien Haas and Thierry Brun were crucial to hold the lab together and help with electrical issues. Further, I would like to thank Alexia Loynton-Ferrand, Wolf Heusermann, and Kai Schleicher from the Biozentrum Image Core Facility who greatly assisted in all confocal microscopy related issues.

A big thank you for useful scientific discussions and else go to Ingrid Felger, Till Voss, Igor Niederwieser, Michael Filarsky, Nicolas Brancucci, Anna Fesser, Eilidh Carrington, Elvira Carrio Gaspar, Maria Grünberg, Travis Basson, Anita Lerch, Eva Hitz, Mirjam Bolz, Raphael Bieri, Nicole Bertschi and Angelika Silbereisen. Substantial for the wellbeing during the PhD were Natalie Hofmann, Rahel Wampfler, Gordana Panic, and Noemi Hiroshige.

I am extremely grateful to having had the opportunity to attend the Summer Course "Biology of Parasitism" 2015 in Woods Hole – this was a unique experience and motivation boost for parasite research. Special thanks to the course directors Kirk Deitsch and Gary Ward and to all the participants. Participating in the antelope programme helped me to put my research into context and not forget the world outside the cell culture lab. I am thankful to all antelope ladies for sharing their experiences as PhD students and allowing a glimpse into other research areas. I enjoyed also the attendance at the SSTMP student meetings for networking with peers in the broader context of parasitology in Switzerland.

For overall support throughout my entire studies I thank my parents, and my entire family (including the Metzler's). I am grateful to my sister pointing out that I am contributing to saving the world. And last but not least an enormous thank you to Mario Metzler, who is there helping, supporting, criticizing, cheering up and much more in all circumstances.

Finally, thank you to all of you – including those I have forgotten to list above!

Table of contents

Abbreviations

aa	amino acid
ACT	artemisinin-based combination therapies
ATS	acid terminal segment
BSA	bovine serum albumin
BSD	blasticidin S deaminase
cAMP	cyclic adenosine monophosphate
Cas9	CRISPR associated protein 9
CD36	cluster of differentiation 36
CIDR	cysteine-rich interdomain regions
Co-IP	co-immunoprecipitation
CRISPR	Clustered Regularly Interspaced Short Palindromic Repeat
CSA	chondroitin sulfate A
C-terminus	carboxy-terminus
DAPI	4',6'-diamidino-2-phenylindole
DBL	Duffy binding ligand
DIC	differential interference contrast
EDV	electron dense vesicle
EPCR	endothelial protein C receptor
EPIC	Exported Protein-Interacting Complex
EPM	erythrocyte plasma membrane
ER	endoplasmic reticulum
ETRAMP	early transcribed membrane protein
EXP2	exported protein 2
GAPDH	glyceraldehyde 3-phosphate dehydrogenase
GFP	green fluorescent protein
HA	hemaglutinin
hDHFR	human dehydrofolate reductase
hpi	hours post infection
HSP	heat shock protein
HT signal	host targeting signal
HR	homology region
ICAM-1	intercellular adhesion molecule-1

iRBC	infected red blood cell
KAHRP	knob-associated histidine-rich protein
KO	knock out
LyMP	lysine-rich membrane-associated PHISTb protein
MAHRP1/2	membrane-associated histidine-rich protein 1/2
MC	Maurer's cleft
MESA	mature parasite-infected erythrocyte surface antigen
MS	mass spectrometry
NPP	new permeation pathway
N-terminus	amino-terminus
NTS	N-terminal segment
PBS	phosphate buffered saline
PCR	polymerase chain reaction
PDEδ	phosphodiesterase δ
PEXEL	*Plasmodium* export element
PfEMP1/3	*Plasmodium falciparum* erythrocyte membrane protein 1/3
PHIST	*Plasmodium* helical interspersed sub-telomeric protein
PKA	protein kinase A
PNEP	PEXEL-negative exported protein
PPM	parasite plasma membrane
PSAC	*Plasmodium* surface anion channel
PTEX	*Plasmodium* translocon of exported proteins
PTP1-6	PfEMP1 transport protein 1-6
PV	parasitophorous vacuole
PVM	parasitophorous vacuole membrane
RBC	red blood cell
RESA	ring-infected erythrocyte surface antigen
REX1/2	ring exported protein 1/2
RIFIN	repetitive interspersed family
SBP1	skeleton binding protein 1
SDS	sodiumdodecylsulfate
SEMP1	small exported membrane protein 1
SERA	serine repeat antigen

SLI	Selection Linked Integration
STARP	sporozoite threonine and asparagine-rich protein
STEVOR	subtelomeric variable open reading frame
SUB1	subtilisin-like protease 1
TM	transmembrane
TRiC	TCP1 ring complex
TRX2	thioredoxin 2
TVN	tubovesicular network
UTR	untranslated region
VAP1	virulence-associated protein 1
VLS	vesicular-like structure
WHO	World Health Organization

Chapter 1

Introduction - Malaria and the Cell Biology of *Plasmodium falciparum*

Malaria – a parasite-caused disease

Malaria is a major global infectious disease with an estimated 216 million cases in 2016 worldwide. The malady represents a huge social and economic burden in the tropical and subtropical endemic areas, mainly in Africa where >90% of an estimated 445,000 malaria deaths worldwide occurred in 2016 (World Health WHO, 2017).

Human malaria is caused by 5 different *Plasmodium* species: *P. falciparum*, *P. vivax*, *P. ovale*, *P. malaria* and *P. knowlesi* which all differ slightly from each other in their biology. *P. falciparum* infection results in malaria tropica, the most severe form of human malaria.

The protozoan parasite *P. falciparum* has a complex lifecycle including insect and human stages (see Figure 1). Sporozoites are transmitted to humans by female *Anopheles* mosquitoes during their blood meal. The injected sporozoites find their way to the liver, enter hepatocytes and start multiplication. Then, merosomes (merozoite-filled vesicles) bud of hepatocytes to the blood stream where thousands of daughter merozoites are released to invade erythrocytes (Sturm et al., 2006). During a 48h intraerythrocytic stage, the parasite grows and multiplies exploiting the infected red blood cells (iRBC) resources. Upon burst of the schizont, merozoites are released and can reinitiate the asexual reproduction cycle. A fraction of blood-stage parasites differentiate into gametocytes (sexual form) which can be transmitted to mosquitoes. In the stomach of the mosquito the male and the female gametocyte fuse to a zygote, undergo meiosis and enter the insect's midgut endothelium as ookinete. There, the ookinete matures and after several days the sporozoites leave towards the mosquito's salivary gland from where they can be transmitted again to the human (White et al., 2014).

During the parasite's life cycle, only the intraerythrocytic stages are responsible for the clinical symptoms. The clinical symptoms of malaria are diverse: initial non-specific symptoms followed by irregular fever, nausea, and vomiting can turn into life-threatening conditions including anemia, coma (cerebral malaria), organ failure and death.

For efficient and successful disease treatment it is essential to reliably and timely diagnose the disease. Standard diagnostics in endemic countries are microscopy of Giemsa stained blood smears and rapid diagnostic tests that detect parasite antigens. Molecular diagnostics by PCR is not adequate for the field setting as it requires sophisticated infrastructure.

For the treatment of malaria several drugs are available and the World Health Organization (WHO) recommends different artemisinin-based combination therapies (ACTs). However, drug resistance against all currently available anti-malarials is emerging or established

(reviewed in Haldar et al., 2018). Despite major efforts, there is no effective, registered vaccine available yet.

Current strategies to control the devastating disease are vector control (e.g. insecticides), exposure prophylaxis (e.g. mosquito nets), and treatment of episodes. Between 2000 and 2015, malaria incidence and death rates dropped globally by 37% and 60%, respectively (Cibulskis et al., 2016). To continue the reduction of the disease the Global Technical Strategy for Malaria 2016–2030 has been set in place by WHO. It aims at a further 90% reduction in global malaria incidence and mortality by 2030 (WHO, 2015). Prerequisite for these ambitious goals towards the elimination of the disease are the maintenance and intensification of the current efforts. Crucial challenges are increasing drug and insecticide resistance as well as overcoming the residual transmission in low transmission areas (Bhatt et al., 2015).

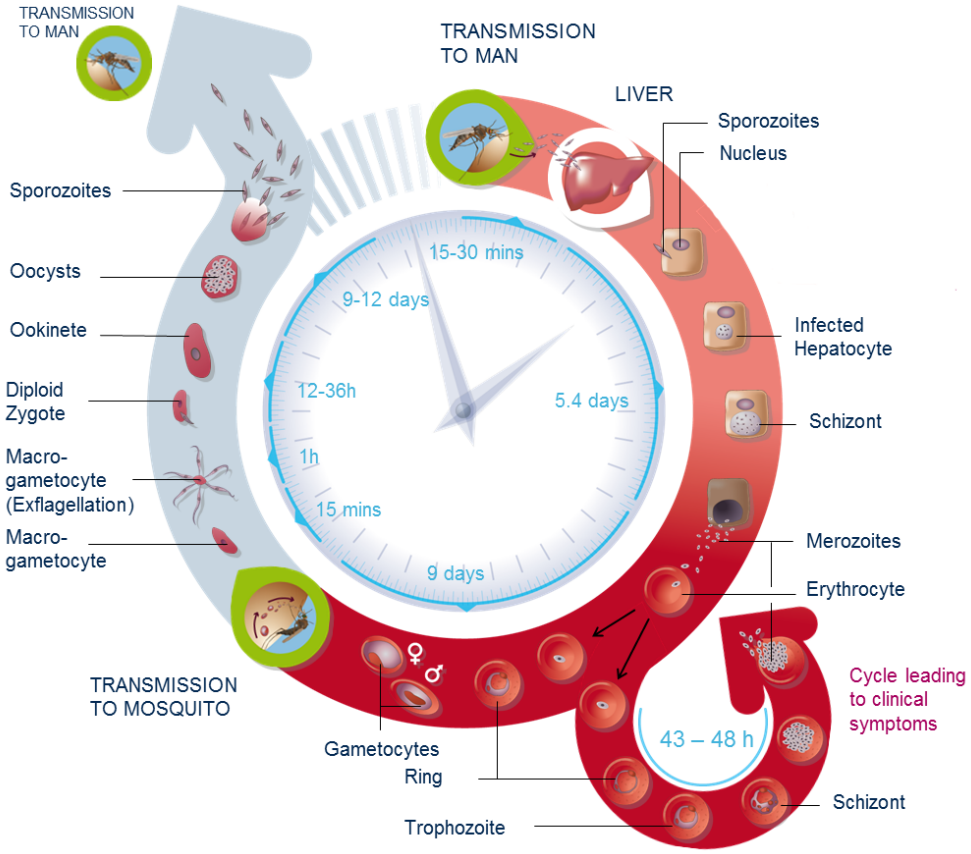

Figure 1: ***P. falciparum*** **life cycle.** The complex parasite life cycle is shown including all stages in the human and mosquito host. The times indicated give an impression on how long the different development stages of the parasite are, e.g. an asexual replication cycle in the blood takes 48 hours, reflected in the clinical symptom of 48h interval fever episodes in malaria tropica (modified from www.mmv.org/malaria-medicines/parasite-lifecycle).

Mechanisms of protein export

The asexually replicating parasites in the blood stream are responsible for the pathogenicity of malaria (Miller et al., 2002). Therefore it is of high interest to better understand *P. falciparum* biology of this life stage. The red blood cell (RBC) is a terminally differentiated cell lacking a nucleus and essential cellular mechanisms e.g. a secretory system and a protein trafficking system. The intracellular parasite *P. falciparum* cannot exploit the host cellular machinery but instead has to install its own processes by extensively remodeling the erythrocyte. In order to proliferate in red blood cells the parasite needs to ensure nutrient uptake, waste disposal and host immune evasion. These host cell adjustments are achieved by protein export (reviewed in de Koning-Ward et al., 2016). Thereby the parasite translocates a massive part of its proteome to the host cell cytosol using novel mechanisms (see Figure 2).

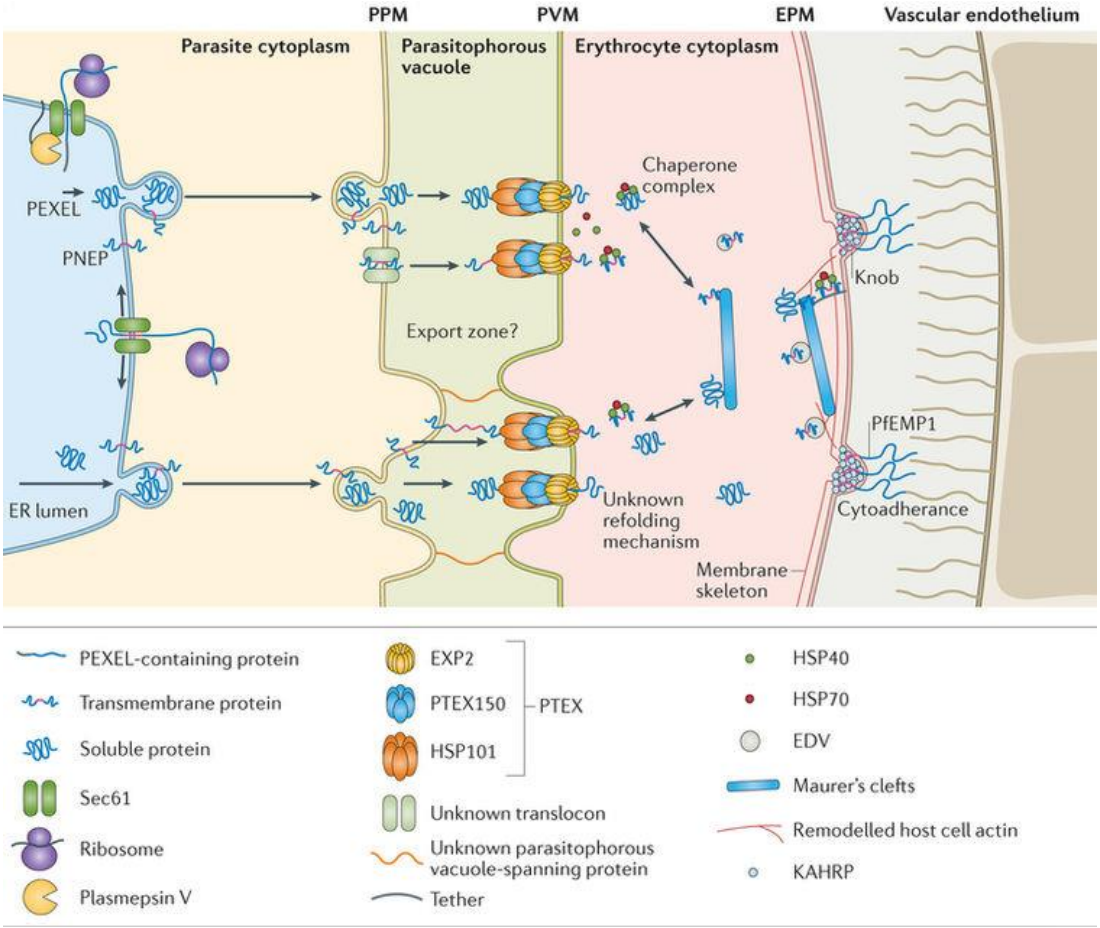

Figure 2: **Overview of the parasite protein export mechanisms.** In order to reach the host cell the parasite proteins need to cross several membranes, including the parasite plasma membrane (PPM), the parasitophorous vacuole membrane (PVM), and possibly the erythrocyte plasma membrane (EPM). Depicted are the different intermediate players involved in the transport mechanisms, e.g. plasmepsin V for PEXEL motif cleavage, the PTEX translocon in the PVM, Maurer's clefts and chaperone complexes Hsp70/Hsp40 (J-dots) in the erythrocyte cytosol (modified from de Koning-Ward et al., 2016).

P. falciparum resides in a parasitophorous vacuole (PV) inside the erythrocyte (Bannister et al., 1975). For the export of proteins the crossing of not only the parasite membrane but also the parasitophorous vacuole membrane (PVM) needs to be ensured.

Plasmodium proteins are translated in the parasite's cytosol and enter the secretory pathway to leave the cell and be exported. It is not entirely clear what signals target the protein to the endoplasmic reticulum (ER) in *P. falciparum.* Most probably, hydrophobic regions at the protein N-terminus function as signal sequences. It was also suggested, that N-terminal sequences may differ between soluble and membrane-associated secretory proteins (Meyer et al., 2017). Nonetheless, other post-translational modifications may be sufficient to target a protein for secretion (rewieved in Przyborski et al., 2016).

The default destination of parasite proteins secreted from the ER is the PV lumen (Deponte et al., 2012).

A common export motif was identified for many parasite proteins that are exported to the host cell cytosol, the *Plasmodium* export element (PEXEL) or host targeting signal (HT). This 5 amino acid signal is composed of RxLxE/D/Q and has been found essential for export into the host cytosol (Hiller et al., 2004, Marti et al., 2004). To this end the PEXEL motif gets cleaved by the aspartic protease plasmepsin V in the ER. The cleavage happens after the leucine and the following amino acid gets acetylated (Boddey et al., 2009). It is the current understanding that the remaining amino acid residues are important for further export of the protein (Gruring et al., 2012, Boddey et al., 2009). However, the exact export mechanism and how it is influenced by the N-terminal acetylation of the protein is presently unknown.

In addition to the classical PEXEL motif, relaxed (Boddey et al., 2013) and non-canonical (Schulze et al., 2015) PEXELs have been described. They differ slightly from the classical PEXEL motif in the amino acid sequence and can be cleaved in a specific sequence context as indicated by findings with different reporter proteins (Schulze et al., 2015). Based on the PEXEL motif approximately 450 *P. falciparum* proteins are predicted to be exported to the host cell (Boddey et al., 2013).

Not all exported *P. falciparum* proteins contain a PEXEL sequence. The PEXEL-negative exported proteins (PNEPs) have some structural similarities among each other but no shared primary sequence features. It is thought that an internal hydrophobic region facilitates their recruitment to the secretory pathway (Spielmann and Gilberger, 2010). Grüring and colleagues showed that the N-terminal sequences of some PNEPs are able to drive export of a reporter protein, indicating a common principle in the export mechanism of those PNEPs

(Gruring et al., 2012). As there are no defined signature motifs for PNEPs a large proportion of them might be missed in predictions of the exportome. More and more PNEPs are identified with surprisingly diverse features, hence it could turn out that PNEPs are not the exception of exported proteins but make up a significant proportion of the exportome (Heiber et al., 2013). Several dozen PNEPs are identified to date in *P. falciparum.* In addition, the ~60 variants of the major virulence factor PfEMP1 (see section below) are PNEPs.

Even though the recognition signals of exported proteins are diverse, there is evidence for shared trafficking mechanisms of PEXEL and PNEP proteins. Experiments with PEXEL and PNEP signals in front of a reporter protein indicate that the N-termini of PNEPs are exchangeable with mature PEXEL proteins. Export of those reporter proteins is still working and indicates shared export pathways for PNEPS and PEXEL proteins relying on the N-terminal sequence of the (mature) protein (Gruring et al., 2012).

A multimeric protein complex called PTEX (*Plasmodium* translocon of exported proteins) has been described as PVM translocon (de Koning-Ward et al., 2009). It consists of 5 different components: HSP101 (ATP-powered unfoldase), EXP2 (pore), PTEX150 (structural component), TRX2 (redox regulation) and PTEX88 (unknown function) (reviewed in de Koning-Ward et al., 2016). Accumulation of PEXEL proteins and PNEPs in the PV upon interference with PTEX proteins PTEX150 and HSP101 indicate that all exported proteins cross the PVM via PTEX (Elsworth et al., 2014, Beck et al., 2014). Further, it was found that exported proteins need to cross the PVM in an unfolded configuration (Gehde et al., 2009, Gruring et al., 2012). The underlying mechanism is unclear.

Target recognition of the PTEX translocon has not been elucidated to date. Some proteins in the PV are resident PV proteins and not meant for export. There are two models for the mechanism of target recognition: 1) bulk secretory flow and 2) PV subcompartments. Bulk secretory flow means that all proteins present in the PV are recognized by PTEX components or other chaperones in order to be translocated (Crabb et al., 2010). The PV subcompartment model suggests sorting of proteins in different areas/compartments of the PV. The protein content of specific compartments (export zones) would then be translocated. Arguing for this latter mechanism is the punctuate localization of PTEX in the PVM (de Koning-Ward et al., 2009, Riglar et al., 2013) and the recent report of an Exported Protein-Interacting Complex (EPIC) in the PV (Batinovic et al., 2017). The authors of that study hypothesize that the complex is involved in protein sorting in the PV as it interacts with PTEX components and exported proteins.

Once the exported proteins crossed all membranes delivery to the final destination must be ensured. There is no host trafficking system that could be highjacked. Thus the parasite has to install its own structures to facilitate protein transport. Proteins reach their destination either by diffusion (soluble proteins) or in case of insoluble membrane proteins by vacuolar transport, in a soluble or chaperone-assisted state (Marti and Spielmann, 2013). Maurer's clefts, parasite-derived membranous structures, are thought to function as protein sorting stations (see chapter below). The ultimate target location is probably hit via specific protein interaction domains.

In summary, the parasite adapted some unconventional pathways in protein export and trafficking. These represent potential drug targets as they differ from host cell properties.

Parasite-induced host cell modifications during the asexual intraerythrocytic cycle

An estimated 10% of the entire *P. falciparum* proteome is exported (Spielmann and Gilberger, 2015). It is assumed that all these proteins fulfill a specific function in the host cell. Additionally, it has been estimated that a quarter of all exported proteins could be essential (Maier et al., 2008). Indeed several modifications of the infected erythrocyte have been studied which will be discussed below (see Figure 3). However the majority of putative exported proteins have not been investigated in detail and their function remains to be elucidated.

The first compartment that exported proteins reach is the PV. The PV represents the interface between the parasite and the host cell and has besides its function in protein export an important role in nutrient uptake and waste disposal of the parasite. The proteome of the PV is increasingly being studied and a recent study identified a novel set of PV residing proteins, including three proteins important for parasite growth (Khosh-Naucke et al., 2017). PV residing proteins are e.g. EPIC components (Batinovic et al., 2017), proteases important for parasite egress (SERAs and SUB1 (Silmon de Monerri et al., 2011, Putrianti et al., 2010)) and PVM spanning proteins with domains in the PV e.g. PTEX components and ETRAMPs (reviewed in Spielmann et al., 2012).

The tubovesicular network (TVN) is a membranous extension from the PVM to the periphery of the iRBC. Its function is unclear, it has been suggested to act as a transport system (e.g. of nutrients) across the parasite (Aikawa, 1971, Lauer et al., 1997).

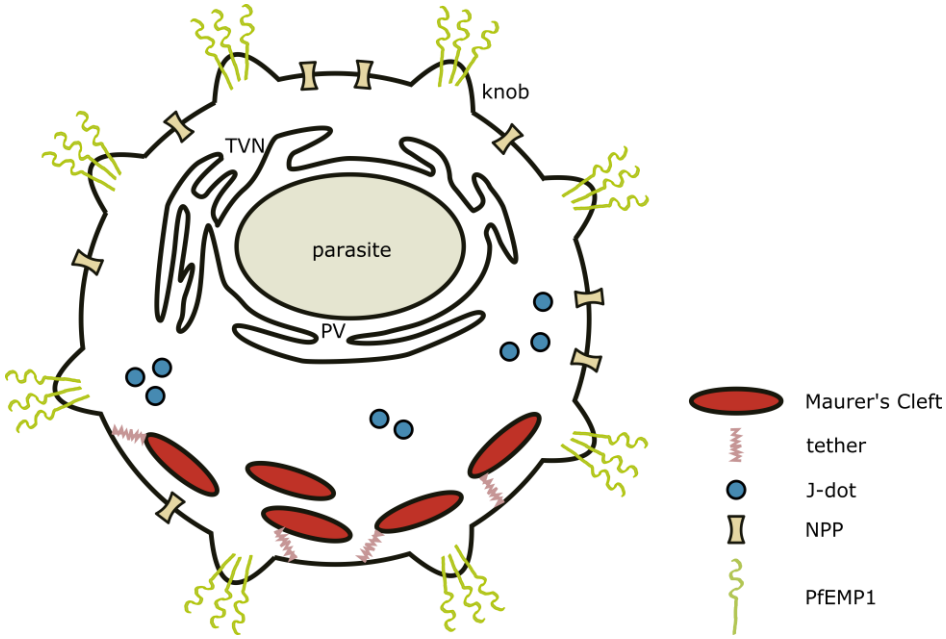

Figure 3: **Parasite-induced host cell modifications.** A wide range of host cell modifications are mediated by exported proteins. The parasite resides in the parasitophorous vacuole (PV) from where the tubovesicular network (TVN) expands. In the erythrocyte cytoplasm Maurer's clefts, Maurer's clefts tethers, and J-dots are installed. Not shown are additional vesicle types. On the erythrocyte surface knobs and PfEMP1 (as representative of variant surface genes) are inserted mediating cytoadhesion and virulence as well as new permeation pathways (NPPs) ensuring nutrient uptake, waste disposal and osmotic balance. Not drawn to scale.

It has been observed that *P. falciparum* infected erythrocytes increase their membrane permeability compared to uninfected erythrocytes which is thought to be due to new permeation pathways (NPPs) (Ginsburg et al., 1985) induced by the parasite. They have two proposed functions (reviewed in Desai, 2014). First, they play a role in nutrient uptake: the parasite retrieves most amino acids from hemoglobin by proteolytic cleavage (Sherman, 1977). However, not all amino acids are present in a sufficient amount. Isoleucine for example does not occur in hemoglobin and also some additional essential compounds for the parasite need to be taken up from the environment, e.g. pantothenic acid (Saliba et al., 1998). Second, the NPPs are important for cation concentration remodeling of the iRBC: the intracellular Na^+ and K^+ concentrations of *P. falciparum* infected erythrocytes are different from uninfected RBCs (Lee et al., 1988). The reasons for the cation remodeling are on one hand the prevention of osmotic lysis of infected cells and on the other hand it is assumed that the growing intracellular parasite adjusts the cation environment to optimize proliferation conditions.

The plasmodial surface anion channel (PSAC) is part of the NPPs (Desai et al., 2000). Yet, the only molecular component of the channel known to date is the CLAG3 protein which either forms the channel alone or interacts with other proteins to form the PSAC (Nguitragool et al., 2011).

Maurer's Clefts (MCs) are parasite-induced organelles established in the host erythrocyte cytosol early after parasite invasion (reviewed in Mundwiler-Pachlatko and Beck, 2013). They are flat, disc-shaped, membranous structures around 500nm in size thought to arise from the PVM (Spycher et al., 2006). MCs have been observed to move rapidly after genesis during the early stages of the intraerythrocytic cycle, later they stay immobilized at the periphery of the iRBC (Gruring et al., 2011). Their function is not well understood but they are assumed to play a crucial role in protein trafficking as putative sorting station because many exported proteins transiently localize to them. Several MC resident proteins have been identified e.g. MAHRP1 (Spycher et al., 2003), SBP1 (Blisnick et al., 2000), REX1 and REX2 (Hawthorne et al., 2004).

Associated to MCs are Maurer's clefts tethers which presumably play a role in anchoring and immobilizing MCs to the erythrocyte membrane. Electron microscopy studies characterized tethers as structures of 200-300nm length and around 30nm diameter with specific MAHRP2 antibody labelling. MAHRP2 is the only resident tether protein identified so far (Pachlatko et al., 2010, Hanssen et al., 2010).

J-dots are yet another structure described in the cytosol of *P. falciparum* iRBCs. They are highly mobile structures much smaller in size than MCs (estimated smaller than 30nm) and putatively involved in transport of exported proteins (Kulzer et al., 2010). The exported *P. falciparum* chaperone complex Hsp70x/Hsp40 has been described to localize to J-dots and possibly facilitate exported protein trafficking (Kulzer et al., 2012).

Exported parasite proteins interfere extensively with the host cytoskeleton organization (see Figure 4) leading to changes in physical properties of the cell, e.g. altered deformability. Most prominent is the formation of knob structures on the surface of iRBCs. These membrane protrusions are built up by the knob-associated histidine-rich protein (KAHRP) and contain the major virulence factor PfEMP1 which is inserted into the erythrocyte membrane (Kriek et al., 2003, Ganguly et al., 2015). Recently, the knob structure has been studied in greater detail and it was found to consist of a spiral structure of a yet unknown protein which is coated by KAHRP and connected to the RBC cytoskeleton by multiple contacts (Watermeyer et al.,

2016). In addition to KAHRP and PfEMP1, many members of the PHISTb protein family are involved in cytoskeleton refurbishment (reviewed in Warncke et al., 2016).

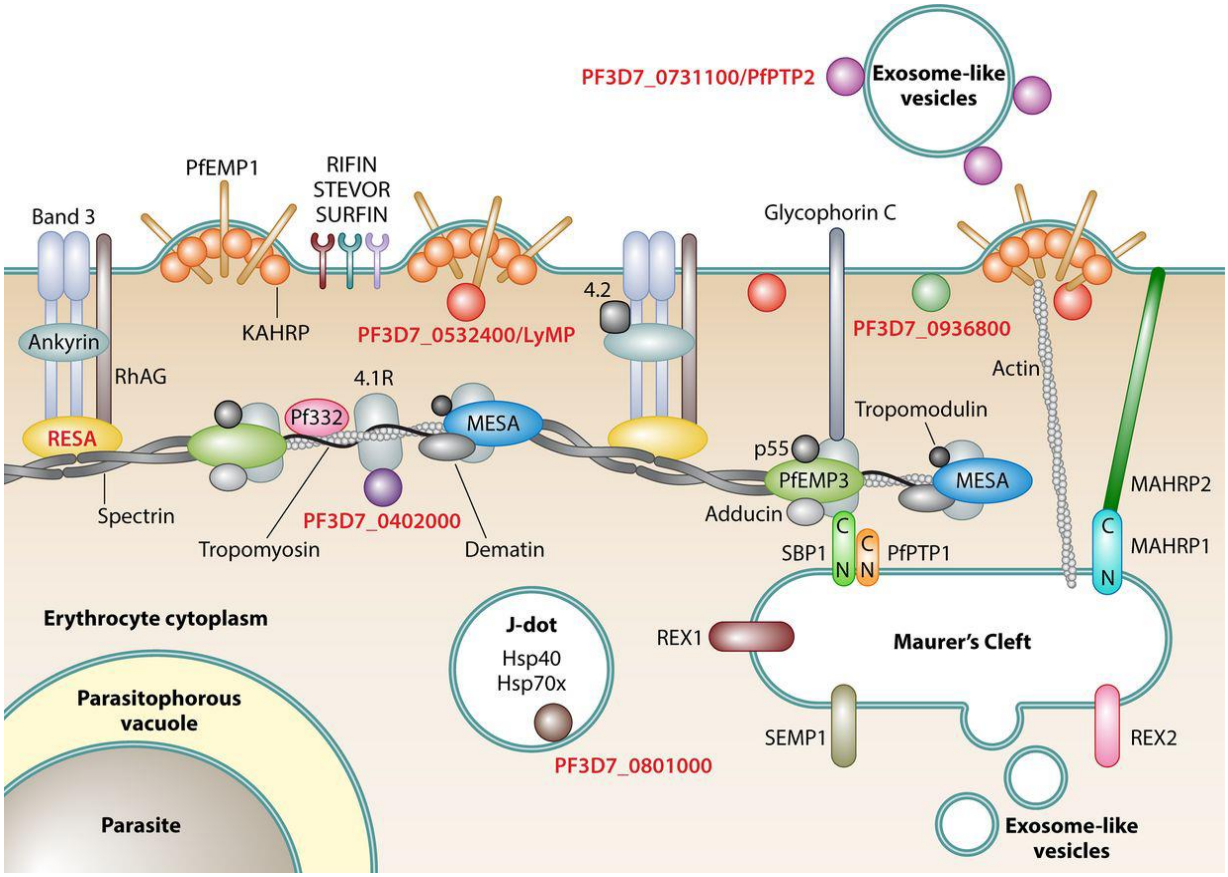

Figure 4: **Erythrocyte cytoskeleton remodeling.** The erythrocyte cytoskeleton is undergoing extensive remodeling by exported proteins. Host erythrocyte proteins are shown in grey scale, in color parasite-derived proteins (modified from Warncke et al., 2016).

Another substantial parasite-mediated host cell modification is the expression of variant surface antigens on the host cell surface. In *P. falciparum* there are three large variant surface antigen families: PfEMP1 (*P. falciparum* erythrocyte membrane protein 1) encoded by the *var* genes, STEVOR (subtelomeric variant open reading frame) encoded by the *stevor* genes, and RIFIN (repetitive interspersed repeats) encoded by the *rif* genes. Their roles have not been entirely understood but an important function of them is binding to host cell receptors thereby mediating on one hand cytoadherence (PfEMP1) and on the other hand rosetting (PfEMP1 (Rowe et al., 1997), STEVOR (Niang et al., 2014), RIFIN (Goel et al., 2015)).
Cytoadherence means the binding of iRBCs to different endothelial host cell receptors in order to sequester in the tissue/vasculature thereby avoiding the passage and elimination in

the spleen. PfEMP1, STEVOR and RIFINs match a broad repertoire of host cell receptors, most extensively studied for PfEMP1. Endothelial cell surface receptors to which different PfEMP1 variants bind, include cluster of differentiation 36 (CD36), chondroitin sulfate A (CSA), intercellular adhesion molecule-1 (ICAM-1), and endothelial protein C receptor (EPCR) (Robinson et al., 2003, Baruch et al., 1996, Fried and Duffy, 1996, Turner et al., 2013).

Rosetting describes the binding of iRBCs to uninfected erythrocytes via parasite ligands and erythrocyte surface receptors. The exact mechanism and function of this phenomenon are still enigmatic but some assumptions exist (reviewed in Yam et al., 2017). First, the uninfected erythrocytes shield the iRBC and the released merozoites form host invasion-inhibitory antibodies (Deans and Rowe, 2006). Second, the uninfected erythrocytes around the iRBC contribute to parasite survival and replication by presenting themselves as new host cells for released merozoites (Wahlgren et al., 1989).

A variety of vesicles has been observed and described in the host cell cytoplasm. Electron microscopy has been instrumental in these studies. Vesicular-like structures (VLSs) are approximately 25nm in size (Hanssen et al., 2008, Kriek et al., 2003, Wickert et al., 2003). Electron dense vesicles (EDVs) are larger, about 80-100 nm (Taraschi et al., 2003, Hanssen et al., 2010). Several exported proteins, e.g. PTP2, PfEMP1, PfEMP3 associate to EDVs and they may have a role in PfEMP1 transport from the MCs to the erythrocyte surface (Hanssen et al., 2010, McMillan et al., 2013, Trelka et al., 2000). Additionally, it has been suggested that extracellular vesicles from iRBCs are immunomodulatory (Mantel et al., 2013), have a function in parasite-to-parasite gene transfer (Regev-Rudzki et al., 2013) and are involved in PfEMP1 display (Sampaio et al., 2018). The existence and proposed functions of those microvesicles are highly disputed.

Aberrant RBC properties like they occur in hemoglobinopathies influence parasite protein export and the structures established by the parasite. For example, in infected sickle cell disease RBC anomalous MCs, actin and knobs structures lead to reduced cytoadherence (Cyrklaff et al., 2011, Kilian et al., 2015). Not surprisingly, the sickle cell trait is highly prevalent in malaria endemic areas (Piel et al., 2010) as heterozygous carriers of the sickle cell hemoglobin (HbS) have a 10-fold lower risk to die from malaria (Aidoo et al., 2002).

PfEMP1 characteristics and transport

PfEMP1 is the major virulence factor of *P. falciparum*. It mediates iRBC cytoadhesion and sequestration thereby contributing greatly to the clinical disease symptoms by disrupting the blood flow in the vasculature.

PfEMP1 is encoded by the *var* gene family which has approximately 60 members (Gardner et al., 2002). All PfEMP1 variants have a similar structure: an N-terminal segment (NTS), varying combinations of Duffy binding ligand (DBL), cysteine-rich inter-domain regions (CIDRs), a transmembrane domain, and the intracellular C-terminal cytoplasmic acid terminal segment (ATS) (Su et al., 1995). The extracellular part of the protein (NTS, DBL, and CIDRs) is highly variable facilitating the interaction with different host cell receptors (Deitsch and Hviid, 2004) and antigenic variation (Biggs et al., 1991). Further, expression of PfEMP1 is mutually exclusive, meaning that one single infected erythrocyte displays exactly one PfEMP1 variant on the surface (Dzikowski et al., 2006). The exact molecular mechanism behind the ability of the parasite to change the expression of the PfEMP1 variant remains elusive. However, the variability in antigenicity and cytoadhesive properties mediated by *var* gene expression switching are assumed to be key properties for host immune response evasion (reviewed in Hviid and Jensen, 2015).

PfEMP1 is displayed at knob structures on the surface of iRBCs (Kriek et al., 2003, Ganguly et al., 2015). An interaction between the PfEMP1 ATS domain and KAHRP has been identified *in vitro* (Waller et al., 1999) but could not be confirmed (Mayer et al., 2012). Further, the PHISTb family protein PFE1605w (LyMP) plays a role in anchoring a subset of PfEMP1s to the host cytoskeleton (Oberli et al., 2014, Oberli et al., 2016).

Despite the crucial role of PfEMP1 surface display in malaria pathology and immunology, our understanding of its transport is only fairly established. A model of PfEMP1 trafficking was proposed by Batinovic and colleagues (see Figure 5, (Batinovic et al., 2017)).

There is evidence implying that the integral membrane protein PfEMP1 is trafficked in a chaperone-assisted manner from the PVM to Maurer's clefts. Components of the human TRiC (TCP1 ring complex, a type II chaperonin complex) support the transport of PfEMP1 (Banumathy et al., 2002, Batinovic et al., 2017). The respective *P. falciparum* TRiC is probably not involved in PfEMP1 delivery (Spillman et al., 2017).

The intermediate stations of PfEMP1 on the way to the erythrocyte membrane are MCs (Kriek et al., 2003). Several MC resident proteins are essential for PfEMP1 presentation on the host cell surface, e.g. MAHRP1 (Spycher et al., 2008), SBP1 (Cooke et al., 2006), PTP2

(Maier et al., 2008) and REX1 (Dixon et al., 2011). Probably, Maurer's clefts proteins stabilize PfEMP1 at the MCs membrane and help target it for further transport.

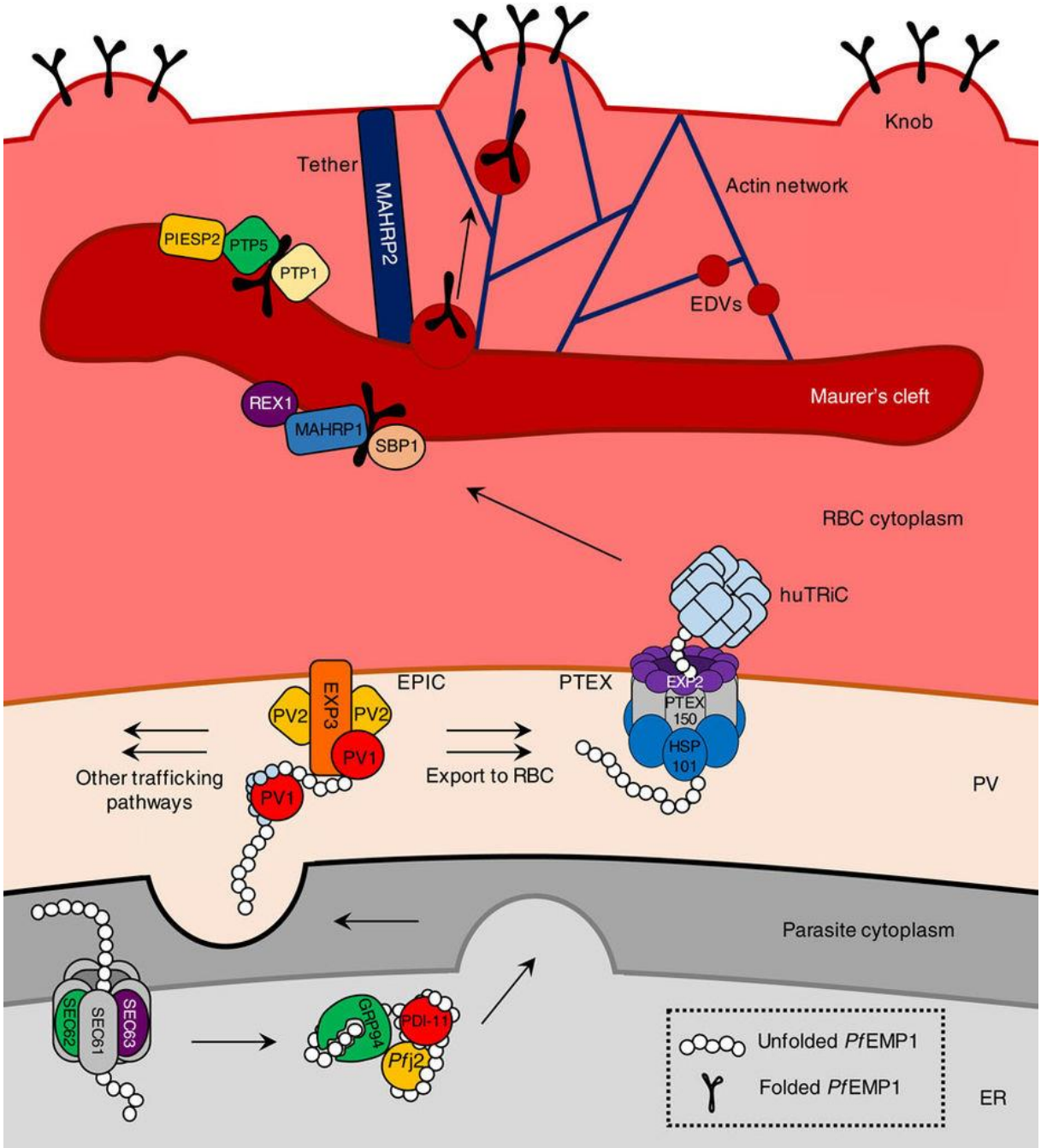

Figure 5: **PfEMP1 trafficking model.** The current understanding of the transport mechanism of the major virulence factor PfEMP1 from the parasite to the erythrocyte membrane is shown including secretion from the endoplasmic reticulum (ER) to the parasitophorous vacuole (PV) where it is recognized by the Exported Protein-Interacting Complex (EPIC), transported through the *Plasmodium* translocon of exported proteins (PTEX) and then with help of the human TCP1 ring complex (huTRiC) shuttled to the Maurer's clefts. There it is inserted in the membrane, putatively packed into electron dense vesicles (EDVs) and transported along tethers to be inserted into knobs (Batinovic et al., 2017).

Electron microscopy studies found PfEMP1 associated to EDVs (Trelka et al., 2000, Cyrklaff et al., 2011). Therefore it is hypothesized that PfEMP1 is transported form Maurer's clefts to the RBC surface in a vesicle-assisted manner (McMillan et al., 2013).
Recently, physical organization of PfEMP1 in the different compartments was investigated by protease protection assays. Those assays revealed that PfEMP1 is non-membrane embedded in the PV (Batinovic et al., 2017) and the N-terminal domain is embedded in MCs (Batinovic et al., 2017, Kriek et al., 2003).
Additional proteins have been reported to have a function in PfEMP1 trafficking, e.g. PTP1-6 (Maier et al., 2008), VAP1 (Nacer et al., 2015), and Hsp70x (Charnaud et al., 2017). However, their exact location and detailed mode of action needs to be elucidated.

Immune evasion strategies and the role of the spleen

To thrive in a host(ile) environment, *P. falciparum* must establish immune evasion strategies. In the human host there are 1) the asymptomatic pre-erythrocytic stages (sporozoite, and the infected liver cell) and 2) the clinically relevant intraerythrocytic stages (asexual and sexual stages) that have to escape the host immune system.
Upon entry of the human body, the sporozoite enters the blood stream, traverses Kupffer cells (liver-resident macrophages) and endothelial cells and subsequently infects hepatocytes. The parasite acquired strategies to suppress the phagocytic characteristics of Kupffer cells thereby avoiding its elimination (Usynin et al., 2007). In the hepatocyte the parasites develop further and modifies selective autophagy processes to its advantage (Prado et al., 2015).
In intraerythrocytic stages the expression of variant surface antigens and the alteration of biomechanical properties of the iRBC are instrumental for immune evasion.
iRBC sequestration mediated by variant surface antigens (see previous section) results in avoidance of iRBC spleen passage which potentially could lead to their removal form the circulation. It has been reported that iRBCs from splenectomized malaria patients lost variant surface antigen expression supporting their importance in spleen passage avoidance (Bachmann et al., 2009). IRBCs have increased stiffness compared to normal erythrocytes (Cranston et al., 1984). This makes them a target of the spleen that recognizes and removes altered erythrocytes from the circulation, e.g. senescent RBCs or iRBCs. Splenomegaly (enlarged spleen) is a typical symptom of malaria patients. Besides filtering aberrant cells (mechanical function), the spleen has also a major role in the immune response to malaria

infection (reviewed in Del Portillo et al., 2012). For example, the spleen red pulp hosts macrophages that are involved in removal of iRBCs by phagocytosis (Yadava et al., 1996). Else, splenic resident classical dendritic cells can take up parasite material and subsequently present *Plasmodium* peptides to T-cells (Sponaas et al., 2006). Splenectomized patients have impaired clearance of the parasite upon drug treatment implicating the crucial role of the organ in parasite removal (Demar et al., 2004). Pitting is an additional function of the spleen. It refers to the removal of the parasite form the erythrocyte, preserving the host erythrocyte (Schnitzer et al., 1972, Chotivanich et al., 2000, Buffet et al., 2011).

The importance of iRBC biomechanical changes in immune evasion is reflected in the deformability properties of gametocytes throughout maturation. Sequestered gametocyte stages II-IV iRBCs have very limited deformability. This probably contributes to their retention in the bone marrow (Tiburcio et al., 2012, Joice et al., 2014). Interestingly, gametocyte stage V iRBCs are highly deformable, presumably allowing the parasite to leave the bone marrow and circulate through the spleen. This is crucial for transmission to the mosquito in order to continue the life cycle (Tiburcio et al., 2012, Aingaran et al., 2012).

Approaches in functional analysis of red blood cell stage *P. falciparum* proteins

The generation of transgenic parasites is an important tool for functional gene and protein studies. Thereby, genetic gene knock out and knock in lines enable a better understanding of the parasites biology. In recent years, great advances have been made in genome editing techniques in *P. falciparum* (reviewed in de Koning-Ward et al., 2015). Transfection-based methods are used for *P. falciparum* asexual red blood cell stages to introduce DNA sequences. Most relevant for this thesis are conventional recombination, the CRISPR-Cas9 system (Ghorbal et al., 2014), and the Selection Linked Integration (SLI) approach (Birnbaum et al., 2017).

There is a broad variety of assays used to investigate cellular processes influenced by the protein/gene of interest. After a basic characterization of the newly generated transgenic cell line (expression and localization studies), more sophisticated experiments are performed to identify putative interaction partners of the protein of interest. Further, functional analysis of knock out cell lines is undertaken.

There is a particular interest in characterizing proteins involved in the processes of parasite virulence and immune evasion in order to better understand parasite biology and identify

intervention targets. Hence, transport and presentation of PfEMP1 on the iRBC as well as biomechanical changes of iRBCs are significant readouts of functional analyses.

The trypsin cleavage assay is commonly used to test for PfEMP1 presentation on the host cell surface. Thereby the iRBCs are trypsin treated in order to cleave the surface exposed part of PfEMP1. Subsequently, PfEMP1 is extracted from the membrane and Western blot analysis is performed using an antibody against the intracellular domain of PfEMP1 which allows conclusions about the exposure of PfEMP1 on the RBC surface. If PfEMP1 is present on the RBC surface and thus cleaved by trypsin, a shorter fragment is detected. If PfEMP1 is not presented on the erythrocyte surface but intracellular and thus is not cleaved by trypsin, a longer fragments (representing full-length, intracellular PfEMP1) is detected.

Another set of assays to assess the quality of PfEMP1 anchoring in the erythrocyte membrane are semi-static binding assays. A culture dish is coated with recombinant human endothelial receptors (e.g. CD36, ICAM-1, CSA) and iRBCs are incubated on it under shaking (semi-static) conditions. The shaking should mimic the blood flow. After incubation bound cells are quantified and conclusions about binding, presentation and anchoring of the expressed PfEMP1 variant can be drawn.

There is a wide range of techniques available to measure biomechanical properties, e.g. deformability of iRBCs, each with advantages and disadvantages. There is the possibility to measure deformability specifically of the iRBC membrane e.g. by micropipette aspiration (Glenister et al., 2002) or atomic force microscopy (Dulinska et al., 2006). In order to assess deformability of the entire iRBC, e.g. microfluidics (Matthews et al., 2017), microsphiltration (Lavazec et al., 2013), or ectacytometry (Dondorp et al., 1999) are used.

Aims

The general aim of this thesis was to further elucidate the role and function of a number of *P. falciparum* exported proteins in the host red blood cell. Protein transport and trafficking mechanisms established by the malaria parasite in the erythrocyte are different from classical mechanisms of the host. Thus a better understanding of the parasite biology could lead to the identification of potential new strategies to target the parasite.

Maurer's clefts (MC) are parasite induced organelles involved in trafficking of exported proteins. Correct and timely delivery of exported proteins to their target site is crucial for the parasite to establish itself in the host cell. A number of exported proteins have been found to localize at the MC either transiently (e.g. PfEMP1) or permanently (e.g. MAHRP1, SBP1, REX1). Putative anchoring structures of MCs are MC tethers, with MAHRP2 as the only resident protein of these structures identified today. In order to better understand the role and function of MCs and MC tethers we performed co-immunoprecipitation experiments with MAHRP1 and MAHRP2 followed by mass spectrometry. By functional characterization of putative interaction partners of these proteins we wanted to expand our understanding of the interaction network of exported proteins and their integration into host cellular structures such as the erythrocyte cytoskeleton. In this project the focus lies on PF3D7_0702500 (also known as PF07_0008), MESA (mature-parasite-infected erythrocyte surface antigen, PF3D7_0500800), and STARP (sporozoite threonine and asparagine-rich protein, PF3D7_0702300) which all were identified in MAHRP2 and/or MAHRP1 co-immunoprecipitation experiments. Of particular interest is their involvement in the PfEMP1 delivery process to the iRBC surface and parasite-induced rigidity changes of the iRBC.

Specific aims:

1) Characterization of PF3D7_0702500, MESA, and STARP (chapter 2, 3, 4)

   Protein characterization will be performed on the basis of transgenic cell lines (introduction of endogenous gene tags and gene knock out). These are going to be generated by applying the recently established CRISPR/Cas9 technology and a novel approach of a combined CRISPR/Cas9-selection-linked integration strategy. Expression and localization of the proteins of interest will be analyzed as well as interaction partners will be identified by co-immunoprecipitation experiments. Phenotypical analysis of knock out cell lines will be undertaken for functional

characterization of the proteins. To this end, special attention of their role in altering the biomechanical properties of the iRBC and in PfEMP1 transport will be paid. Adopted methods will include growth assay, microsphiltration (see aim 2), trypsin cleavage assay and binding assay.

2) Assessment of iRBC rigidity changes as protein functional readout after genetic manipulation of the parasite (chapter 2 and 3) and upon spiroindolone KAF246 treatment (chapter 5)

   Biomechanical alterations of the host erythrocyte are instrumental for parasite virulence and immune evasion. One method to assess these is microsphiltration. The microsphiltration technique will be learnt during a research visit in Paris and subsequently established at the Swiss TPH during my thesis. This versatile tool will be used to assess rigidity changes a) during the parasite life cycle in knock out cell lines (functional protein studies) and b) upon anti-malarial drug exposure. To this, a study on the effect of spiroindolones on iRBCs deformability will be performed in collaboration with the Parasite Chemotherapy Unit, Swiss TPH.

References

AIDOO, M., TERLOUW, D. J., KOLCZAK, M. S., MCELROY, P. D., TER KUILE, F. O., KARIUKI, S., NAHLEN, B. L., LAL, A. A. & UDHAYAKUMAR, V. 2002. Protective effects of the sickle cell gene against malaria morbidity and mortality. *Lancet,* 359**,** 1311-2.

AIKAWA, M. 1971. Parasitological review. Plasmodium: the fine structure of malarial parasites. *Exp Parasitol,* 30**,** 284-320.

AINGARAN, M., ZHANG, R., LAW, S. K., PENG, Z., UNDISZ, A., MEYER, E., DIEZ-SILVA, M., BURKE, T. A., SPIELMANN, T., LIM, C. T., SURESH, S., DAO, M. & MARTI, M. 2012. Host cell deformability is linked to transmission in the human malaria parasite Plasmodium falciparum. *Cell Microbiol,* 14**,** 983-93.

BACHMANN, A., ESSER, C., PETTER, M., PREDEHL, S., VON KALCKREUTH, V., SCHMIEDEL, S., BRUCHHAUS, I. & TANNICH, E. 2009. Absence of erythrocyte sequestration and lack of multicopy gene family expression in Plasmodium falciparum from a splenectomized malaria patient. *PLoS One,* 4**,** e7459.

BANNISTER, L. H., BUTCHER, G. A., DENNIS, E. D. & MITCHELL, G. H. 1975. Structure and invasive behaviour of Plasmodium knowlesi merozoites in vitro. *Parasitology,* 71**,** 483-91.

BANUMATHY, G., SINGH, V. & TATU, U. 2002. Host chaperones are recruited in membrane-bound complexes by Plasmodium falciparum. *J Biol Chem,* 277**,** 3902-12.

BARUCH, D. I., GORMELY, J. A., MA, C., HOWARD, R. J. & PASLOSKE, B. L. 1996. Plasmodium falciparum erythrocyte membrane protein 1 is a parasitized erythrocyte receptor for adherence to CD36, thrombospondin, and intercellular adhesion molecule 1. *Proc Natl Acad Sci U S A,* 93**,** 3497-502.

BATINOVIC, S., MCHUGH, E., CHISHOLM, S. A., MATTHEWS, K., LIU, B., DUMONT, L., CHARNAUD, S. C., SCHNEIDER, M. P., GILSON, P. R., DE KONING-WARD, T. F., DIXON, M. W. A. & TILLEY, L. 2017. An exported protein-interacting complex involved in the trafficking of virulence determinants in Plasmodium-infected erythrocytes. *Nat Commun,* 8**,** 16044.

BECK, J. R., MURALIDHARAN, V., OKSMAN, A. & GOLDBERG, D. E. 2014. PTEX component HSP101 mediates export of diverse malaria effectors into host erythrocytes. *Nature,* 511**,** 592-5.

BHATT, S., WEISS, D. J., CAMERON, E., BISANZIO, D., MAPPIN, B., DALRYMPLE, U., BATTLE, K., MOYES, C. L., HENRY, A., ECKHOFF, P. A., WENGER, E. A., BRIET, O., PENNY, M. A., SMITH, T. A., BENNETT, A., YUKICH, J., EISELE, T. P., GRIFFIN, J. T., FERGUS, C. A., LYNCH, M., LINDGREN, F., COHEN, J. M., MURRAY, C. L. J., SMITH, D. L., HAY, S. I., CIBULSKIS, R. E. & GETHING, P. W. 2015. The effect of malaria control on Plasmodium falciparum in Africa between 2000 and 2015. *Nature,* 526**,** 207-211.

BIGGS, B. A., GOOZE, L., WYCHERLEY, K., WOLLISH, W., SOUTHWELL, B., LEECH, J. H. & BROWN, G. V. 1991. Antigenic variation in Plasmodium falciparum. *Proc Natl Acad Sci U S A,* 88**,** 9171-4.

BIRNBAUM, J., FLEMMING, S., REICHARD, N., SOARES, A. B., MESEN-RAMIREZ, P., JONSCHER, E., BERGMANN, B. & SPIELMANN, T. 2017. A genetic system to study Plasmodium falciparum protein function. *Nat Methods,* 14**,** 450-456.

BLISNICK, T., MORALES BETOULLE, M. E., BARALE, J. C., UZUREAU, P., BERRY, L., DESROSES, S., FUJIOKA, H., MATTEI, D. & BRAUN BRETON, C. 2000. Pfsbp1, a Maurer's cleft Plasmodium falciparum protein, is associated with the erythrocyte skeleton. *Mol Biochem Parasitol,* 111**,** 107-21.

BODDEY, J. A., CARVALHO, T. G., HODDER, A. N., SARGEANT, T. J., SLEEBS, B. E., MARAPANA, D., LOPATICKI, S., NEBL, T. & COWMAN, A. F. 2013. Role of plasmepsin V in export of diverse protein families from the Plasmodium falciparum exportome. *Traffic,* 14**,** 532-50.

BODDEY, J. A., MORITZ, R. L., SIMPSON, R. J. & COWMAN, A. F. 2009. Role of the Plasmodium export element in trafficking parasite proteins to the infected erythrocyte. *Traffic,* 10**,** 285-99.

BUFFET, P. A., SAFEUKUI, I., DEPLAINE, G., BROUSSE, V., PRENDKI, V., THELLIER, M., TURNER, G. D. & MERCEREAU-PUIJALON, O. 2011. The pathogenesis of Plasmodium falciparum malaria in humans: insights from splenic physiology. *Blood,* 117**,** 381-92.

CHARNAUD, S. C., DIXON, M. W. A., NIE, C. Q., CHAPPELL, L., SANDERS, P. R., NEBL, T., HANSSEN, E., BERRIMAN, M., CHAN, J. A., BLANCH, A. J., BEESON, J. G., RAYNER, J. C., PRZYBORSKI, J. M., TILLEY, L., CRABB, B. S. & GILSON, P. R. 2017. The exported chaperone Hsp70-x supports virulence functions for Plasmodium falciparum blood stage parasites. *PLoS One,* 12**,** e0181656.

CHOTIVANICH, K., UDOMSANGPETCH, R., DONDORP, A., WILLIAMS, T., ANGUS, B., SIMPSON, J. A., PUKRITTAYAKAMEE, S., LOOAREESUWAN, S., NEWBOLD, C. I. & WHITE, N. J. 2000. The mechanisms of parasite clearance after antimalarial treatment of Plasmodium falciparum malaria. *J Infect Dis,* 182**,** 629-33.

CIBULSKIS, R. E., ALONSO, P., APONTE, J., AREGAWI, M., BARRETTE, A., BERGERON, L., FERGUS, C. A., KNOX, T., LYNCH, M., PATOUILLARD, E., SCHWARTE, S., STEWART, S. & WILLIAMS, R. 2016. Malaria: Global progress 2000 - 2015 and future challenges. *Infect Dis Poverty,* 5**,** 61.

COOKE, B. M., BUCKINGHAM, D. W., GLENISTER, F. K., FERNANDEZ, K. M., BANNISTER, L. H., MARTI, M., MOHANDAS, N. & COPPEL, R. L. 2006. A Maurer's cleft-associated protein is essential for expression of the major malaria virulence antigen on the surface of infected red blood cells. *J Cell Biol,* 172**,** 899-908.

CRABB, B. S., DE KONING-WARD, T. F. & GILSON, P. R. 2010. Protein export in Plasmodium parasites: from the endoplasmic reticulum to the vacuolar export machine. *Int J Parasitol,* 40**,** 509-13.

CRANSTON, H. A., BOYLAN, C. W., CARROLL, G. L., SUTERA, S. P., WILLIAMSON, J. R., GLUZMAN, I. Y. & KROGSTAD, D. J. 1984. Plasmodium falciparum maturation abolishes physiologic red cell deformability. *Science,* 223**,** 400-3.

CYRKLAFF, M., SANCHEZ, C. P., KILIAN, N., BISSEYE, C., SIMPORE, J., FRISCHKNECHT, F. & LANZER, M. 2011. Hemoglobins S and C interfere with actin remodeling in Plasmodium falciparum-infected erythrocytes. *Science,* 334**,** 1283-6.

DE KONING-WARD, T. F., DIXON, M. W., TILLEY, L. & GILSON, P. R. 2016. Plasmodium species: master renovators of their host cells. *Nat Rev Microbiol,* 14**,** 494-507.

DE KONING-WARD, T. F., GILSON, P. R., BODDEY, J. A., RUG, M., SMITH, B. J., PAPENFUSS, A. T., SANDERS, P. R., LUNDIE, R. J., MAIER, A. G., COWMAN, A. F. & CRABB, B. S. 2009. A newly discovered protein export machine in malaria parasites. *Nature,* 459**,** 945-9.

DE KONING-WARD, T. F., GILSON, P. R. & CRABB, B. S. 2015. Advances in molecular genetic systems in malaria. *Nat Rev Microbiol,* 13**,** 373-87.

DEANS, A. M. & ROWE, J. A. 2006. Plasmodium falciparum: Rosettes do not protect merozoites from invasion-inhibitory antibodies. *Exp Parasitol,* 112**,** 269-73.

DEITSCH, K. W. & HVIID, L. 2004. Variant surface antigens, virulence genes and the pathogenesis of malaria. *Trends Parasitol,* 20**,** 562-6.

DEL PORTILLO, H. A., FERRER, M., BRUGAT, T., MARTIN-JAULAR, L., LANGHORNE, J. & LACERDA, M. V. 2012. The role of the spleen in malaria. *Cell Microbiol,* 14**,** 343-55.

DEMAR, M., LEGRAND, E., HOMMEL, D., ESTERRE, P. & CARME, B. 2004. Plasmodium falciparum malaria in splenectomized patients: two case reports in French Guiana and a literature review. *Am J Trop Med Hyg,* 71**,** 290-3.

DEPONTE, M., HOPPE, H. C., LEE, M. C., MAIER, A. G., RICHARD, D., RUG, M., SPIELMANN, T. & PRZYBORSKI, J. M. 2012. Wherever I may roam: protein and membrane trafficking in P. falciparum-infected red blood cells. *Mol Biochem Parasitol,* 186**,** 95-116.

DESAI, S. A. 2014. Why do malaria parasites increase host erythrocyte permeability? *Trends Parasitol,* 30**,** 151-9.

DESAI, S. A., BEZRUKOV, S. M. & ZIMMERBERG, J. 2000. A voltage-dependent channel involved in nutrient uptake by red blood cells infected with the malaria parasite. *Nature,* 406**,** 1001-5.

DIXON, M. W., KENNY, S., MCMILLAN, P. J., HANSSEN, E., TRENHOLME, K. R., GARDINER, D. L. & TILLEY, L. 2011. Genetic ablation of a Maurer's cleft protein prevents assembly of the Plasmodium falciparum virulence complex. *Mol Microbiol,* 81**,** 982-93.

DONDORP, A. M., ANGUS, B. J., CHOTIVANICH, K., SILAMUT, K., RUANGVEERAYUTH, R., HARDEMAN, M. R., KAGER, P. A., VREEKEN, J. & WHITE,

N. J. 1999. Red blood cell deformability as a predictor of anemia in severe falciparum malaria. *Am J Trop Med Hyg,* 60**,** 733-7.

DULINSKA, I., TARGOSZ, M., STROJNY, W., LEKKA, M., CZUBA, P., BALWIERZ, W. & SZYMONSKI, M. 2006. Stiffness of normal and pathological erythrocytes studied by means of atomic force microscopy. *J Biochem Biophys Methods,* 66**,** 1-11.

DZIKOWSKI, R., FRANK, M. & DEITSCH, K. 2006. Mutually exclusive expression of virulence genes by malaria parasites is regulated independently of antigen production. *PLoS Pathog,* 2**,** e22.

ELSWORTH, B., MATTHEWS, K., NIE, C. Q., KALANON, M., CHARNAUD, S. C., SANDERS, P. R., CHISHOLM, S. A., COUNIHAN, N. A., SHAW, P. J., PINO, P., CHAN, J. A., AZEVEDO, M. F., ROGERSON, S. J., BEESON, J. G., CRABB, B. S., GILSON, P. R. & DE KONING-WARD, T. F. 2014. PTEX is an essential nexus for protein export in malaria parasites. *Nature,* 511**,** 587-91.

FRIED, M. & DUFFY, P. E. 1996. Adherence of Plasmodium falciparum to chondroitin sulfate A in the human placenta. *Science,* 272**,** 1502-4.

GANGULY, A. K., RANJAN, P., KUMAR, A. & BHAVESH, N. S. 2015. Dynamic association of PfEMP1 and KAHRP in knobs mediates cytoadherence during Plasmodium invasion. *Sci Rep,* 5**,** 8617.

GARDNER, M. J., HALL, N., FUNG, E., WHITE, O., BERRIMAN, M., HYMAN, R. W., CARLTON, J. M., PAIN, A., NELSON, K. E., BOWMAN, S., PAULSEN, I. T., JAMES, K., EISEN, J. A., RUTHERFORD, K., SALZBERG, S. L., CRAIG, A., KYES, S., CHAN, M. S., NENE, V., SHALLOM, S. J., SUH, B., PETERSON, J., ANGIUOLI, S., PERTEA, M., ALLEN, J., SELENGUT, J., HAFT, D., MATHER, M. W., VAIDYA, A. B., MARTIN, D. M., FAIRLAMB, A. H., FRAUNHOLZ, M. J., ROOS, D. S., RALPH, S. A., MCFADDEN, G. I., CUMMINGS, L. M., SUBRAMANIAN, G. M., MUNGALL, C., VENTER, J. C., CARUCCI, D. J., HOFFMAN, S. L., NEWBOLD, C., DAVIS, R. W., FRASER, C. M. & BARRELL, B. 2002. Genome sequence of the human malaria parasite Plasmodium falciparum. *Nature,* 419**,** 498-511.

GEHDE, N., HINRICHS, C., MONTILLA, I., CHARPIAN, S., LINGELBACH, K. & PRZYBORSKI, J. M. 2009. Protein unfolding is an essential requirement for transport across the parasitophorous vacuolar membrane of Plasmodium falciparum. *Mol Microbiol,* 71**,** 613-28.

GHORBAL, M., GORMAN, M., MACPHERSON, C. R., MARTINS, R. M., SCHERF, A. & LOPEZ-RUBIO, J. J. 2014. Genome editing in the human malaria parasite Plasmodium falciparum using the CRISPR-Cas9 system. *Nat Biotechnol,* 32**,** 819-21.

GINSBURG, H., KUTNER, S., KRUGLIAK, M. & CABANTCHIK, Z. I. 1985. Characterization of permeation pathways appearing in the host membrane of Plasmodium falciparum infected red blood cells. *Mol Biochem Parasitol,* 14**,** 313-22.

GLENISTER, F. K., COPPEL, R. L., COWMAN, A. F., MOHANDAS, N. & COOKE, B. M. 2002. Contribution of parasite proteins to altered mechanical properties of malaria-infected red blood cells. *Blood,* 99**,** 1060-3.

GOEL, S., PALMKVIST, M., MOLL, K., JOANNIN, N., LARA, P., AKHOURI, R. R., MORADI, N., OJEMALM, K., WESTMAN, M., ANGELETTI, D., KJELLIN, H., LEHTIO, J., BLIXT, O., IDESTROM, L., GAHMBERG, C. G., STORRY, J. R., HULT, A. K., OLSSON, M. L., VON HEIJNE, G., NILSSON, I. & WAHLGREN, M. 2015. RIFINs are adhesins implicated in severe Plasmodium falciparum malaria. *Nat Med,* 21**,** 314-7.

GRURING, C., HEIBER, A., KRUSE, F., FLEMMING, S., FRANCI, G., COLOMBO, S. F., FASANA, E., SCHOELER, H., BORGESE, N., STUNNENBERG, H. G., PRZYBORSKI, J. M., GILBERGER, T. W. & SPIELMANN, T. 2012. Uncovering common principles in protein export of malaria parasites. *Cell Host Microbe,* 12**,** 717-29.

GRURING, C., HEIBER, A., KRUSE, F., UNGEFEHR, J., GILBERGER, T. W. & SPIELMANN, T. 2011. Development and host cell modifications of Plasmodium falciparum blood stages in four dimensions. *Nat Commun,* 2**,** 165.

HALDAR, K., BHATTACHARJEE, S. & SAFEUKUI, I. 2018. Drug resistance in Plasmodium. *Nat Rev Microbiol*.

HANSSEN, E., CARLTON, P., DEED, S., KLONIS, N., SEDAT, J., DERISI, J. & TILLEY, L. 2010. Whole cell imaging reveals novel modular features of the exomembrane system of the malaria parasite, Plasmodium falciparum. *Int J Parasitol,* 40**,** 123-34.

HANSSEN, E., SOUGRAT, R., FRANKLAND, S., DEED, S., KLONIS, N., LIPPINCOTT-SCHWARTZ, J. & TILLEY, L. 2008. Electron tomography of the Maurer's cleft organelles of Plasmodium falciparum-infected erythrocytes reveals novel structural features. *Mol Microbiol,* 67**,** 703-18.

HAWTHORNE, P. L., TRENHOLME, K. R., SKINNER-ADAMS, T. S., SPIELMANN, T., FISCHER, K., DIXON, M. W., ORTEGA, M. R., ANDERSON, K. L., KEMP, D. J. & GARDINER, D. L. 2004. A novel Plasmodium falciparum ring stage protein, REX, is located in Maurer's clefts. *Mol Biochem Parasitol,* 136**,** 181-9.

HEIBER, A., KRUSE, F., PICK, C., GRURING, C., FLEMMING, S., OBERLI, A., SCHOELER, H., RETZLAFF, S., MESEN-RAMIREZ, P., HISS, J. A., KADEKOPPALA, M., HECHT, L., HOLDER, A. A., GILBERGER, T. W. & SPIELMANN, T. 2013. Identification of new PNEPs indicates a substantial non-PEXEL exportome and underpins common features in Plasmodium falciparum protein export. *PLoS Pathog,* 9**,** e1003546.

HILLER, N. L., BHATTACHARJEE, S., VAN OOIJ, C., LIOLIOS, K., HARRISON, T., LOPEZ-ESTRANO, C. & HALDAR, K. 2004. A host-targeting signal in virulence proteins reveals a secretome in malarial infection. *Science,* 306**,** 1934-7.

HVIID, L. & JENSEN, A. T. 2015. PfEMP1 - A Parasite Protein Family of Key Importance in Plasmodium falciparum Malaria Immunity and Pathogenesis. *Adv Parasitol,* 88**,** 51-84.

JOICE, R., NILSSON, S. K., MONTGOMERY, J., DANKWA, S., EGAN, E., MORAHAN, B., SEYDEL, K. B., BERTUCCINI, L., ALANO, P., WILLIAMSON, K. C., DURAISINGH, M. T., TAYLOR, T. E., MILNER, D. A. & MARTI, M. 2014. Plasmodium falciparum transmission stages accumulate in the human bone marrow. *Sci Transl Med,* 6**,** 244re5.

KHOSH-NAUCKE, M., BECKER, J., MESEN-RAMIREZ, P., KIANI, P., BIRNBAUM, J., FROHLKE, U., JONSCHER, E., SCHLUTER, H. & SPIELMANN, T. 2017. Identification of novel parasitophorous vacuole proteins in P. falciparum parasites using BioID. *Int J Med Microbiol*.

KILIAN, N., SRISMITH, S., DITTMER, M., OUERMI, D., BISSEYE, C., SIMPORE, J., CYRKLAFF, M., SANCHEZ, C. P. & LANZER, M. 2015. Hemoglobin S and C affect protein export in Plasmodium falciparum-infected erythrocytes. *Biol Open,* 4**,** 400-10.

KRIEK, N., TILLEY, L., HORROCKS, P., PINCHES, R., ELFORD, B. C., FERGUSON, D. J., LINGELBACH, K. & NEWBOLD, C. I. 2003. Characterization of the pathway for transport of the cytoadherence-mediating protein, PfEMP1, to the host cell surface in malaria parasite-infected erythrocytes. *Mol Microbiol,* 50**,** 1215-27.

KULZER, S., CHARNAUD, S., DAGAN, T., RIEDEL, J., MANDAL, P., PESCE, E. R., BLATCH, G. L., CRABB, B. S., GILSON, P. R. & PRZYBORSKI, J. M. 2012. Plasmodium falciparum-encoded exported hsp70/hsp40 chaperone/co-chaperone complexes within the host erythrocyte. *Cell Microbiol,* 14**,** 1784-95.

KULZER, S., RUG, M., BRINKMANN, K., CANNON, P., COWMAN, A., LINGELBACH, K., BLATCH, G. L., MAIER, A. G. & PRZYBORSKI, J. M. 2010. Parasite-encoded Hsp40 proteins define novel mobile structures in the cytosol of the P. falciparum-infected erythrocyte. *Cell Microbiol,* 12**,** 1398-420.

LAUER, S. A., RATHOD, P. K., GHORI, N. & HALDAR, K. 1997. A membrane network for nutrient import in red cells infected with the malaria parasite. *Science,* 276**,** 1122-5.

LAVAZEC, C., DEPLAINE, G., SAFEUKUI, I., PERROT, S., MILON, G., MERCEREAU-PUIJALON, O., DAVID, P. H. & BUFFET, P. 2013. Microsphiltration: a microsphere matrix to explore erythrocyte deformability. *Methods Mol Biol,* 923**,** 291-7.

LEE, P., YE, Z., VAN DYKE, K. & KIRK, R. G. 1988. X-ray microanalysis of Plasmodium falciparum and infected red blood cells: effects of qinghaosu and chloroquine on potassium, sodium, and phosphorus composition. *Am J Trop Med Hyg,* 39**,** 157-65.

MAIER, A. G., RUG, M., O'NEILL, M. T., BROWN, M., CHAKRAVORTY, S., SZESTAK, T., CHESSON, J., WU, Y., HUGHES, K., COPPEL, R. L., NEWBOLD, C., BEESON, J. G., CRAIG, A., CRABB, B. S. & COWMAN, A. F. 2008. Exported proteins required for virulence and rigidity of Plasmodium falciparum-infected human erythrocytes. *Cell,* 134**,** 48-61.

MANTEL, P. Y., HOANG, A. N., GOLDOWITZ, I., POTASHNIKOVA, D., HAMZA, B., VOROBJEV, I., GHIRAN, I., TONER, M., IRIMIA, D., IVANOV, A. R., BARTENEVA, N. & MARTI, M. 2013. Malaria-infected erythrocyte-derived microvesicles mediate cellular communication within the parasite population and with the host immune system. *Cell Host Microbe,* 13**,** 521-34.

MARTI, M., GOOD, R. T., RUG, M., KNUEPFER, E. & COWMAN, A. F. 2004. Targeting malaria virulence and remodeling proteins to the host erythrocyte. *Science,* 306**,** 1930-3.

MARTI, M. & SPIELMANN, T. 2013. Protein export in malaria parasites: many membranes to cross. *Curr Opin Microbiol,* 16**,** 445-51.

MATTHEWS, K., DUFFY, S. P., MYRAND-LAPIERRE, M. E., ANG, R. R., LI, L., SCOTT, M. D. & MA, H. 2017. Microfluidic analysis of red blood cell deformability as a means to assess hemin-induced oxidative stress resulting from Plasmodium falciparum intraerythrocytic parasitism. *Integr Biol (Camb),* 9**,** 519-528.

MAYER, C., SLATER, L., ERAT, M. C., KONRAT, R. & VAKONAKIS, I. 2012. Structural analysis of the Plasmodium falciparum erythrocyte membrane protein 1 (PfEMP1) intracellular domain reveals a conserved interaction epitope. *J Biol Chem,* 287**,** 7182-9.

MCMILLAN, P. J., MILLET, C., BATINOVIC, S., MAIORCA, M., HANSSEN, E., KENNY, S., MUHLE, R. A., MELCHER, M., FIDOCK, D. A., SMITH, J. D., DIXON, M. W. & TILLEY, L. 2013. Spatial and temporal mapping of the PfEMP1 export pathway in Plasmodium falciparum. *Cell Microbiol,* 15**,** 1401-18.

MEYER, C., BARNIOL, L., HISS, J. A. & PRZYBORSKI, J. M. 2017. The N-terminal extension of the P. falciparum GBP130 signal peptide is irrelevant for signal sequence function. *Int J Med Microbiol*.

MILLER, L. H., BARUCH, D. I., MARSH, K. & DOUMBO, O. K. 2002. The pathogenic basis of malaria. *Nature,* 415**,** 673-9.

MUNDWILER-PACHLATKO, E. & BECK, H. P. 2013. Maurer's clefts, the enigma of Plasmodium falciparum. *Proc Natl Acad Sci U S A,* 110**,** 19987-94.

NACER, A., CLAES, A., ROBERTS, A., SCHEIDIG-BENATAR, C., SAKAMOTO, H., GHORBAL, M., LOPEZ-RUBIO, J. J. & MATTEI, D. 2015. Discovery of a novel and conserved Plasmodium falciparum exported protein that is important for adhesion of PfEMP1 at the surface of infected erythrocytes. *Cell Microbiol,* 17**,** 1205-16.

NGUITRAGOOL, W., BOKHARI, A. A., PILLAI, A. D., RAYAVARA, K., SHARMA, P., TURPIN, B., ARAVIND, L. & DESAI, S. A. 2011. Malaria parasite clag3 genes determine channel-mediated nutrient uptake by infected red blood cells. *Cell,* 145**,** 665-77.

NIANG, M., BEI, A. K., MADNANI, K. G., PELLY, S., DANKWA, S., KANJEE, U., GUNALAN, K., AMALADOSS, A., YEO, K. P., BOB, N. S., MALLERET, B., DURAISINGH, M. T. & PREISER, P. R. 2014. STEVOR is a Plasmodium falciparum erythrocyte binding protein that mediates merozoite invasion and rosetting. *Cell Host Microbe,* 16**,** 81-93.

OBERLI, A., SLATER, L. M., CUTTS, E., BRAND, F., MUNDWILER-PACHLATKO, E., RUSCH, S., MASIK, M. F., ERAT, M. C., BECK, H. P. & VAKONAKIS, I. 2014. A Plasmodium falciparum PHIST protein binds the virulence factor PfEMP1 and comigrates to knobs on the host cell surface. *Faseb j,* 28**,** 4420-33.

OBERLI, A., ZURBRUGG, L., RUSCH, S., BRAND, F., BUTLER, M. E., DAY, J. L., CUTTS, E. E., LAVSTSEN, T., VAKONAKIS, I. & BECK, H. P. 2016. Plasmodium falciparum Plasmodium helical interspersed subtelomeric proteins contribute to

cytoadherence and anchor P. falciparum erythrocyte membrane protein 1 to the host cell cytoskeleton. *Cell Microbiol,* 18**,** 1415-28.

PACHLATKO, E., RUSCH, S., MULLER, A., HEMPHILL, A., TILLEY, L., HANSSEN, E. & BECK, H. P. 2010. MAHRP2, an exported protein of Plasmodium falciparum, is an essential component of Maurer's cleft tethers. *Mol Microbiol,* 77**,** 1136-52.

PIEL, F. B., PATIL, A. P., HOWES, R. E., NYANGIRI, O. A., GETHING, P. W., WILLIAMS, T. N., WEATHERALL, E. J. & HAYB, S. I. 2010. Global distribution of the sickle cell gene and geographical confirmation of the malaria hypothesis. *Nat. Commun.***,** 104.

PRADO, M., EICKEL, N., DE NIZ, M., HEITMANN, A., AGOP-NERSESIAN, C., WACKER, R., SCHMUCKLI-MAURER, J., CALDELARI, R., JANSE, C. J., KHAN, S. M., MAY, J., MEYER, C. G. & HEUSSLER, V. T. 2015. Long-term live imaging reveals cytosolic immune responses of host hepatocytes against Plasmodium infection and parasite escape mechanisms. *Autophagy,* 11**,** 1561-79.

PRZYBORSKI, J. M., NYBOER, B. & LANZER, M. 2016. Ticket to ride: export of proteins to the Plasmodium falciparum-infected erythrocyte. *Mol Microbiol,* 101**,** 1-11.

PUTRIANTI, E. D., SCHMIDT-CHRISTENSEN, A., ARNOLD, I., HEUSSLER, V. T., MATUSCHEWSKI, K. & SILVIE, O. 2010. The Plasmodium serine-type SERA proteases display distinct expression patterns and non-essential in vivo roles during life cycle progression of the malaria parasite. *Cell Microbiol,* 12**,** 725-39.

REGEV-RUDZKI, N., WILSON, D. W., CARVALHO, T. G., SISQUELLA, X., COLEMAN, B. M., RUG, M., BURSAC, D., ANGRISANO, F., GEE, M., HILL, A. F., BAUM, J. & COWMAN, A. F. 2013. Cell-cell communication between malaria-infected red blood cells via exosome-like vesicles. *Cell,* 153**,** 1120-33.

RIGLAR, D. T., ROGERS, K. L., HANSSEN, E., TURNBULL, L., BULLEN, H. E., CHARNAUD, S. C., PRZYBORSKI, J., GILSON, P. R., WHITCHURCH, C. B., CRABB, B. S., BAUM, J. & COWMAN, A. F. 2013. Spatial association with PTEX complexes defines regions for effector export into Plasmodium falciparum-infected erythrocytes. *Nat Commun,* 4**,** 1415.

ROBINSON, B. A., WELCH, T. L. & SMITH, J. D. 2003. Widespread functional specialization of Plasmodium falciparum erythrocyte membrane protein 1 family members to bind CD36 analysed across a parasite genome. *Mol Microbiol,* 47**,** 1265-78.

ROWE, J. A., MOULDS, J. M., NEWBOLD, C. I. & MILLER, L. H. 1997. P. falciparum rosetting mediated by a parasite-variant erythrocyte membrane protein and complement-receptor 1. *Nature,* 388**,** 292-5.

SALIBA, K. J., HORNER, H. A. & KIRK, K. 1998. Transport and metabolism of the essential vitamin pantothenic acid in human erythrocytes infected with the malaria parasite Plasmodium falciparum. *J Biol Chem,* 273**,** 10190-5.

SAMPAIO, N. G., EMERY, S., GARNHAM, A., TAN, Q. Y., SISQUELLA, X., PIMENTEL, M. A., REGEV-RUDZKI, N., SCHOFIELD, L. & ERIKSSON, E. M. 2018.

Extracellular vesicles from early-stage P. falciparum-infected red blood cells contain PfEMP1 and induce transcriptional changes in human monocytes. *Cell Microbiol*.

SCHNITZER, B., SODEMAN, T., MEAD, M. L. & CONTACOS, P. G. 1972. Pitting function of the spleen in malaria: ultrastructural observations. *Science,* 177**,** 175-7.

SCHULZE, J., KWIATKOWSKI, M., BORNER, J., SCHLUTER, H., BRUCHHAUS, I., BURMESTER, T., SPIELMANN, T. & PICK, C. 2015. The Plasmodium falciparum exportome contains non-canonical PEXEL/HT proteins. *Mol Microbiol,* 97**,** 301-14.

SHERMAN, I. W. 1977. Amino acid metabolism and protein synthesis in malarial parasites. *Bull World Health Organ,* 55**,** 265-76.

SILMON DE MONERRI, N. C., FLYNN, H. R., CAMPOS, M. G., HACKETT, F., KOUSSIS, K., WITHERS-MARTINEZ, C., SKEHEL, J. M. & BLACKMAN, M. J. 2011. Global identification of multiple substrates for Plasmodium falciparum SUB1, an essential malarial processing protease. *Infect Immun,* 79**,** 1086-97.

SPIELMANN, T. & GILBERGER, T. W. 2010. Protein export in malaria parasites: do multiple export motifs add up to multiple export pathways? *Trends Parasitol,* 26**,** 6-10.

SPIELMANN, T. & GILBERGER, T. W. 2015. Critical Steps in Protein Export of Plasmodium falciparum Blood Stages. *Trends Parasitol,* 31**,** 514-25.

SPIELMANN, T., MONTAGNA, G. N., HECHT, L. & MATUSCHEWSKI, K. 2012. Molecular make-up of the Plasmodium parasitophorous vacuolar membrane. *Int J Med Microbiol,* 302**,** 179-86.

SPILLMAN, N. J., BECK, J. R., GANESAN, S. M., NILES, J. C. & GOLDBERG, D. E. 2017. The chaperonin TRiC forms an oligomeric complex in the malaria parasite cytosol. *Cell Microbiol,* 19.

SPONAAS, A. M., CADMAN, E. T., VOISINE, C., HARRISON, V., BOONSTRA, A., O'GARRA, A. & LANGHORNE, J. 2006. Malaria infection changes the ability of splenic dendritic cell populations to stimulate antigen-specific T cells. *J Exp Med,* 203**,** 1427-33.

SPYCHER, C., KLONIS, N., SPIELMANN, T., KUMP, E., STEIGER, S., TILLEY, L. & BECK, H. P. 2003. MAHRP-1, a novel Plasmodium falciparum histidine-rich protein, binds ferriprotoporphyrin IX and localizes to the Maurer's clefts. *J Biol Chem,* 278**,** 35373-83.

SPYCHER, C., RUG, M., PACHLATKO, E., HANSSEN, E., FERGUSON, D., COWMAN, A. F., TILLEY, L. & BECK, H. P. 2008. The Maurer's cleft protein MAHRP1 is essential for trafficking of PfEMP1 to the surface of Plasmodium falciparum-infected erythrocytes. *Mol Microbiol,* 68**,** 1300-14.

STURM, A., AMINO, R., VAN DE SAND, C., REGEN, T., RETZLAFF, S., RENNENBERG, A., KRUEGER, A., POLLOK, J. M., MENARD, R. & HEUSSLER, V. T. 2006. Manipulation of host hepatocytes by the malaria parasite for delivery into liver sinusoids. *Science,* 313**,** 1287-90.

SU, X. Z., HEATWOLE, V. M., WERTHEIMER, S. P., GUINET, F., HERRFELDT, J. A., PETERSON, D. S., RAVETCH, J. A. & WELLEMS, T. E. 1995. The large diverse gene family var encodes proteins involved in cytoadherence and antigenic variation of Plasmodium falciparum-infected erythrocytes. *Cell,* 82**,** 89-100.

TARASCHI, T. F., O'DONNELL, M., MARTINEZ, S., SCHNEIDER, T., TRELKA, D., FOWLER, V. M., TILLEY, L. & MORIYAMA, Y. 2003. Generation of an erythrocyte vesicle transport system by Plasmodium falciparum malaria parasites. *Blood,* 102**,** 3420-6.

TIBURCIO, M., NIANG, M., DEPLAINE, G., PERROT, S., BISCHOFF, E., NDOUR, P. A., SILVESTRINI, F., KHATTAB, A., MILON, G., DAVID, P. H., HARDEMAN, M., VERNICK, K. D., SAUERWEIN, R. W., PREISER, P. R., MERCEREAU-PUIJALON, O., BUFFET, P., ALANO, P. & LAVAZEC, C. 2012. A switch in infected erythrocyte deformability at the maturation and blood circulation of Plasmodium falciparum transmission stages. *Blood,* 119**,** e172-80.

TRELKA, D. P., SCHNEIDER, T. G., REEDER, J. C. & TARASCHI, T. F. 2000. Evidence for vesicle-mediated trafficking of parasite proteins to the host cell cytosol and erythrocyte surface membrane in Plasmodium falciparum infected erythrocytes. *Mol Biochem Parasitol,* 106**,** 131-45.

TURNER, L., LAVSTSEN, T., BERGER, S. S., WANG, C. W., PETERSEN, J. E., AVRIL, M., BRAZIER, A. J., FREETH, J., JESPERSEN, J. S., NIELSEN, M. A., MAGISTRADO, P., LUSINGU, J., SMITH, J. D., HIGGINS, M. K. & THEANDER, T. G. 2013. Severe malaria is associated with parasite binding to endothelial protein C receptor. *Nature,* 498**,** 502-5.

USYNIN, I., KLOTZ, C. & FREVERT, U. 2007. Malaria circumsporozoite protein inhibits the respiratory burst in Kupffer cells. *Cell Microbiol,* 9**,** 2610-28.

WAHLGREN, M., CARLSON, J., UDOMSANGPETCH, R. & PERLMANN, P. 1989. Why do Plasmodium falciparumm-infected erythrocytes form spontaneous erythrocyte rosettes? *Parasitol Today,* 5**,** 183-5.

WALLER, K. L., COOKE, B. M., NUNOMURA, W., MOHANDAS, N. & COPPEL, R. L. 1999. Mapping the binding domains involved in the interaction between the Plasmodium falciparum knob-associated histidine-rich protein (KAHRP) and the cytoadherence ligand P. falciparum erythrocyte membrane protein 1 (PfEMP1). *J Biol Chem,* 274**,** 23808-13.

WARNCKE, J. D., VAKONAKIS, I. & BECK, H. P. 2016. Plasmodium Helical Interspersed Subtelomeric (PHIST) Proteins, at the Center of Host Cell Remodeling. *Microbiol Mol Biol Rev,* 80**,** 905-27.

WATERMEYER, J. M., HALE, V. L., HACKETT, F., CLARE, D. K., CUTTS, E. E., VAKONAKIS, I., FLECK, R. A., BLACKMAN, M. J. & SAIBIL, H. R. 2016. A spiral scaffold underlies cytoadherent knobs in Plasmodium falciparum-infected erythrocytes. *Blood,* 127**,** 343-51.

WHITE, N. J., PUKRITTAYAKAMEE, S., HIEN, T. T., FAIZ, M. A., MOKUOLU, O. A. & DONDORP, A. M. 2014. Malaria. *Lancet,* 383**,** 723-35.

WHO 2015. Global Technical Strategy for Malaria 2016–2030

WHO 2017. World malaria report 2017.

WICKERT, H., WISSING, F., ANDREWS, K. T., STICH, A., KROHNE, G. & LANZER, M. 2003. Evidence for trafficking of PfEMP1 to the surface of P. falciparum-infected erythrocytes via a complex membrane network. *Eur J Cell Biol,* 82**,** 271-84.

YADAVA, A., KUMAR, S., DVORAK, J. A., MILON, G. & MILLER, L. H. 1996. Trafficking of Plasmodium chabaudi adami-infected erythrocytes within the mouse spleen. *Proc Natl Acad Sci U S A,* 93**,** 4595-9.

YAM, X. Y., NIANG, M., MADNANI, K. G. & PREISER, P. R. 2017. Three Is a Crowd - New Insights into Rosetting in Plasmodium falciparum. *Trends Parasitol,* 33**,** 309-320.

Chapter 2

Characterization of PF3D7_0702500, an exported protein contributing to *P. falciparum* virulence

Data in preparation for manuscript

Characterization of PF3D7_0702500, an exported protein contributing to P. falciparum virulence

Introduction

Plasmodium falciparum is the causative agent of the most severe form of human malaria and accountable for an estimated 445,000 deaths in 2016 (World Health WHO, 2017). The asexual development of the protozoan parasite within the red blood cell (RBC) is associated with clinical symptoms of the disease, while the sexual forms (gametocytes) are crucial for transmission to the mosquito and thus the maintenance of the life cycle. Erythrocytes are highly specialized cells lacking organelles and specific cellular mechanisms e.g. a protein trafficking system. *P. falciparum* extensively modifies the red blood cell to thrive. Essential changes mediate host immune evasion and enable nutrient uptake. The refurbishment process is driven by parasite proteins that are exported to the host cell. To ensure proper protein delivery to target sites, the parasite needs to establish a trafficking system as no existing host pathways can be exploited. Maurer's clefts are parasite-derived organelles installed in the cytoplasm of the infected RBC (reviewed in Mundwiler-Pachlatko and Beck, 2013). Their function is not entirely clear but they are thought to be important sorting stations of already exported proteins. Depletion of several resident Maurer's clefts proteins prevents *P. falciparum* erythrocyte membrane protein 1 (PfEMP1) presentation on the erythrocyte surface e.g. MAHRP1 (Spycher et al., 2008), SBP1 (Cooke et al., 2006), and REX1 (Dixon et al., 2011). PfEMP1 is the major virulence factor of *P. falciparum* mediating cytoadherence of infected erythrocytes to the microvasculature enabling the parasite to avoid spleen passage resulting in clearance from the circulation (Hviid and Jensen, 2015).

P. falciparum exports ~10% of its entire proteome to the erythrocyte cytoplasm (Spielmann and Gilberger, 2015). This enormous number hints at the critical role of host cell refurbishment for parasite development. Thus, a better understanding of the function of exported proteins and in particular of PfEMP1 trafficking mechanisms could lead to the identification of new targets for therapy, or even lead towards a vaccination with attenuated parasites.

Exported proteins can be divided in two groups: 1) those that carry a common *Plasmodium* export element (PEXEL) motif (RxLxE/Q/D) (Hiller et al., 2004, Marti et al., 2004), and 2) those devoid of a PEXEL motif which are summarized as PEXEL-negative exported proteins (PNEPs). PNEPs have structural similarities but no shared primary sequence features and they are therefore difficult to predict. A study from Heiber and colleagues suggested that there are several dozens of PNEPs in *P. falciparum* (Heiber et al., 2013).

In order to elucidate the interaction network of exported proteins, their functions, and their integration into host cellular structures we previously performed co-immunoprecipitation experiments with SEMP1 (a Maurer's clefts protein) (Dietz et al., 2014) and MAHRP2 (a Maurer's cleft's tether protein) (unpublished). One of the common putative interaction partners identified by mass spectrometry was the PNEP PF3D7_0702500.

Here, we characterized the PNEP PF3D7_0702500 which is expressed throughout the intraerythrocytic stages and localizes to electron-dense structures. Our results suggest that PF3D7_0702500 contributes to efficient transport of PfEMP1 between Maurer's clefts and the erythrocyte membrane, or its reduced anchoring at the cytoskeleton.

Methods

Cell culture and transfections

P. falciparum 3D7 was cultured and transfected as described (Moll et al., 2013). Transfected parasites were positively selected with 10nM WR99210 (Jacobs Pharmaceuticals, Cologne, Germany), 5mg/ ml blasticidin (Sigma-Aldrich, Inc.), negative selection was done with 1µM 5-Fluorocytosine (Valeant Pharmaceuticals, Laval, CA).

Plasmid constructs

3xHA-tagging at the 3' end generating PF3D7_0702500-3xHA was achieved using a combined CRISPR-Cas9/SLI approach (Ghorbal et al., 2014, Birnbaum et al., 2017). Homology regions between 400-550bp were designed, and a gRNA close to the genes 5' end was chosen using the CHOPCHOP software (Labun et al., 2016, Montague et al., 2014). The gRNA recognition sequence was mutated on the homology plasmid sequences to avoid cleavage of successfully tagged endogenous protein. Mutations were introduced with PCR primers. The homology regions and gRNA were PCR amplified using primers listed in Supplementary Table 1 and cloned into pCRISPR_HA2ABSD using the In-Fusion® HD Cloning Kit (Clontech® Laboratories, Inc.). pCRISPR_HA2ABSD contains the Cas9, the gRNA, and the integration cassette flanked by homology regions. The integration cassette consists of the 3xHA-tag and a blasticidine resistance gene separated by a 2A skip peptide (Szymczak et al., 2004) and a *hrp2* terminator. The blasticidine gene lacks a promotor and can only be expressed after successful integration into the target locus. The skip peptide triggers a

ribosomal skip mechanism and thus impairs normal peptide bond formation preventing the attachment of the selection marker to the target protein (Donnelly et al., 2001).
The PF3D7_0702500 KO was generated with a two plasmid CRISPR-Cas9 approach using pUF_Cas9 and pL7 (obtained from Ghorbal et al., 2014). 350-500bp homology regions were designed and a gRNA was chosen as described. The homology regions and gRNA were PCR amplified using primers listed in Supplementary Table 1 and cloned into pL7 using the In-Fusion® HD Cloning Kit (Clontech® Laboratories, Inc.).

Western blot analysis

Parasite saponin lysates were run on 4-12% Bis/Tris precast gels (NuPAGE®, Life Technologies) according to the manufacturers' protocol. Protein transfer was performed with the iBlot 2.0 (Life Technologies). Subsequently the membrane was blocked with 10% skimmed milk/TNT (0.1% Tween in 100mM Tris, 150mM NaCl-buffer) and probed with a first antibody in 3% skimmed milk/TNT at room temperature for 2h or overnight. After 6 washes for 5min with TNT the secondary antibody conjugated to HRP was incubated in the respective dilution in 3% skimmed milk/TNT for 2h at room temperature. After another 6 washes for 5min with TNT the signal was detected by Super Signal West Pico Chemiluminescent Substrate (Thermo Scientific) or LumiGlo Reserve Chemiluminescent Substrate (Seracare) according to the manufacturers' protocol. The antibodies used were: rabbit α-MAHRP1 (1:5'000), rat α-HA (Roche, 1:1'000), mouse α-GAPDH (1:20'000), rabbit α-PFE1605w (1:1'000), mouse α-ATS (1:500), goat α-mouse-HRP (Pierce, 1:5'000), α-rat-HRP (Pierce, 1:10'000), goat α-rabbit-HRP (Pierce, 1:10'000).

Fluorescence microscopy

Thin blood smears of infected parasite cultures were fixed in ice-cold 60% methanol/40% acetone for 2min. After air-drying of the smear, a small circle was drawn with a hydrophobic pen and the respective area was blocked with 3% BSA/PBS for 1h at room temperature in a humidified chamber. Then, the cells were incubated with mouse α-MAHRP1 (1:100), rabbit α-MAHRP2 (1:100), mouse α-ATS (1:50), rat α-HA (Roche, 1:100), mouse α-GFP (Roche, 1:100), mouse α-PFI1780w (1:1000) in 3% BSA/PBS for minimum 2h at room temperature in a humidified chamber. After 3 washes with 3% BSA/PBS for 7min the secondary antibody (goat α-mouse Alexa488, goat α-rabbit Alexa488, goat α-rabbit Alexa568, goat α-rat

Alexa568 (all Invitrogen, 1:200)) was applied in 3% BSA/PBS for a minimum of 1h at room temperature in a humidified chamber. After another 3 wash steps with 3% BSA/PBS for 7min each a coverslip was mounted with 2µl VECTASHIELD® with DAPI (Vector Laboratories Inc.). For imaging a 63x oil-immersion lens (1.4 numerical aperture) on a Leica 5000 B microscope was used. The images were obtained by using the software Leica ApplicationSuite 4.4. and analyzed using FiJi (Schindelin et al., 2012).

Confocal microscopy

2.5ml of infected parasite cultures were pelleted and all subsequent steps were performed in Eppendorf tubes. Cells were fixed for 30min in 1ml 4% formaldehyde/0.01% glutaraldehyde in PBS on a rotator at room temperature. After washing 6 times with PBS, membrane permeabilization was achieved by incubating the pellet for 10 min in 500 µl 0.1% Triton X-100 in PBS at room temperature on a rotator followed by 3 washes in PBS. Unspecific binding sites from glutaraldehyde were blocked by incubating the sample for 10min in 500µl 0.1mg/ml $NaBH_4$ in PBS at room temperature on a rotator. After 3 times washing with PBS, blocking was performed in 3% BSA/PBS for 1h at room temperature on a rotator. The first antibody (rat α-HA (Roche, 1:100), mouse α-GFP (Roche, 1:100), mouse α-PFI1780w (1:1000), mouse α-ATS (1:50)) was diluted in 100µl 3% BSA/PBS and incubated 1-2h at room temperature on a rotator. Then 5 wash steps with PBS were performed. The secondary antibody (goat α-mouse Alexa488, goat α-rat Alexa568, both Invitrogen, 1:200) was diluted in 3% BSA/PBS and incubated 1-2h at room temperature on a rotator in the dark. After 5 PBS washes, the cell pellet was resuspended in 50-100µl PBS and mixed 1:1 with VECTASHIELD® with DAPI (Vector Laboratories Inc.). Approximately 5µl of cells were put on a microscopy slide, covered by a coverslip which was fixed and sealed with nail polish. The slides were imaged with a Zeiss LSM 700 confocal microscope (Carl Zeiss GmbH, Jena, Germany), with a 63x oil-immersion lens (1.4 numerical aperture). Colocalization analysis was performed with deconvoluted pictures (Huygens Remote Manager, Ponti et al., 2007) by using Fiji (JACoP plugin, Schindelin et al., 2012).

Solubility assay

10ml asynchronous parasite infected cell cultures were lysed in 0.03% saponin for 10min on ice. Cell pellets were washed 3x with PBS and resuspended in 200µl 5mM Tris-Cl (pH 8)

with cOmplete protease inhibitor cocktail (Roche). The sample was frozen at -80°C. After centrifugation for 10min at 16'000g at 4°C the supernatant was saved as hypotonic fraction (soluble protein fraction). The pellet was washed 5 times in 5mM Tris-Cl (pH 8) and then resuspended in 200µl 0.1 M Na_2CO_3 (pH 11) with protease inhibitor and incubated 30min on ice. After centrifugation for 10min at 16'000g at 4°C the supernatant was saved as carbonate fraction (peripheral membrane protein fraction). The pellet was washed 5 times in 0.1M Na_2CO_3 (pH 11) and then resuspended in 200µl 1% Triton-X-100 in PBS with protease inhibitor and incubated 30min on ice. After centrifugation for 10min at 16'000 g at 4°C the supernatant was saved as integral fraction (integral membrane protein fraction). The remaining pellet was resuspended in 200µl 4% SDS/0.5% Triton-X-114/.5x PBS and defined as Triton insoluble fraction. Equal amounts of all fractions were assessed by Western blot.

Co-Immunoprecipitation

150ml synchronized parasite culture was harvested by Percoll to enrich late stages. Proteins were cross-linked with 1% formaldehyde in culture media for 30min on a rotator at 37°C. Cross-linking was stopped by adding glycine to a final concentration of 0.3M. The red blood cells were subsequently lysed with 0.03% saponin for 10min at 4°C. Afterwards the pellet was resuspended in sonication buffer (50mM Tris-HCl pH 8, 10mM EDTA, 1% SDS, cOmplete protease inhibitor cocktail) and sonicated for 15min (30 sec on/30 sec off) in a Bioruptor UCD-300. The fraction containing the protein of interest (bait) was determined by Western blot analysis. For the Co-immunoprecipitation the sample and the control were divided into 4 replicates each. 350µl sonication supernatant was mixed with 350µl 2x binding buffer (50mM Tris-HCl pH 7.4, 300mM NaCl, 2% Nonidet 40, cOmplete protease inhibitor cocktail) and for the negative control additionally 75µg HA-peptide (Sigma) was added. Samples were mixed with 80µl PierceTM α-HA Magnetic Beads (Thermo Scientific) and incubated at 4°C overnight at 25rpm. Beads were pelleted with a magnet and washed 4 times with washing buffer (50mM Tris-HCl pH 7.4, 150mM NaCl, 1mM EDTA, 1% Nonidet 40, cOmplete protease inhibitor cocktail). Finally, the beads were incubated with 30µl elution buffer (0.5mg/ml HA-peptide in 1x binding buffer) at 25rpm for 2h at 4°C. The supernatant was kept as elution, and mixed with sample buffer. The eluted fraction was analyzed by Silver Gel (SilverQuest, Invitrogen) and Western blot before LC-MS/MS analysis.

MS sample preparation

Samples were loaded onto a 4%-12% gradient Bis-Tris gel (Thermo) and run in 1x MOPS buffer at 180V for 10min. Each lane was sliced, minced and transferred to an Eppendorf reaction tube. In gel digest was performed as previously described (Bluhm et al., 2016) and samples stored on StageTips (Rappsilber et al., 2007) until measurement. Alternatively, for biotin proximity ligation experiments, the beads were directly incubated in 2mM DTT/50mM ammoniumbicarbonate buffer (Sigma-Aldrich) and subsequently alkylated with 5mM iodoacetamide (Sigma-Aldrich). Digestions were performed with 200ng of trypsin (Sigma-Aldrich) in 2M urea/50mM ammoniumbicarbonate buffer at room temperature overnight. Tryptic peptides were stored on StageTips (Rappsilber et al., 2007) until measurement.

MS measurement

The digested peptides of the samples were separated on a 25-cm reverse-phase capillary (75 µM inner diameter, New Objective) packed with Reprosil C18 material (Dr. Maisch GmbH). Elution of the peptides was achieved with a 2h gradient from 2%-40% Buffer acetonitrile followed by a 95% acetonitrile wash-out at 200nl/min on an Easy LC1000 HPLC system (Thermo). Mass spectrometry measurements were performed with a Q Exactive Plus mass spectrometer (Thermo) operated with a Top10 data-dependent MS/MS acquisition method per full scan. Spray voltage was set to 2.2-2.4 kV.

MS data analysis

MS raw data was analyzed using MaxQuant v1.5.2.8 (Cox and Mann, 2008) with standard settings and activated match between runs and LFQ quantitation features. The search was performed against a Human Uniprot database (81,194 entries) and the *Plasmodium falciparum* PlasmoDB 9.3 database (5,538 entries). The proteinGroups file was filtered for known contaminants and reverse hits prior to statistical analysis (Welch t-test). Data was plotted using the R environment (http://www.R-project.org).

Growth assay

Asynchronous parasite infected cell cultures were set up at 0.2% parasitemia. Parasitemia was determined by flow cytometry and followed over 5 days. Parasites were stained with SYBR® Green I nucleic acid gel stain (Sigma-Aldrich) 1:5000 for 20min at 37°C in the dark, washed

3x with culture medium and 100’000 cells were assessed with a BD FACSCalibur. The experiment was performed in biological triplicates, standard deviations were calculated and exponential curves fitted to the data points.

Deformability assay

Microsphiltration experiments were performed as described by Lavazec et al. (2013). Tightly synchronized parasite cultures (600µl, 0.5-10% parasitemia, 1.5% hematocrit) were passed under flow (60ml/h) through a microsphere matrix consisting of solder powder beads from 5-15µm and 15-25µm diameter (Industrie des Poudres Sphériques, Annemasse, France). After rinsing the column with 5ml of culture medium, parasitemia of input and flow through samples were assessed by flow cytometry. Parasites were stained with SYBR® Green I nucleic acid gel stain (Sigma-Aldrich) 1:5000 for 20min at 37°C in the dark, washed 3x with culture medium and 100’000 cells were assessed with a BD FACSCalibur. All experiments were performed in technical triplicates. Retention rates (in %) were calculated as 1−(parasitemia flow through sample/parasitemia input sample).

Binding assay

Semi-static binding assays were performed as published previously (Oberli et al., 2016). Human CD36 recombinant protein (Sino Biological, China) was spotted on wells of eight-chamber cell culture glass slides (Falcon, Big Flats, NY, USA) with 50µg/ml concentrations and incubated overnight at 4°C to allow proteins to absorb to the surface. The wells were blocked with 1% BSA/PBS for 1h at 37°C. Parasite cultures were washed twice with RPMI-HEPES and spotted onto immobilized CD36 and cultured for 2h under continuous and simultaneous shaking (140rpm, proBlot 25 Rocker; Labnet International Inc., NY, USA) (105rpm, Lab-Therm LT-W, Kühner, Switzerland) at 37°C. Non-bound erythrocytes were removed by six gentle washes with RPMI-HEPES with simultaneous shaking for 2min. Bound iRBCs were fixed with 2% glutaraldehyde in RPMI-HEPES overnight, stained with 10% Giemsa for 1h and microscopically counted. Results are shown as relative mean number of parasites bound per square millimeter and normalized to 1% parasitemia and 3D7. The experiment was performed in biological triplicates.

Trypsin cleavage assay

Percoll-purified late stage parasites were digested for 15min at 37°C either in 100µg/ml L-(tosylamido-2-phenyl) ethyl chloromethyl ketone-treated trypsin (Sigma)/PBS or in trypsin and 1mg/ml soybean trypsin inhibitor (Sigma)/PBS. The reaction was stopped by adding soybean trypsin inhibitor to a 1mg/ml final concentration. PfEMP1 extraction and subsequent Western blot analysis was performed as previously described (Van Schravendijk et al., 1993, Waterkeyn et al., 2000).

PfEMP1 expression typing by quantitative real-time PCR

PfEMP1 transcript diversity in the respective parasite cultures was performed as previously described (Dahlback et al., 2007). Total RNA was extracted from ring stage infected red blood cells dissolved in RiboZol (Amresco). Subsequently, qRT-PCR was performed on complementary DNA synthesized from total RNA with gene specific primers for each 3D7 *var* gene to determine relative copy numbers compared to internal control transcripts.

Immunoelectron microscopy

For immunoelectron microscopy, mature parasites were knob-selected, purified by Percoll density gradient, fixed in 2% paraformaldehyde/ 0.2% glutaraldehyde in phosphate buffer pH7.4, half of them were treated with Tetanolysin (Sigma) and prepared according to Tokuyasu (1973). Ultrathin sections (70nm) prepared on a FC7/UC7-ultramicrotome (Leica) at -120°C were immuno-gold labeled with rabbit α-HA (dilution 1:60, Invitrogen) or rabbit α-MAHRP2 (dilution 1:20) antibodies and finally decorated with 5 or 10nm protein A-gold (1:70) (UMC, Utrecht, The Netherlands). Sections were stained with 4% uranyl acetate/methylcellulose (1:9) and examined with a Tecnai G2 Spirit or CM100 Philips transmission electron microscope (TEM) at 80kV.

Results

Expression and localization of PF3D7_0702500

PF3D7_0702500 is located on chromosome 7 and has a two exon structure encoding a 253 amino acid long protein with a predicted transmembrane domain.

We used a combined CRISPR/Cas9-SLI approach (Ghorbal et al., 2014, Birnbaum et al., 2017) to introduce a 3xHA-tag at the PF3D7_0702500 C-terminal end (Figure 1A). Correct integration of the tag-cassette was verified by PCR (data not shown). The expression of the fusion-protein was analyzed by Western blot (Figure 1B) and a signal running at around 40kDa was observed although the calculated molecular weight of PF3D7_0702500-3xHA is 31kDa. As expected there was no HA-signal detected in the 3D7 control lysate. The faint band above 50kDa is PF3D7_0702500-3xHA-2A-BSD, where the skip peptide was not cleaved efficiently (α-bsd Western blot not shown).

Information about expression and localization of PF3D7_0702500-3xHA throughout the asexual intraerythrocytic life cycle was obtained by time course immunofluorescence assays and Western blot analysis (Figures 1C and D). PF3D7_0702500-3xHA is expressed and exported throughout the entire asexual life cycle with a peak in the late trophozoite/schizont fraction, and the protein localizes in a punctuate manner in the infected red blood cell (iRBC) cytosol. Well-known structures in the erythrocyte cytosol are Maurer's clefts and Maurer's clefts tethers. Co-labeling immunofluorescence assays with MAHRP1 (resident Maurer's cleft protein) and MAHRP2 (resident Maurer's cleft tether protein) showed partial overlap of the signal indicating a partial localization of PF3D7_0702500-3xHA at Maurer's clefts and tether structures (Figure 1E).

The high-resolution subcellular localization of PF3D7_0702500-3xHA was determined by immunoelectron microscopy of ultrathin sections (Figure 2). PF3D7_0702500-3xHA was found to localize to electron-dense structures approximately 25 nm in diameter and 100 nm in length. They were found in proximity to Maurer's clefts, tethers, and the iRBC membrane.

In a solubility assay, PF3D7_0702500-3xHA was recovered in the hypotonic fraction indicating behavior as a soluble protein similar to GAPDH which was used as control (Figure 1F, first and second panel). In contrast, the carbonate fraction contains peripheral membrane proteins, e.g. PFE1605w (Figure 1F, third panel), and in the Triton-X100 fraction integral membrane proteins such as MAHRP1 are found (Figure 1F, forth panel).

Interaction partners of PF3D7_0702500

To identify interacting proteins of PF3D7_0702500 we performed co-immunoprecipitation (Co-IP) experiments of PF3D7_0702500-3xHA followed by mass spectrometry. Protein extracts of trophozoite PF3D7_0702500-3xHA iRBCs were analyzed. Potential interacting proteins of PF3D7_0702500-3xHA were eluted from α-HA-beads by competition with soluble HA peptide. As a negative control excess HA peptide was added to the protein extract during the binding step. Four sample replicates each were analyzed by mass spectrometry. The Δ value describes how enriched a protein was found in the sample compared to the negative control. We have identified a total number of 94 *P. falciparum* and human proteins positively enriched in the PF3D7_0702500-3xHA sample compared to the control sample (see Supplementary Table 2). Table 1 shows a list of 19 exported *Plasmodium* proteins identified in the Co-IP. We detected Maurer's clefts proteins (e.g. MAHRP1, SBP1, REX1) and proteins localizing to the erythrocyte cytoskeleton (e.g. MESA, PFE1605w, PHISTb family proteins). Further, we found several human proteins localizing to the erythrocyte membrane and cytoskeleton proteins such as 55 kDa erythrocyte membrane protein, spectrin alpha and beta chain, ankyrin-1, band 4.1, band 7 and band 4.2 (Table 2).

Colocalization analysis with confocal microscopy was performed to verify the potential *P. falciparum* interaction partners of PF3D7_0702500-3xHA. For MAHRP1, MAHRP2, Hsp70x, REX1, SBP1, MESA, PFE1605w, and PFI1780w specific antibodies were available. Additionally, the PF3D7_0702500-3xHA cell line was transfected to episomally overexpress PF3D7_0402000-GFP or PF3D7_0801000-GFP. These double transfected cell lines PF3D7_0702500-3xHA/PF3D7_0402000-GFP and PF3D7_0702500-3xHA/ PF3D7_0801000-GFP were used for colocalization studies using α-HA- and α-GFP-antibodies. Huygens deconvolution and intensity-based colocalization analysis with the JACoP plugin identified PFI1780w, PF3D7_0402000-GFP and PF3D7_0801000-GFP as strongly colocalizing to PF3D7_0702500-3xHA with Pearson's coefficients >0.9 and Maender's coefficients >0.9 (Figure 3 A and B). In a next step, the double PF3D7_0702500-3xHA/PF3D7_0402000-GFP and PF3D7_0702500-3xHA/ PF3D7_0801000-GFP cell lines were analysed by immunoelectron microscopy. No colocalization of PF3D7_0702500-3xHA and PF3D7_0402000-GFP or PF3D7_0702500-3xHA and PF3D7_0801000-GFP was observed. PF3D7_0402000-GFP was found at the iRBC cytoskeleton and PF3D7_0801000-GFP at the iRBC cytoskeleton and at Maurer's clefts (Supplementary Figure 1).

Phenotypical analysis of PF3D7_0702500

To investigate the function of PF3D7_0702500 a knock out (KO) parasite line was generated using a CRISPR/Cas9 approach. A *hDHFR* resistance cassette was introduced to disrupt the gene and enable positive selection of transgenic parasites. The gene disruption was confirmed by PCR (Figure 4A) and Southern blot (data not shown).

The PF3D7_0702500 KO was viable indicating that the respective gene is dispensable in culture. There was no significant growth difference between the PF3D7_0702500 KO cell line and wildtype 3D7 parasites (Figure 4B).

Deformability of iRBC is important for the passage of iRBCs through small capillaries and to avoid clearance in the spleen. With microsphiltration cell deformability is assessed by mimicking the function of a spleen (Deplaine et al., 2011). We used highly synchronous parasite cultures in ring and trophozoite stages and the deformability measured by retention rates of the KO cell line was not significantly different to 3D7 infected iRBCs (Figure 4C).

Similarly to deformability, the presentation of PfEMP1 on the iRBC surface is crucial for the parasite as it confers cytoadherence and allows avoidance of spleen passage. We measured cytoadherence to CD36 in semi-static binding in which the KO cell line was significantly reduced when compared to 3D7 (Figure 5A). CD36 binding depends on the expressed PfEMP1 variant and since no pre-selection of PfEMP1 expression was done before the experiments we determined the PfEMP1 repertoire expressed which was similar in both cell lines (Figure 5B).

To verify that the reduced binding is not due to a lack of PfEMP1 on the iRBC surface, a trypsin cleavage assay was performed. In both cell lines PfEMP1 is present on the surface of the host erythrocyte (Figure 5C). Immunofluorescence assays with antibodies against the ATS-domain of PfEMP1 showed no difference in signal at the Maurer's clefts indicating correct transport of PfEMP1 to the clefts (Figure 5D). However, it is not possible with this antibody to test the presence of PfEMP1 at the erythrocyte membrane.

To further investigate the relationship between PF3D7_0702500 and PfEMP1, colocalization analysis of trophozoite PF3D7_0702500-3xHA and PfEMP1 (α-ATS antibody) was performed (Figure 5E). Partial overlap of the signals was observed.

We have previously shown that MAHRP1 is essential for PfEMP1 presentation on the iRBC surface (Spycher et al., 2008). Therefore PF3D7_0702500 was endogenously 3xHA-tagged in a MAHRP1 KO cell line and the localization of PF3D7_0702500-3xHA was checked in a

PfEMP1 export depleted host cell. PF3D7_0702500-3xHA localization was not affected by lack of PfEMP1 (Figure 5E).

Discussion

Within an approach of better understanding the role and interactions of exported proteins associated with Maurer's clefts and Maurer's clefts tethers, we have characterized the PNEP PF3D7_0702500 and suggest a function in anchoring PfEMP1 or facilitating PfEMP1 transport from Maurer's clefts to the iRBC membrane.

To study PF3D7_0702500 in detail, a PF3D7_0702500-3xHA and a PF3D7_0702500 KO cell line were generated. The chosen CRISPR/Cas9 and combined CRISPR/Cas9–SLI approaches enabled the establishment of knock out and knock in cell lines in an efficient way. Endogenous PF3D7_0702500 3x-HA-tagging allowed us to study its expression and localization in the native environment (not overexpressed under an exogenous promoter). PF3D7_0702500-3xHA is present in the iRBC cytoplasm throughout the entire intraerythrocytic life cycle. The peak of PF3D7_0702500-3xHA expression seems during later life stages, putatively reflecting the importance of the protein in the second half of the red blood cell cycle.

By immunoelectron microscopy we found PF3D7_0702500-3xHA localizing to electron dense structures. They resemble the uncoated vesicular-like structures (VLS) described before (Kriek et al., 2003, Wickert et al., 2003, Hanssen et al., 2008). Uncoated VLS are spherical, and ~25-30nm in size, generally they are poorly defined. Cyrklaff and colleagues observed vesicles in various sizes (20nm to >200nm) attached to actin filaments connecting Maurer's clefts with the knobs and hypothesize that they may have a role in the transport of cargo (Cyrklaff et al., 2011).

The solubility assay revealed soluble-protein-like behavior of PF3D7_0702500-3xHA. This is in line with its localization to non-membranous structures observed by electron microscopy. However, the TMHMM tool (Krogh et al., 2001, Sonnhammer et al., 1998) predicts a transmembrane domain between aa 32-50 in PF3D7_0702500. We suggest that the predicted transmembrane domain functions rather as signal peptide, as for PNEPs a hydrophobic N-terminal region was described to be important as export element (Spielmann and Gilberger, 2010). Previously we have shown that the predicted transmembrane domain of MAHRP2 clearly is not a functional transmembrane domain (Pachlatko et al., 2010). This shows that the

TMHMM tool is a prediction program only and that additional experiments are needed to confirm its predictions.

Alternatively, PF3D7_0702500 aa 48-52 (KYIRS) could be a non-canonical, so far unknown PEXEL variant (Schulze et al., 2015). A putatively cleaved PF3D7_0702500 would have a molecular weight of around 22kDa. Thus one could hypothesize that the observed 40kDa band on the Western blot (Figure 1B) corresponds to a dimer of the protein.

We suggest a shuttling function of PF3D7_0702500 containing structures between Maurer's clefts and the iRBC membrane. The identification of putative interaction partners resident to both structures supports this thesis. Of the 18 exported proteins that are possibly interacting with PF3D7_0702500-3xHA, 7 have been described to be involved in trafficking or anchoring PfEMP1 to the iRBC surface: MAHRP1 (Spycher et al., 2008), SBP1 (Cooke et al., 2006), REX1 (McHugh et al., 2015), Hsp70-x (Charnaud et al., 2017), PFE1605w (Oberli et al., 2016), PTP5 and PTP6 (Maier et al., 2008). Further, we could validate a previously found MAHRP2 interaction with PF3D7_0702500 (unpublished), since we identified MAHRP2 in the immunoprecipitation with PF3D7_0702500.

Following up the putative interaction partners we narrowed down the candidates for direct interaction by confocal microscopy followed by colocalization analysis. PFI1780w, PF3D7_0801000-GFP and PF3D7_0402000-GFP were identified in close proximity of PF3D7_0702500-3xHA. All of them belong to the *Plasmodium* Helical Interspersed Subtelomeric (PHIST) protein family (reviewed in Warncke et al., 2016). PFI1780w belongs to the PHISTc subfamily, its function is unknown. It has been shown to interact with the ATS domain of PfEMP1 in vitro (Mayer et al., 2012) and localizes to the iRBC periphery with ATS (Oberli et al., 2014). However, it is not co-transported with PfEMP1 (Oberli et al., 2014). PF3D7_0801000 also belongs to the PHISTc subfamily and is a soluble protein present in the PV lumen, the iRBC cytosol and localizes to J-dots. The *P. yoellii* orthologue PcyPHIST/CVC-81_{95} localizes to caveola-vesicle complex (CVC) structures that are not produced in *P. falciparum* (Akinyi et al., 2012). PF3D7_0402000 is a PHISTa subfamily protein that has been reported to interact with the human cytoskeleton protein band 4.1R (Parish et al., 2013). It is noteworthy that a Co-IP using the ATS domain of var2CSA identified PF3D7_0702500 and PF3D7_0801000 (unpublished) suggesting a complex of these three proteins. In contrast, immunoelectron microscopy did not confirm a close physical association of PF3D7_0702500-3xHA neither with PF3D7_0402000-GFP nor

PF3D7_0801000-GFP. PF3D7_0402000-3xHA was found at the cytoskeleton. PF3D7_0801000-GFP localized to Maurer's clefts and the cytoskeleton but not to the PF3D7_0702500-3xHA-labelled electron-dense structures (Supplementary Figure 1). Thus, it is rather unlikely that there is a direct interaction of the two proteins, however a function in the same complex (e.g. an indirect interaction) cannot be excluded.

Phenotypical analysis of the PF3D7_0702500 KO cell line revealed reduced binding to the endothelial receptor CD36. Binding capacity of iRBCs to different receptor molecules depends on the PfEMP1 variant that is expressed in parasite culture. To exclude that the observed reduced binding of the PF3D7_0702500 KO cell line is due to a different dominantly expressed PfEMP1 variant, *var* gene expression analysis was performed. In line with our previous observations, the most dominantly expressed PfEMP1 variant was PF07_0048 in both cultures which belongs to the upsC group. PF07_0048, PFD0615c, PFL1955w, PFD0625c, and MAL6P1.252, the most frequently expressed PfEMP1 variants in both cultures are CD36 binders (Robinson et al., 2003, Oberli et al., 2016). We found PfEMP1 correctly surface-presented in a PF3D7_0702500 KO trypsin cleavage assay and the Western blot does not explicitly indicate a reduced amount of (cleaved) PfEMP1 in PF3D7_0702500 KO compared to wildtype. However, the quantification of PfEMP1 molecules transported to the surface in order to find out whether PF3D7_0702500 plays a role in efficient PfEMP1 delivery will be challenging. Preliminary evidence for an interaction of PF3D7_0702500-3xHA and PfEMP1 in the erythrocyte cytosol was obtained by confocal colocalization analysis. Further analysis of the electron-dense structures PF3D7_0702500-3xHA localizes to will hopefully give more insights whether they are involved in PfEMP1 shuttling.

Another possible explanation of the reduced CD36 binding of PF3D7_0702500 KO iRBCs is a defective anchoring of PfEMP1 in the erythrocyte membrane. In other instances PFE1605w has been shown to comigrate with PfEMP1 but not to be involved in PfEMP1 transport. The reduced binding to CD36 (but not to other endothelial receptors) upon PFE1605w knock down was explained by different interactions of PFE1605w with various PfEMP1 molecules (Oberli et al., 2016). Additional binding assays with preselected PF3D7_0702500 KO and wildtype iRBCs binding to CSA, ICAM-1, or EPCR could clarify the PfEMP1 variant specificity of PF3D7_0702500.

In conclusion, we characterized the PNEP PF3D7_0702500 and suggest a function in efficient delivery or anchoring of PfEMP1 to the iRBC surface. The complete understanding of PfEMP1 transport to the iRBC surface will enable new approaches in fighting this devastating pathogen.

Acknowledgements

We would like to thank the following colleagues for sharing antibodies: Brian Cooke (α-ATS), Claudia Daubenberger (α-GAPDH). Jan Warncke kindly provided the PF3D7_0402000-GFP and PF3D7_0801000-GFP transfection constructs. We thank Henning Stahlberg and his team at the C-CINA, Biozentrum, University of Basel, for the access to the electron microscopy facility and the Image Core Facility, Biozentrum, University of Basel, for the access and support for confocal microscopy.

References

AKINYI, S., HANSSEN, E., MEYER, E. V., JIANG, J., KORIR, C. C., SINGH, B., LAPP, S., BARNWELL, J. W., TILLEY, L. & GALINSKI, M. R. 2012. A 95 kDa protein of Plasmodium vivax and P. cynomolgi visualized by three-dimensional tomography in the caveola-vesicle complexes (Schuffner's dots) of infected erythrocytes is a member of the PHIST family. *Mol Microbiol,* 84**,** 816-31.

BIRNBAUM, J., FLEMMING, S., REICHARD, N., SOARES, A. B., MESEN-RAMIREZ, P., JONSCHER, E., BERGMANN, B. & SPIELMANN, T. 2017. A genetic system to study Plasmodium falciparum protein function. *Nat Methods,* 14**,** 450-456.

BLUHM, A., CASAS-VILA, N., SCHEIBE, M. & BUTTER, F. 2016. Reader interactome of epigenetic histone marks in birds. *Proteomics,* 16**,** 427-36.

CHARNAUD, S. C., DIXON, M. W. A., NIE, C. Q., CHAPPELL, L., SANDERS, P. R., NEBL, T., HANSSEN, E., BERRIMAN, M., CHAN, J. A., BLANCH, A. J., BEESON, J. G., RAYNER, J. C., PRZYBORSKI, J. M., TILLEY, L., CRABB, B. S. & GILSON, P. R. 2017. The exported chaperone Hsp70-x supports virulence functions for Plasmodium falciparum blood stage parasites. *PLoS One,* 12**,** e0181656.

COOKE, B. M., BUCKINGHAM, D. W., GLENISTER, F. K., FERNANDEZ, K. M., BANNISTER, L. H., MARTI, M., MOHANDAS, N. & COPPEL, R. L. 2006. A Maurer's cleft-associated protein is essential for expression of the major malaria virulence antigen on the surface of infected red blood cells. *J Cell Biol,* 172**,** 899-908.

CYRKLAFF, M., SANCHEZ, C. P., KILIAN, N., BISSEYE, C., SIMPORE, J., FRISCHKNECHT, F. & LANZER, M. 2011. Hemoglobins S and C interfere with actin remodeling in Plasmodium falciparum-infected erythrocytes. *Science,* 334**,** 1283-6.

DAHLBACK, M., LAVSTSEN, T., SALANTI, A., HVIID, L., ARNOT, D. E., THEANDER, T. G. & NIELSEN, M. A. 2007. Changes in var gene mRNA levels during erythrocytic development in two phenotypically distinct Plasmodium falciparum parasites. *Malar J,* 6**,** 78.

DEPLAINE, G., SAFEUKUI, I., JEDDI, F., LACOSTE, F., BROUSSE, V., PERROT, S., BILIGUI, S., GUILLOTTE, M., GUITTON, C., DOKMAK, S., AUSSILHOU, B., SAUVANET, A., CAZALS HATEM, D., PAYE, F., THELLIER, M., MAZIER, D., MILON, G., MOHANDAS, N., MERCEREAU-PUIJALON, O., DAVID, P. H. & BUFFET, P. A. 2011. The sensing of poorly deformable red blood cells by the human spleen can be mimicked in vitro. *Blood,* 117**,** e88-95.

DIETZ, O., RUSCH, S., BRAND, F., MUNDWILER-PACHLATKO, E., GAIDA, A., VOSS, T. & BECK, H. P. 2014. Characterization of the small exported Plasmodium falciparum membrane protein SEMP1. *PLoS One,* 9**,** e103272.

DIXON, M. W., KENNY, S., MCMILLAN, P. J., HANSSEN, E., TRENHOLME, K. R., GARDINER, D. L. & TILLEY, L. 2011. Genetic ablation of a Maurer's cleft protein prevents assembly of the Plasmodium falciparum virulence complex. *Mol Microbiol,* 81**,** 982-93.

DONNELLY, M. L., LUKE, G., MEHROTRA, A., LI, X., HUGHES, L. E., GANI, D. & RYAN, M. D. 2001. Analysis of the aphthovirus 2A/2B polyprotein 'cleavage' mechanism indicates not a proteolytic reaction, but a novel translational effect: a putative ribosomal 'skip'. *J Gen Virol,* 82**,** 1013-25.

GHORBAL, M., GORMAN, M., MACPHERSON, C. R., MARTINS, R. M., SCHERF, A. & LOPEZ-RUBIO, J. J. 2014. Genome editing in the human malaria parasite Plasmodium falciparum using the CRISPR-Cas9 system. *Nat Biotechnol,* 32**,** 819-21.

HANSSEN, E., SOUGRAT, R., FRANKLAND, S., DEED, S., KLONIS, N., LIPPINCOTT-SCHWARTZ, J. & TILLEY, L. 2008. Electron tomography of the Maurer's cleft organelles of Plasmodium falciparum-infected erythrocytes reveals novel structural features. *Mol Microbiol,* 67**,** 703-18.

HEIBER, A., KRUSE, F., PICK, C., GRURING, C., FLEMMING, S., OBERLI, A., SCHOELER, H., RETZLAFF, S., MESEN-RAMIREZ, P., HISS, J. A., KADEKOPPALA, M., HECHT, L., HOLDER, A. A., GILBERGER, T. W. & SPIELMANN, T. 2013. Identification of new PNEPs indicates a substantial non-PEXEL exportome and underpins common features in Plasmodium falciparum protein export. *PLoS Pathog,* 9**,** e1003546.

HILLER, N. L., BHATTACHARJEE, S., VAN OOIJ, C., LIOLIOS, K., HARRISON, T., LOPEZ-ESTRANO, C. & HALDAR, K. 2004. A host-targeting signal in virulence proteins reveals a secretome in malarial infection. *Science,* 306**,** 1934-7.

HVIID, L. & JENSEN, A. T. 2015. PfEMP1 - A Parasite Protein Family of Key Importance in Plasmodium falciparum Malaria Immunity and Pathogenesis. *Adv Parasitol,* 88**,** 51-84.

KRIEK, N., TILLEY, L., HORROCKS, P., PINCHES, R., ELFORD, B. C., FERGUSON, D. J., LINGELBACH, K. & NEWBOLD, C. I. 2003. Characterization of the pathway for transport of the cytoadherence-mediating protein, PfEMP1, to the host cell surface in malaria parasite-infected erythrocytes. *Mol Microbiol,* 50**,** 1215-27.

KROGH, A., LARSSON, B., VON HEIJNE, G. & SONNHAMMER, E. L. 2001. Predicting transmembrane protein topology with a hidden Markov model: application to complete genomes. *J Mol Biol,* 305**,** 567-80.

LABUN, K., MONTAGUE, T. G., GAGNON, J. A., THYME, S. B. & VALEN, E. 2016. CHOPCHOP v2: a web tool for the next generation of CRISPR genome engineering. *Nucleic Acids Res,* 44**,** W272-6.

LAVAZEC, C., DEPLAINE, G., SAFEUKUI, I., PERROT, S., MILON, G., MERCEREAU-PUIJALON, O., DAVID, P. H. & BUFFET, P. 2013. Microsphiltration: a microsphere matrix to explore erythrocyte deformability. *Methods Mol Biol,* 923**,** 291-7.

MAIER, A. G., RUG, M., O'NEILL, M. T., BROWN, M., CHAKRAVORTY, S., SZESTAK, T., CHESSON, J., WU, Y., HUGHES, K., COPPEL, R. L., NEWBOLD, C., BEESON, J. G., CRAIG, A., CRABB, B. S. & COWMAN, A. F. 2008. Exported proteins required for virulence and rigidity of Plasmodium falciparum-infected human erythrocytes. *Cell,* 134**,** 48-61.

MARTI, M., GOOD, R. T., RUG, M., KNUEPFER, E. & COWMAN, A. F. 2004. Targeting malaria virulence and remodeling proteins to the host erythrocyte. *Science,* 306**,** 1930-3.

MAYER, C., SLATER, L., ERAT, M. C., KONRAT, R. & VAKONAKIS, I. 2012. Structural analysis of the Plasmodium falciparum erythrocyte membrane protein 1 (PfEMP1) intracellular domain reveals a conserved interaction epitope. *J Biol Chem,* 287**,** 7182-9.

MCHUGH, E., BATINOVIC, S., HANSSEN, E., MCMILLAN, P. J., KENNY, S., GRIFFIN, M. D., CRAWFORD, S., TRENHOLME, K. R., GARDINER, D. L., DIXON, M. W. & TILLEY, L. 2015. A repeat sequence domain of the ring-exported protein-1 of Plasmodium falciparum controls export machinery architecture and virulence protein trafficking. *Mol Microbiol,* 98**,** 1101-14.

MOLL, K., KANEKO, A., SCHERF, A. & WAHLGREN, M. 2013. Methods in Malaria Research (MR4/ATCC) 6th Edition.

MONTAGUE, T. G., CRUZ, J. M., GAGNON, J. A., CHURCH, G. M. & VALEN, E. 2014. CHOPCHOP: a CRISPR/Cas9 and TALEN web tool for genome editing. *Nucleic Acids Res,* 42**,** W401-7.

MUNDWILER-PACHLATKO, E. & BECK, H. P. 2013. Maurer's clefts, the enigma of Plasmodium falciparum. *Proc Natl Acad Sci U S A,* 110**,** 19987-94.

OBERLI, A., SLATER, L. M., CUTTS, E., BRAND, F., MUNDWILER-PACHLATKO, E., RUSCH, S., MASIK, M. F., ERAT, M. C., BECK, H. P. & VAKONAKIS, I. 2014. A Plasmodium falciparum PHIST protein binds the virulence factor PfEMP1 and comigrates to knobs on the host cell surface. *Faseb j,* 28**,** 4420-33.

OBERLI, A., ZURBRUGG, L., RUSCH, S., BRAND, F., BUTLER, M. E., DAY, J. L., CUTTS, E. E., LAVSTSEN, T., VAKONAKIS, I. & BECK, H. P. 2016. Plasmodium falciparum Plasmodium helical interspersed subtelomeric proteins contribute to cytoadherence and anchor P. falciparum erythrocyte membrane protein 1 to the host cell cytoskeleton. *Cell Microbiol,* 18**,** 1415-28.

PACHLATKO, E., RUSCH, S., MULLER, A., HEMPHILL, A., TILLEY, L., HANSSEN, E. & BECK, H. P. 2010. MAHRP2, an exported protein of Plasmodium falciparum, is an essential component of Maurer's cleft tethers. *Mol Microbiol,* 77**,** 1136-52.

PARISH, L. A., MAI, D. W., JONES, M. L., KITSON, E. L. & RAYNER, J. C. 2013. A member of the Plasmodium falciparum PHIST family binds to the erythrocyte cytoskeleton component band 4.1. *Malar J,* 12**,** 160.

PONTI, A., GULATI, A., BÄCKER, V. & SCHWARB, P. 2007. Huygens Remote Manager: a Web Interface for High-Volume Batch Deconvolution. *Imaging & Microscopy* 2**,** 57-58.

RAPPSILBER, J., MANN, M. & ISHIHAMA, Y. 2007. Protocol for micro-purification, enrichment, pre-fractionation and storage of peptides for proteomics using StageTips. *Nat Protoc,* 2**,** 1896-906.

ROBINSON, B. A., WELCH, T. L. & SMITH, J. D. 2003. Widespread functional specialization of Plasmodium falciparum erythrocyte membrane protein 1 family members to bind CD36 analysed across a parasite genome. *Mol Microbiol,* 47**,** 1265-78.

SCHINDELIN, J., ARGANDA-CARRERAS, I., FRISE, E., KAYNIG, V., LONGAIR, M., PIETZSCH, T., PREIBISCH, S., RUEDEN, C., SAALFELD, S., SCHMID, B., TINEVEZ, J. Y., WHITE, D. J., HARTENSTEIN, V., ELICEIRI, K., TOMANCAK, P. & CARDONA, A. 2012. Fiji: an open-source platform for biological-image analysis. *Nat Methods,* 9**,** 676-82.

SCHULZE, J., KWIATKOWSKI, M., BORNER, J., SCHLUTER, H., BRUCHHAUS, I., BURMESTER, T., SPIELMANN, T. & PICK, C. 2015. The Plasmodium falciparum exportome contains non-canonical PEXEL/HT proteins. *Mol Microbiol,* 97**,** 301-14.

SONNHAMMER, E. L., VON HEIJNE, G. & KROGH, A. 1998. A hidden Markov model for predicting transmembrane helices in protein sequences. *Proc Int Conf Intell Syst Mol Biol,* 6**,** 175-82.

SPIELMANN, T. & GILBERGER, T. W. 2010. Protein export in malaria parasites: do multiple export motifs add up to multiple export pathways? *Trends Parasitol,* 26**,** 6-10.

SPIELMANN, T. & GILBERGER, T. W. 2015. Critical Steps in Protein Export of Plasmodium falciparum Blood Stages. *Trends Parasitol,* 31**,** 514-25.

SPYCHER, C., RUG, M., PACHLATKO, E., HANSSEN, E., FERGUSON, D., COWMAN, A. F., TILLEY, L. & BECK, H. P. 2008. The Maurer's cleft protein MAHRP1 is essential for trafficking of PfEMP1 to the surface of Plasmodium falciparum-infected erythrocytes. *Mol Microbiol,* 68**,** 1300-14.

SZYMCZAK, A. L., WORKMAN, C. J., WANG, Y., VIGNALI, K. M., DILIOGLOU, S., VANIN, E. F. & VIGNALI, D. A. 2004. Correction of multi-gene deficiency in vivo using a single 'self-cleaving' 2A peptide-based retroviral vector. *Nat Biotechnol,* 22**,** 589-94.

TOKUYASU, K. T. 1973. A technique for ultracryotomy of cell suspensions and tissues. *J Cell Biol,* 57**,** 551-65.

VAN SCHRAVENDIJK, M. R., PASLOSKE, B. L., BARUCH, D. I., HANDUNNETTI, S. M. & HOWARD, R. J. 1993. Immunochemical characterization and differentiation of two approximately 300-kD erythrocyte membrane-associated proteins of Plasmodium falciparum, PfEMP1 and PfEMP3. *Am J Trop Med Hyg,* 49**,** 552-65.

WARNCKE, J. D., VAKONAKIS, I. & BECK, H. P. 2016. Plasmodium Helical Interspersed Subtelomeric (PHIST) Proteins, at the Center of Host Cell Remodeling. *Microbiol Mol Biol Rev,* 80**,** 905-27.

WATERKEYN, J. G., WICKHAM, M. E., DAVERN, K. M., COOKE, B. M., COPPEL, R. L., REEDER, J. C., CULVENOR, J. G., WALLER, R. F. & COWMAN, A. F. 2000. Targeted mutagenesis of Plasmodium falciparum erythrocyte membrane protein 3 (PfEMP3) disrupts cytoadherence of malaria-infected red blood cells. *Embo j,* 19**,** 2813-23.

WHO 2017. World malaria report 2017.

WICKERT, H., WISSING, F., ANDREWS, K. T., STICH, A., KROHNE, G. & LANZER, M. 2003. Evidence for trafficking of PfEMP1 to the surface of P. falciparum-infected erythrocytes via a complex membrane network. *Eur J Cell Biol,* 82**,** 271-84.

Table 1

Protein ID	Gene product	# peptides	Δ neg. Ctrl/ 008HA
PF3D7_0501200	PIESP2	12	-6.773990856
PF3D7_0501000	unknown function	7	-5.787175304
PF3D7_1370300	MAHRP1	6	-5.285842133
PF3D7_0831700	Hsp70x	18	-5.220433306
PF3D7_1002100	PTP5	2	-5.202451978
PF3D7_0501300	SBP1	3	-4.978448644
PF3D7_0801000	PHISTc	16	-4.912530452
PF3D7_0402000	PHISTa	2	-4.455466261
PF3D7_1353200	MAHRP2	2	-4.435114524
PF3D7_1201000	PHISTb	6	-4.288180089
PF3D7_0935900	REX1	4	-3.935197171
PF3D7_0500800	MESA	26	-3.422706071
PF3D7_0936800 (PFI1780w)	PHISTc	7	-3.342773302
PF3D7_0301700	unknown function	4	-3.043488065
PF3D7_0702500	*008*	*6*	*-2.902204979*
PF3D7_0532400 (PFE1605w)	LyMP	6	-2.88787158
PF3D7_1302000	PTP6	3	-2.817701929
PF3D7_0731300	PHISTb	6	-2.645594119
PF3D7_0424600	PHISTb	5	-2.466183066

Δ008HA/neg. Ctrl values describe how enriched a protein was found in the sample compared to the negative control

Table 2

Protein name	localization	# peptides	Δ neg. Ctrl/ 008HA
55 kDa erythrocyte membrane protein	cytoskeleton	13	-5.302959798
Spectrin alpha chain, erythrocytic 1	cytoskeleton	86	-4.612724604
Spectrin beta chain, erythrocytic	cytoskeleton	75	-4.604611571
Ankyrin-1	cytoskeleton	46	-4.424931921
Protein 4.1	cytoskeleton	14	-4.361392497
Erythrocyte band 7 integral membrane protein	membrane	9	-4.353384156
Erythrocyte membrane protein band 4.2	cytoskeleton	12	-3.699836611
Alpha-adducin	cytoskeleton	7	-2.336905069
Band 3 anion transport protein	membrane	26	-2.303382461
Solute carrier family 2, facilitated glucose transporter member 1	membrane	5	-2.257730862
Blood group Rh(CE) and Rh(D) polypeptide	membrane	2	-2.086344643

Δ008HA/neg. Ctrl values describe how enriched a protein was found in the sample compared to the negative control

Supplementary Table 1

008-HA 5HR fw	5'TATCGTGGAACCGTATTCG
008-HA 5HR rv	5'TACATGAGCTTCATTAGTGTTTAAAC
008-HA 3HR fw	5'TAGAAAGTTAATATTCTGTTGTA
008-HA 3HR rv	5'GTATCGAACTGTGATTAACAAC
008-HA gRNA	5'GAAGCTCATGTATAAGAGAG
008 KO 5HR fw	5'TTGGAACTTGTCCTGGAAATAGC
008 KO 5HR rv	5'TCTTCATCGAATACGGTTCCAC
008 KO 3HR fw	5'GGGTGAAGGAACTCATAGTGCAG
008 KO 3HR rv	5'ACGCTACTTTCGGTTGTACTTGAG
008 KO gRNA	5'GGGCTTTGGTCTTTTTATGG

Supplementary Table 2

Protein.IDs	difference_cont_bait
PF3D7_0501200	-6.773990856
PF3D7_0501000	-5.787175304
Q00013;B4DZV5;G3XAI1;C9J9J4;A8MTH1;C9JB34;A6NFY0;F8WC84;F8WDV6	-5.302959798
PF3D7_1370300	-5.285842133
PF3D7_0731600;PF3D7_0215300	-5.249766821
PF3D7_0831700;H0YIE7;F5H3L8;B7Z4V2;P48741;P38646	-5.220433306
PF3D7_1002100	-5.202451978
PF3D7_0501300	-4.978448644
PF3D7_0801000	-4.912530452
P02549-2;P02549	-4.612724604
P11277;P11277-2;Q59FP5;P11277-3;E7EV95;H0YJE6;F8W6C1;Q01082-3;Q01082-2;Q01082;A4QPE4;C9JRP8;E9PDB1;Q9H254-2;Q9H254-4;Q9H254	-4.604611571
PF3D7_0402000	-4.455466261
PF3D7_1353200	-4.435114524
E7EVE3;P16157-11;P16157-9;P16157-6;P16157-7;P16157-4;P16157-13;P16157-10;P16157-15;P16157-8;P16157-5;P16157-16;P16157-3;P16157;P16157-21;P16157-12;P16157-14;E7EVX7;P16157-2;H0YBS0;H0YAY8;H0Y3N0;E9PE32;Q12955;D6RCB2;B7Z651;D6RHE1;E9PHW9;F8WEF9;Q01484-5;Q01484-2;Q01484;Q01484-4;D6RHY3;F5H4S1;E7EMJ1;H0YH59	-4.424931921
P11171-4;P11171-3;P11171-2;P11171;C9JTS2;E9PEW9;P11171-7;E9PEX0;P11171-6;P11171-5	-4.361392497
B4E2V5;P27105;E7EQ93;B1AM77	-4.353384156
PF3D7_1201000	-4.288180089
PF3D7_0930300	-4.267905071
PF3D7_1129100	-4.078256003
PF3D7_1222300	-4.058759451
PF3D7_1116800	-4.055115297
PF3D7_0626800	-4.019720588
PF3D7_0935900	-3.935197171
PF3D7_1108600	-3.829733706
Q4KKX0;P16452;P16452-2;F5H563	-3.699836611
PF3D7_1105600	-3.540294422
PF3D7_1420700;E7ENN3;E9PEL9;Q8NF91-7;Q8NF91-4;Q8NF91;E7EQI5	-3.494556582
PF3D7_1311800	-3.471377727
PF3D7_0500800	-3.422706071
PF3D7_1468700	-3.402925323

PF3D7_0936800	-3.342773302
PF3D7_1135400	-3.291047966
PF3D7_0608800	-3.27958905
PF3D7_1134000	-3.25433546
PF3D7_0929400	-3.233700196
PF3D7_1471100	-3.210423132
PF3D7_0905400	-3.183660648
PF3D7_1253400;PF3D7_1372400	-3.138109395
PF3D7_0301700	-3.043488065
PF3D7_0917900	-3.040921244
PF3D7_0827900	-3.01272185
PF3D7_1104400	-3.009933525
PF3D7_0925900	-2.939527142
PF3D7_0207600	-2.909279067
PF3D7_0702500	-2.902204979
PF3D7_0818900;B4DEF7	-2.888332904
PF3D7_0532400	-2.88787158
PF3D7_1016400;PF3D7_0500900	-2.867775879
PF3D7_0220000	-2.865305318
PF3D7_1324900	-2.851009613
PF3D7_1334500	-2.820359098
PF3D7_1302000	-2.817701929
P30043	-2.766800674
PF3D7_1001600	-2.753000688
PF3D7_1012400	-2.725844681
PF3D7_1343000	-2.684417401
PF3D7_0731300	-2.645594119
PF3D7_1149000	-2.616642863
PF3D7_0708400	-2.602773267
PF3D7_0922200	-2.558195623
PF3D7_1117700;B4DV51	-2.551456659
PF3D7_0826700	-2.513981891
PF3D7_0424600	-2.466183066
PF3D7_0513300	-2.454389159
PF3D7_1454400	-2.390940866
PF3D7_1462800	-2.360910041
E7EV99;E7ENY0;P35611-2;A2A3N8;P35611;P35611-3;Q86XM2;Q96D30;H0Y9H2;H0YFD8;D6RF25	-2.336905069
P02730	-2.303382461
PF3D7_0922500	-2.295772376
F8WC15;P11166;C9JIM8;G8JLF4	-2.257730862
PF3D7_1344200	-2.236572502
PF3D7_1016300;PF3D7_0937000	-2.222297833

PF3D7_1338300	-2.213690167
PF3D7_0708800	-2.203540261
PF3D7_0627500	-2.169432048
F5H3A6;F5H423;P84077;P61204;F5H0C7;B7ZB63;C9J1Z8;P84085	-2.167934667
PF3D7_0525100	-2.147509739
PF3D7_0730800.2;PF3D7_0730800.1	-2.142732776
PF3D7_1120100	-2.136314494
PF3D7_1436300	-2.115351048
E7EQ47;E7EWZ5;F5GXQ4;Q5VSJ9;P18577-9;P18577-4;P18577-10;P18577-11;Q02161;P18577;F5GXS3	-2.086344643
PF3D7_1451100	-2.083355215
Q13228-2;Q13228;B4E1F3;A6PVX1;A6PVW9;H0Y532;F2Z2W8;F8WCR4	-2.07990333
P11142;E7ET08;E9PKE3;P11142-2;E9PN89;E9PNE6;A8K7Q2;E9PQQ4;E9PQK7;E9PK54;E9PLF4;P54652;E9PI65;E9PN25;E9PPY6;B3KUS2;E9PM13;E9PS65	-2.059212733
PF3D7_0619400	-2.023129184
PF3D7_1408100	-2.020645974
P04040	-2.017058069
P68871;F8W6P5;A8MUF7;E9PBW4;E9PBX7;P69892;P69891;P02100	-2.009647969
PF3D7_1033200	-2.004682032
P69905;G3V1N2;P02008	-2.00165627
PF3D7_1407900	-1.982823521
PF3D7_1408600;Q5JR95;P62241	-1.921689126
P00915;E5RHP7;E5RH81;E5RFE7;E5RIF9;E5RG43;H0YBE2;E5RGU8;E5RFL2;E5RG81;E5RJI8;E5RII2;E5RJF6;E5RHS7	-1.919765098
PF3D7_1129000	-1.699495735
B7Z5J4;B7Z576;Q9UI42;F5H0B9;C9J6N7	1.992897592
P22531;Q96RM1;P35326;P35325;P22532;Q9BYE4;F5H1V2	2.071557368
PF3D7_0320900	2.148427061
B4DEB1;Q71DI3;Q16695;P84243;P68431;Q5TEC6;Q6NXT2	3.2467262

Figure legends

Figure 1: **PF3D7_0702500-3xHA is expressed throughout the intraerythrocytic life cycle.** A: Schematic representation of endogenous tagging strategy using a combined CRISPR/Cas9-SLI approach. 5' and 3' homology regions (HRs) flank an integration cassette consisting of the tag (e.g. 3xHA), a 2A skip peptide, a blasticidine (bsd) resistance including a terminator. On the same plasmid, the Cas9 and the gRNA are included. The black arrow indicates the gRNA recognition site close to the 3' terminus of the gene of interest. Not drawn to scale. B: Western blot analysis of 3D7 and PF3D7_0702500-3xHA saponin lysates. The membranes were probed with HA antibody and GAPDH antibody as loading control. C: Time course immunofluorescence assay. Scale bar 2µm. D: Time course Western blot analysis of PF3D7_0702500-3xHA expressing parasites. The membrane was probed with HA antibody and GAPDH antibody as loading control. E: Co-labelling immunofluorescence assay of PF3D7_0702500-3xHA with MAHRP1, and MAHRP2 respectively. Scale bar 2µm. F: Western blot analysis from PF3D7_0702500-3xHA solubility assay. Membranes were probed with HA, GAPDH, PFE1605w, and MAHRP1 antibodies. Lanes represent hypotonic lysis fraction, Na_2CO_3 fraction, Triton X-100-soluble fraction, and the remaining insoluble fraction.

Figure 2: **PF3D7_0702500-3xHA localizes to electron-dense structures.** Immunoelectron microscopy of iRBCs expressing PF3D7_0702500-3xHA. Small 5nm gold conjugated Protein A indicating α-HA antibody (arrow), large 10nm gold conjugated Protein A decorating α-MAHRP2 antibody (triangle). Knobs (K), Maurer's clefts (MC), and Maurer's clefts tethers (T) are indicated. Scale bar 500nm (A), 200nm (B).

Figure 3: **Colocalization of PF3D7_0702500-3xHA with PF3D7_0801000-GFP, PF3D7_0402000-GFP, and PFI1780w (PF3D7_0936800-GFP).** A: Confocal microscopy pictures of PF3D7_0801000-GFP, PF3D7_0402000-GFP, and PFI1780w (PF3D7_0936800-GFP) colocalization analysis with PF3D7_0702500-3xHA. Scale bar 2µm. B: Table of Pearson's coefficient, and Maenders' coefficients. M1 indicates the fraction of PF3D7_0801000-GFP/PF3D7_0402000-GFP/PFI1780w (PF3D7_0936800-GFP) overlapping with PF3D7_0702500-3xHA, M2 indicates the fraction of PF3D7_0702500-3xHA overlapping with PF3D7_0801000-GFP/PF3D7_0402000-GFP/PFI1780w (PF3D7_0936800-GFP).

Figure 4: **Phenotypical analysis of PF3D7_0702500 KO.** A: A PF3D7_0702500 KO cell line was generated by CRISP/Cas9 replacing the gene of interest with a *hDHFR* resistance cassette. Correct integration of the *hDHFR* cassette was assessed by PCR spanning the integration sites. Expected PCR product sizes are for 3D7 no product, for PF3D7_0702500 KO 642bp for 5'HR, 883bp for 3'HR. B: Growth assay of 3D7 wild type and PF3D7_0702500 KO iRBCs. C: Deformability assay of tightly synchronized 3D7 wild type and PF3D7_0702500 KO ring and trophozoite iRBCs. Shown are retention rates and standard deviations of means of 6 replicates.

Figure 5: **PF3D7_0702500 KO shows impaired virulence.** A: Semi-static CD36 binding assay. Shown is the mean of relative binding of trophozoite 3D7 and PF3D7_0702500 KO iRBCs to CD36 of 3 biological replicates. Error bar shows standard deviation. B: Pie charts show the PfEMP1 transcript distribution in the 3D7 wildtype and PF3D7_0702500 KO cell line. Each color represents a different PfEMP1 variant. C: Western blot analysis of trypsin cleavage assay of 3D7 wildtype and PF3D7_0702500 KO iRBCs. –T is negative control, +T is sample with added trypsin. The membrane was probed with ATS-antibody. D: PfEMP1 immunofluorescence assay (ATS antibody) of 3D7 and PF3D7_0702500 KO iRBCs. Scale bar 2µm. E: Immunofluorescence assay of PF3D7_0702500-3xHA in wildtype and MAHRP1 KO background. Scale bar 2µm.

Supplementary Figure 1: **Immunoelectron microscopy of PF3D7_0702500-3xHA with PF3D7_0402000-GFP and PF3D7_0801000-GFP.** A: PF3D702500-3xHA/ PF3D7_0402000-GFP expressing cell line with small 5nm gold conjugated Protein A indicating α-GFP antibody (triangle), large 10nm gold conjugated Protein A decorating α-HA antibody. B: PF3D702500-3xHA/PF3D7_0801000-GFP expressing cells with small 5nm gold conjugated Protein A indicating α-GFP antibody (triangle), large 10nm gold conjugated Protein A decorating α-HA antibody. Scalebar 1µm.

Figure 1

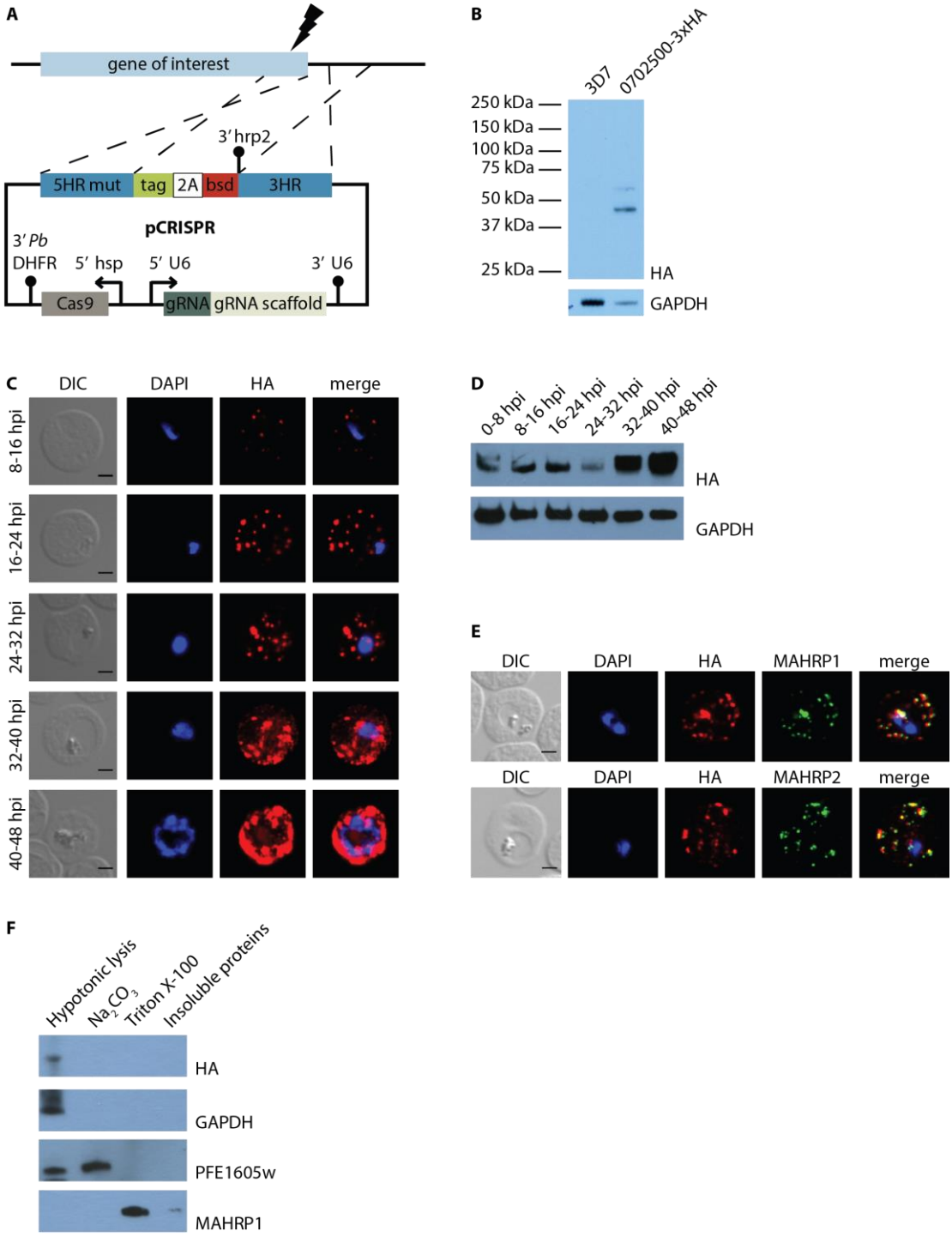
A
gene of interest
3′ hrp2
5HR mut
tag
2A
bsd
3HR
pCRISPR
3′ Pb DHFR
5′ hsp
5′ U6
3′ U6
Cas9
gRNA
gRNA scaffold
B
3D7
0702500-3xHA
250 kDa
150 kDa
100 kDa
75 kDa
50 kDa
37 kDa
25 kDa
HA
GAPDH
C
DIC
DAPI
HA
merge
8-16 hpi
16-24 hpi
24-32 hpi
32-40 hpi
40-48 hpi
D
0-8 hpi
8-16 hpi
16-24 hpi
24-32 hpi
32-40 hpi
40-48 hpi
HA
GAPDH
E
DIC
DAPI
HA
MAHRP1
merge
DIC
DAPI
HA
MAHRP2
merge
F
Hypotonic lysis
Na2CO3
Triton X-100
Insoluble proteins
HA
GAPDH
PFE1605w
MAHRP1

Figure 2

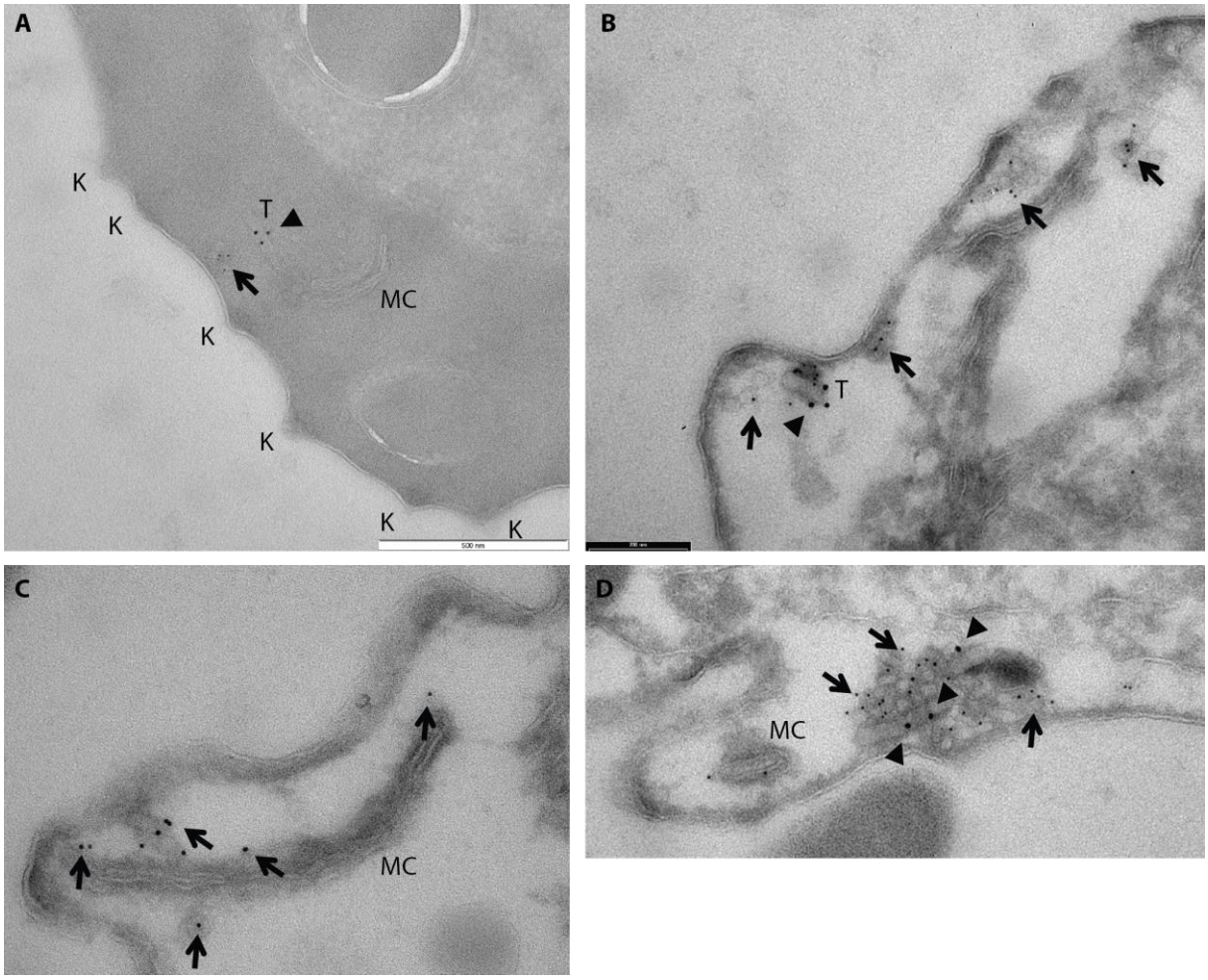

Figure 3

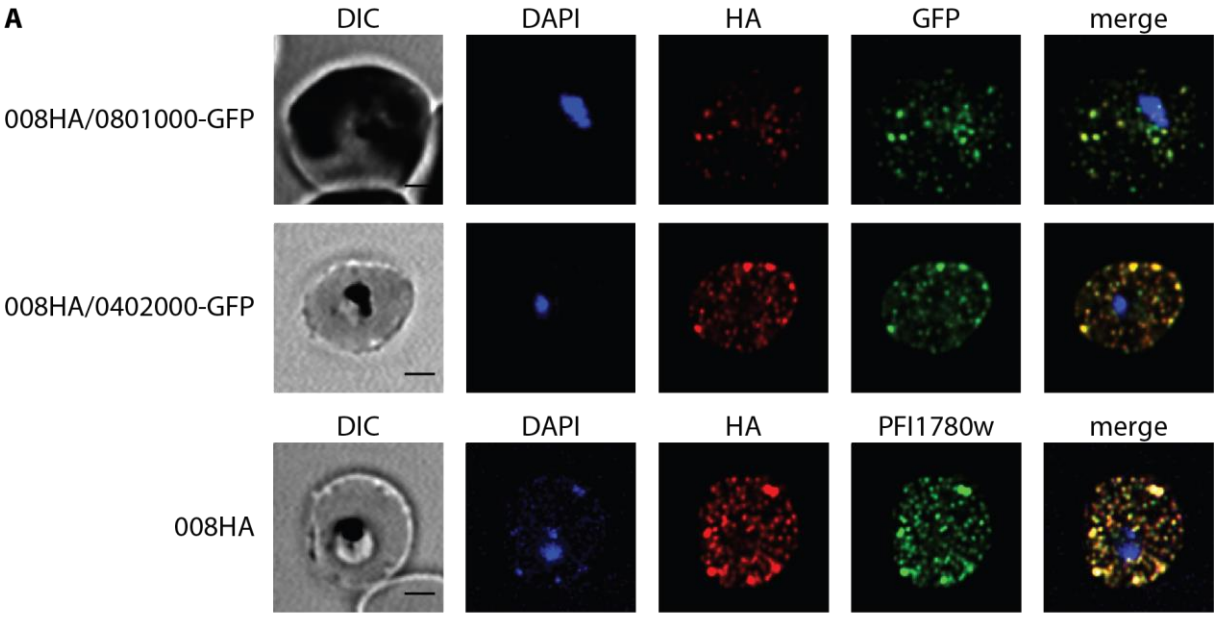

B

	Pearson's coefficient	Threshold Maenders ' coefficient M1	Threshold Maenders ' coefficient M2
PF3D7_0801000	0.907	0.805	0.87
PF3D7_0402000	0.939	0.945	0.783
PFI1780w	0.949	0.940	0.884

Figure 4

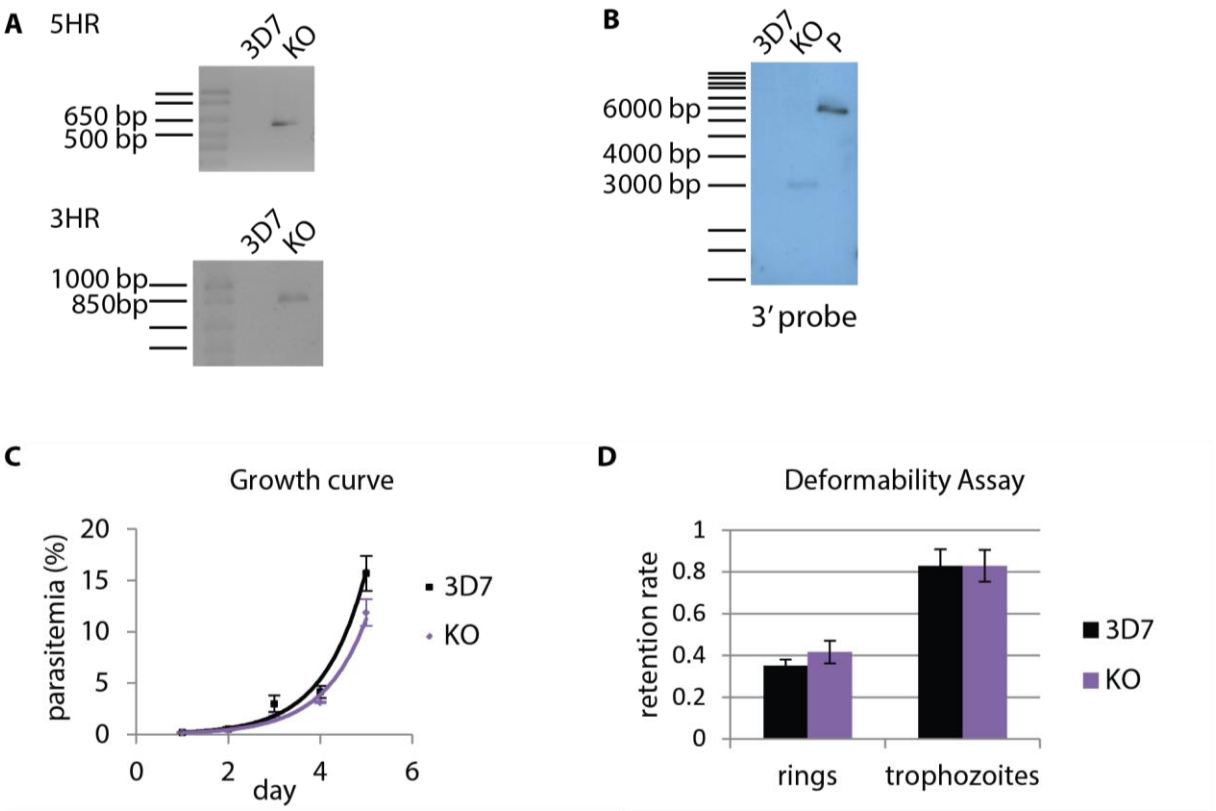
A
5HR
3D7
KO
650 bp
500 bp
3HR
3D7
KO
1000 bp
850bp
B
3D7
KO
P
6000 bp
4000 bp
3000 bp
3′ probe
C
Growth curve
parasitemia (%)
20
15
10
5
0
0
2
4
6
day
3D7
KO
D
Deformability Assay
retention rate
1
0.8
0.6
0.4
0.2
0
rings
trophozoites
3D7
KO

Figure 5

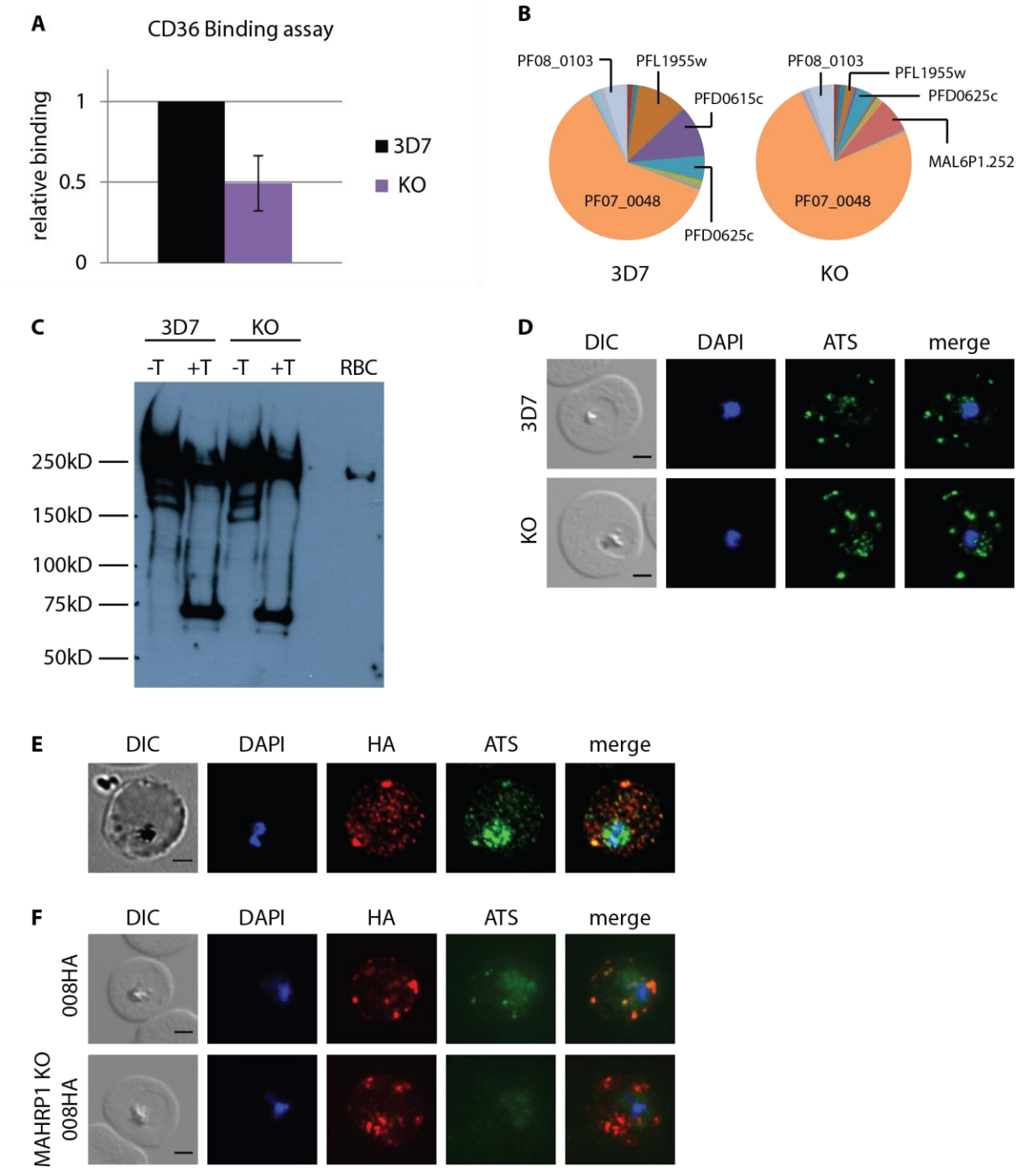
A
CD36 Binding assay
relative binding
1
0.5
0
3D7
KO
B
PF08_0103
PFL1955w
PFD0615c
PF07_0048
PFD0625c
3D7
PF08_0103
PFL1955w
PFD0625c
MAL6P1.252
PF07_0048
KO
C
3D7
KO
-T
+T
-T
+T
RBC
250kD
150kD
100kD
75kD
50kD
D
DIC
DAPI
ATS
merge
3D7
KO
E
DIC
DAPI
HA
ATS
merge
F
DIC
DAPI
HA
ATS
merge
008HA
MAHRP1 KO
008HA

Supplementary Figure 1

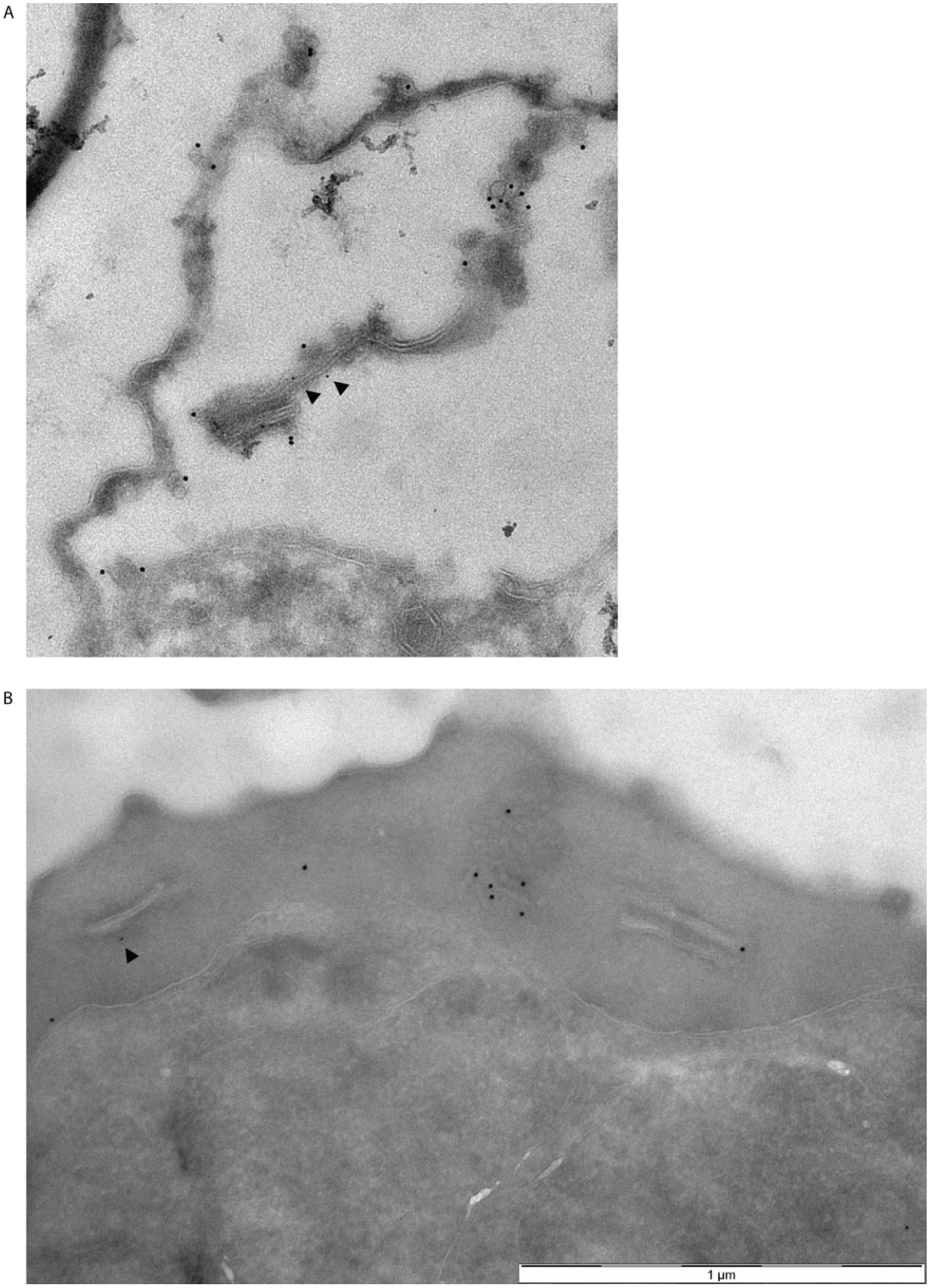

Chapter 3

Functional characterization of the *Plasmodium falciparum* mature erythrocyte surface antigen (MESA)

Functional characterization of the Plasmodium falciparum mature erythrocyte surface antigen (MESA)

Introduction

Host cell cytoskeleton remodeling by the parasite *P. falciparum* contributes significantly to its virulence and persistence in the human red blood cell. A large number of exported parasite proteins interact with the host cytoskeleton. MESA (PfEMP2, PF3D7_0500800) was one of the first described parasite proteins to associate to the inside of the iRBC membrane (Coppel et al., 1986, Howard et al., 1988). It contains a PEXEL motif, which is functional in combination with an embedded signal peptide to direct the protein to the RBC cytosol (Black et al., 2008). MESA is expressed in trophozoite and schizont stages of the asexual red blood cell cycle (Coppel et al., 1988).

The 168kDa protein has a 19-residue region near the N-terminus binding to the erythrocyte membrane skeletal protein band 4.1 (Lustigman et al., 1990, Bennett et al., 1997, Kun et al., 1999). This motif is also known as MEC motif (MESA erythrocyte cytoskeleton binding, Kilili and LaCount, 2011) and present in several other exported *P. falciparum* protein (e.g. some PHISTb family members), putatively targeting them to the erythrocyte cytoskeleton (Warncke et al., 2016).

In vitro studies with recombinant MESA and band 4.1 revealed competition between the human phosphoprotein p55 that regulates plasma membrane stability (Chishti, 1998), and MESA for band 4.1 interaction (Lustigman et al., 1990, Waller et al., 2003). Band 4.1 that interacts with spectrin and actin is crucial for the cytoskeleton deformability. Further, band 4.1 ensures mechanical stability of the RBC by connecting the cytoskeleton to the membrane via glycophorin C. Interestingly, MESA accumulates in the erythrocyte cytosol of band 4.1 deficient erythrocytes and the iRBCs show poor survival (Magowan et al., 1995). Unbound MESA thus seems detrimental or even toxic to the host erythrocyte. The relationship between band 4.1 and MESA could reflect a structural function of MESA in modulating the protein interactions in the host cytoskeleton in order to facilitate parasite survival (Waller et al., 2003).

Phosphorylation is a prevalent post-transcriptional modification of RBC cytoskeleton proteins to regulate mechanical properties of the RBC cytoskeleton. MESA is also a phosphoprotein, the phosphorylation sites have been predicted (Collins et al., 2014). It was found that the kinase responsible for MESA phosphorylation is probably shared with the band 4.1 phosphorylating kinase and is sensitive to casein kinase inhibitors (Magowan et al., 1998).

MESA was also discussed as a diagnostic marker as it was found in malaria patient serum by mass spectrometry analysis (Zainudin et al., 2015). Further, in a mass-spectrometry-based proteomic approach it was identified as overexpressed in samples from patients with cerebral malaria compared to uncomplicated malaria samples. This may indicate an association of MESA with the pathophysiology of cerebral malaria (Bertin et al., 2016).

We have identified MESA in a MAHRP2 co-immunoprecipitation experiment aiming at the identification of Maurer's clefts tether interacting proteins (unpublished). MESA is a well-known protein localizing to the erythrocyte cytoskeleton, but no specific function has been assigned to it yet. It has been hypothesized that MESA has a structural role in remodeling the host cell, thus putatively interfering with the iRBC deformability. Here, we endogenously GFP-tagged MESA in order to identify interaction partners of the protein by immunoprecipitation experiments. Further we generated a 5' MESA knock out (KO) parasite cell line for functional analysis of the protein. We assessed growth, deformability and cytoadherence properties of the knock out cell line but were not able to assign a function to the protein nor were we able to describe a distinct phenotype in the knock out cell line.

Methods

Cell culture and transfections

P. falciparum 3D7 was cultured and transfected as described (Moll et al., 2013). For positive selection of transfected parasites 10nM WR99210 (Jacobs Pharmaceuticals, Cologne, Germany), and 5mg/ml blasticidin (Sigma-Aldrich, Inc.) were used.

Plasmid constructs

The endogenous MESA-GFP tagged cell line was generated using a combined CRISPR-Cas9/SLI approach (Ghorbal et al., 2014, Birnbaum et al., 2017). Homology regions between 300-1000bp were designed, and a gRNA was chosen with the CHOPCHOP software (Labun et al., 2016, Montague et al., 2014). Mutations of the gRNA recognition sequence were introduced by gene synthesis (GenScript, USA) of the containing homology region in order to avoid recleavage of the successfully tagged endogenous gene. The homology regions and gRNA were PCR amplified using primers listed in Table 1 and cloned into pCRISPR_GFP2ABSD using the In-Fusion® HD Cloning Kit (Clontech® Laboratories, Inc.). pCRISPR_GFP2ABSD contains the Cas9, the gRNA within the gRNA scaffold, and the

integration cassette flanked by the 5' and 3' homology regions. The integration cassette consists of the GFP-tag and a *bsd* selection marker separated by a 2A skip peptide (Szymczak et al., 2004) and followed by a terminator. The selection marker lacks a promotor and can only be expressed after successful integration into the target locus. The skip peptide triggers a ribosomal skip mechanism and thus impairs normal peptide bond formation preventing the attachment of the selection marker to the target protein (Donnelly et al., 2001).
The single cross-over MESA KO cell line was generated with the pH plasmid including a 5' stretch of the MESA gene. The homology region was PCR amplified using the primers listed in Supplementary Table 1 and cloned with *EcoRI* and *BamHI* into the plasmid.

Western blot analysis

Parasite saponin lysates were run on 4-12% Bis/Tris precast gels (NuPAGE®, Life Technologies) according to the manufacturer's protocol. Protein transfer was performed with the iBlot 2.0 (Life Technologies). Subsequently, the membrane was blocked with 10% skimmed milk/TNT (100mM Tris, 150mM NaCl, 0.1% Tween) and probed with the first antibody in 3% skimmed milk/TNT at room temperature for 2h-O/N. After 6 washes for 5min with TNT the secondary antibody conjugated to HRP was incubated in the respective dilution in 3% skimmed milk/TNT for 2h at room temperature. After another 6 washes for 5min with TNT the signal was detected by Super Signal West Pico Chemiluminescent Substrate (Thermo Scientific) or LumiGlo Reserve Chemiluminescent Substrate (Seracare) according to the manufacturer's protocol. The antibodies used were: mouse α-GFP (Roche, 1:250), mouse α-GAPDH (1:20'000), goat α-mouse-HRP (Pierce, 1:5000).

Immunofluorescence Assay

Thin blood smears of parasite cultures were fixed in ice-cold 60% methanol/40% acetone for 2min. After air-drying of the smear, a small well was drawn with a hydrophobic pen and the respective area was blocked with 3% BSA/PBS for 1h at room temperature in a humidified chamber. Then, the cells were incubated with mouse α-GFP (Roche, 1:100), rabbit α-MESA (1:200), rabbit α-RESA (1:200), rabbit α-MAHRP2 (1:100), mouse α-PFI1780w (1:1000), rabbit α-PFE1605w (1:100), rabbit α-band 4.1 (Abcam, 1:100), and rabbit α-spectrin (Abcam, 1:100) in 3% BSA/PBS for minimum 2h at room temperature in a humidified chamber. After 3 washes with 3% BSA/PBS for 7min the secondary antibody (goat α-mouse Alexa488, goat

α-rabbit Alexa488, goat α-rabbit Alexa568, goat α-rat Alexa568; all Invitrogen, 1:200) was applied in the appropriate dilution in 3% BSA/PBS for minimum 1h at room temperature in a humidified chamber. After another 3 wash steps with 3% BSA/PBS for 7min each, a coverslip was mounted with 2µl VECTASHIELD® with DAPI (Vector Laboratories Inc.). For imaging a 63x oil-immersion lens (1.4 numerical aperture) on a Leica 5000 B microscope was used. The images were obtained by using the software Leica ApplicationSuite 4.4. and analyzed using Fiji (Schindelin et al., 2012).

Erythrocyte Cytoskeleton Imaging

First, coverslips were functionalized to prepare erythrocyte binding (Aebersold et al., 1986). To this end the coverslips were cleaned with Ethanol and ddH_2O and dried with compressed air. Then, the coverslips were immersed for 60sec in 2% 3-Aminopropyltriethoxysilane (Pierce)/dry acetone (Sigma) at room temperature. Subsequently, the coverslips were rinsed with acetone and air dried. 300µl fresh 1mM BS3 cross linker (Pierce)/PBS was placed on the surface of each silyated coverslip and incubated for 30min at room temperature. Then, the coverslips were washed 3 times with 300µl PBS. Next, 300µl 0.1mg/ml Erythroagglutinating phytohemoagglutinin (PHA-E, EY-Labs/Lubio) were applied on the silyated-BS3-coupled coverslip and incubated for 1-2h at room temperature in a humidified chamber. After rinsing the coverslips 3 times with PBS, they were incubated in 0.1M Glycine/PBS for 15min at room temperature. After another 3 washes with PBS, binding and shearing of erythrocytes was performed as published (Shi et al., 2013). In brief, 150µl of 4% hematocrit iRBCs/PBS were pipetted on the activated coverslip and allowed to adhere for 1-3h at 37°C in a humidified chamber. To shear and lyse the iRBCs a 10ml syringe with a 23G needle was used to flush the cells on the coverslip with 5P8-10 buffer (5mM Na_2HPO_4/NaH_2PO_4, 10mM NaCl, pH8) from a 20° angle 3 times. The coverslip was washed twice with ddH_2O before proceeding with an immunofluorescence assay.

Co-immunoprecipitation

150ml synchronized parasite culture was harvested by Percoll purification to enrich late stage parasites. Proteins were cross-linked with 1% formaldehyde in culture media for 30min on a rotator at 37°C. Cross-linking was stopped by adding glycine to a final concentration of 0.3M. The red blood cells were subsequently lysed with 0.03% saponin for 10min at 4°C.

Afterwards the pellet was resuspended in sonication buffer (10mM Tris-HCl pH 8, 0.5mM EDTA, 0.2% SDS, cOmplete protease inhibitor cocktail (Roche)) and sonicated for 15min (30 sec on/30 sec off) in a Bioruptor UCD-300. Western blot analysis was performed to confirm the soluble fraction to contain the protein of interest. For the co-immunoprecipitation the sample and the control were divided into 4 replicates each. 350µl sonication supernatant was mixed with 350µl dilution buffer (10mM Tris-HCl pH 7.4, 150mM NaCl, 0.5 mM EDTA, 0.5% Nonidet 40, cOmplete protease inhibitor cocktail (Roche)). Samples were mixed with 25µl GFP-Trap®_MA Magnetic Agarose Beads (Chromotek) and incubated at 4°C and 25rpm overnight. Then, beads were pelleted with a magnet and washed 4 times with dilution buffer. Finally, the beads were mixed with 30µl 4x LDS sample buffer (Invitrogen) and boiled 10min at 95°C. The supernatant was collected as elution. The fractions were analyzed by Silver Gel (SilverQuest, Invitrogen) and Western blot before mass spectrometry analysis.

MS sample preparation

Samples were loaded onto a 4%-12% gradient Bis-Tris gel (Thermo) and run in 1x MOPS buffer at 180V for 10min. Each lane was sliced, minced and transferred to an Eppendorf reaction tube. In gel digest was performed as previously described (Bluhm et al., 2016) and samples stored on StageTips (Rappsilber et al., 2007) until measurement. Alternatively, for biotin proximity ligation experiments, the beads were directly incubated in 2mM DTT/50mM ammonium bicarbonate buffer (Sigma-Aldrich) and subsequently alkylated with 5mM iodoacetamide (Sigma-Aldrich). Digestions were performed with 200ng of trypsin (Sigma-Aldrich) in 2M urea/50mM ammonium bicarbonate buffer at room temperature overnight. Tryptic peptides were stored on StageTips (Rappsilber et al., 2007) until measurement.

MS measurement

The digested peptides of the samples were separated on a 25-cm reverse-phase capillary (75µM inner diameter, New Objective) packed with Reprosil C18 material (Dr. Maisch GmbH). Elution of the peptides was achieved with a 2h gradient from 2%-40% Buffer acetonitrile followed by a 95% acetonitrile wash-out at 200nl/min on an Easy LC1000 HPLC system (Thermo). Mass spectrometry measurements were performed with a Q Exactive Plus mass spectrometer (Thermo) operated with a Top10 data-dependent MS/MS acquisition method per full scan. Spray voltage was set to 2.2-2.4kV.

MS data analysis

MS raw data was analyzed using MaxQuant v1.5.2.8 (Cox and Mann, 2008) with standard settings and activated match between runs and LFQ quantitation features. The search was performed against a Human Uniprot database (81,194 entries) and the Plasmodium falciparum PlasmoDB 9.3 database (5,538 entries). The proteinGroups file was filtered for known contaminants and reverse hits prior to statistical analysis (Welch t-test). Data was plotted using the R environment.

Southern blot

Genomic DNA was isolated by phenol/chloroform extraction of saponin lysed parasites. gDNA was digested with *AflIII* & *AflII* restriction enzymes, separated on a 0.8% agarose gel and transferred onto a Amersham Hybond-N+ membrane (GE Healthcare). Blots were probed with ^{32}P-dATP-labelled probe fragments. As probe, the 5' stretch MESA homology region of the pH-MESA KO plasmid was used.

Growth assay

Asynchronous parasite cultures were set up at 0.2% parasitemia. Parasitemia was determined by flow cytometry and followed over 5 days. Parasites were stained with SYBR® Green I nucleic acid gel stain (Sigma-Aldrich) 1:5000 for 20min at 37°C in the dark, washed 3x with culture medium and 100'000 cells were assessed with a BD FACSCalibur. The experiment was performed in biological triplicates, standard deviations were calculated and exponential curves fitted to the data points.

Binding assay

Semi-static binding assays were performed as published before (Oberli et al., 2016). 100µl 50µg/ml human CD36 recombinant protein (Sino Biological, China) was applied into wells of eight-chamber cell culture glass slides (Falcon, Big Flats, NY, USA) and incubated overnight at 4°C to allow proteins to absorb to the surface. The wells were blocked with 1% BSA/PBS for 1h at 37°C. Parasite cultures were washed twice with RPMI-HEPES and spotted onto the immobilized CD36 and cultured for 2h under continuous and simultaneous shaking (140 rpm, proBlot 25 Rocker; Labnet International Inc., NY, USA) (105 rpm, Lab-Therm LT-W, Kühner, Switzerland) at 37°C. Non-bound erythrocytes were removed by six gentle washes

with RPMI-HEPES with simultaneous shaking for 2min. Bound iRBCs were fixed with 2% glutaraldehyde in RPMI-HEPES overnight, stained with 10% Giemsa for 1h and microscopically counted. Results are shown as mean number of parasites bound per square millimeter and normalized to 1% parasitemia. The experiment was performed in biological triplicates.

Microsphiltration

Microsphiltration experiments were performed as described in Lavazec et al. (2013). Tightly synchronized parasite cultures (600µl, 0.5-10% parasitemia, 1.5% hematocrit) were passed under flow (60ml/h) through a microsphere matrix consisting of solder powder beads from 5-15µm and 15-25µm diameter (Industrie des Poudres Sphériques, Annemasse, France). After rinsing the column with 5ml of culture medium, parasitemia of input and flow-through samples were assessed by flow cytometry. Parasites were stained with SYBR® Green I nucleic acid gel stain (Sigma-Aldrich) 1:5000 for 20min at 37°C in the dark, washed 3x with culture medium and 100’000 cells were assessed with a BD FACSCalibur. All experiments were performed in technical triplicates. Retention rates were calculated as 1−(parasitemia flow through sample/parasitemia input sample).

Scanning electron microscopy

For scanning electron microscopy mature parasites were knob-selected, purified by Percoll density gradient and fixed in 2.5% PBS for 1 hour at room temperature. After transfer to coverslips preliminary coated with Poly-L-lysine, the samples were dehydrated in increasing concentration of ethanol (10% v/v, 25% v/v, 50% v/v, 75% v/v, 90% v/v and 2 x 100% v/v, 10min each), critical point dryed and finally sputtered with 5nm Platinum (LEICA EM ACE600). The micrographs were taken with a SEM Versa 3D (FEI) at 5kV.

Results

Expression and localization of MESA

We generated a cell line with endogenously tagged MESA as a tool for protein characterization. To that end, a CRISPR/Cas9-SLI approach was used to introduce a GFP-tag at the MESA C-terminus. Correct integration of the tag-cassette was checked by PCR (data not shown). MESA-GFP protein expression was confirmed by Western blot and

immunofluorescence analysis (Figure 1A and B). In Western blot analysis no GFP was detected in the 3D7 control. The MESA-GFP signal runs higher (>250kDa) as its calculated molecular weight of 202kDa. In immunofluorescence microscopy the signal of both MESA antibody and GFP antibody localize to the iRBC periphery (Figure 1B).

To confirm published expression data of MESA, Western blot and immunofluorescence analysis throughout the intraerythrocytic life cycle were performed (Figure 1C and D). As the MESA antibody is not suitable for Western blot analysis, Western blot was performed with MESA-GFP parasites, and immunofluorescence analysis with 3D7 wildtype and MESA-GFP (data not shown) parasites. We found MESA expression as expected in the second half of the intraerythrocytic life cycle in trophozoite and schizont stages.

MESA localizes to the cytoskeleton of iRBCs (Coppel et al., 1988) and is not surface exposed as the name misleadingly indicates. In fluorescence microscopy we observe MESA at the periphery of red blood cells (Figure 1B and D). We performed cytoskeleton imaging where the inside of RBCs can be investigated by immunofluorescence assay after the cells were bound to a glass slide and opened with shear stress. The cytosolic face of the membrane and attached cytoskeleton is exposed on the surface of the glass slide. By immunofluorescence imaging MESA was identified specifically in iRBCs (Figure 1E). Glycophorin A/B staining serves as control for shearing of the RBCs; if the cells were not open, the stain would cover all the area and not only label the contours of the cells.

Interaction partners of MESA

To identify putative interacting proteins of MESA-GFP co-immunoprecipitation with α-GFP beads (GFP-trap, Chromotek) followed by mass spectrometry was performed. MESA-GFP protein extracts of trophozoite stages were analyzed, as negative control 3D7 wildtype parasites were used. We have identified a total number of 53 proteins positively enriched in the MESA-GFP compared to the control sample (see Supplementary Table 2). Among those were several exported *Plasmodium* (Table 1) and human (Table 2) proteins.

In order to confirm association of MESA with candidates from the co-immunoprecipitation experiment, co-labelling fluorescence imaging analysis was performed.

For *Plasmodium* proteins we used antibodies against GFP or MESA combined with PFE1605w or PFI1780w, in MESA-GFP or 3D7 cell lines. Additionally, a cell line episomally expressing PF3D7_0424600-GFP was probed with MESA and GFP antibodies

(Figure 2A). Limited overlap with the MESA signal was observed with PFE1605w and PFI1780w, but significant overlap was seen with another PHISTb protein, PF3D7_0424600-GFP, and MESA.

For human interaction candidates, we used the MESA-GFP cell line and co-labelled with GFP, band 4.1, and spectrin antibodies (Figure 2B). We found a good overlap of the GFP signal with band 4.1 or the spectrin signals.

Functional analysis of MESA

In order to investigate protein function, a MESA KO cell line was generated by single cross-over homologous recombination. A *hDHFR* resistance cassette was introduced to disrupt the gene and enable positive selection of transgenic parasites. Successful knock out was confirmed by PCR (data not shown) and Southern blot (Figure 3A). There is some residual plasmid in the MESA KO parasite cell line, which is usually lost over the course of several generations. The MESA KO was viable indicating that the respective gene is dispensable. We assessed growth of the MESA KO compared to wildtype 3D7 and found no significant growth difference (Figure 3B).

To check whether MESA has an influence on PfEMP1 presentation and anchorage on the iRBC membrane, we performed a semi-static binding assay to CD36 (Figure 3C). We found MESA KO have similar binding to CD36 as 3D7.

Further, we assessed deformability of MESA KO by microsphiltration (Figure 3D). With that method, cell deformability is assessed by passing cells under flow through a microsphere matrix consisting of different-sized beads mimicking the cell passage through the spleen. Less deformable cell are more prone to be retained in the matrix, flexible cells can pass the matrix easily. The experiments were performed with highly synchronous parasite cultures at different time points in the life cycle stage (22hpi, 28hpi, 34hpi and 40hpi). Retention percentages of 45.8±8.7%, 71.5±17.7%, 72.1±8.4%, 86.7±3.7% for 3D7 and 51.6±13.1%, 68.1±9.0%, 70.7±9.8%, 90.6±6.9% for MESA KO at 22hpi, 28hpi, 34hpi and 40hpi were observed, respectively (see Figure 3D). In summary, no significant differences in retention rates between MESA KO and 3D7 wildtype were found.

MESA localizes to the erythrocyte cytoskeleton close to knob structures. With scanning electron microscopy we investigated morphology of knobs in MESA KO iRBCs (Figure 3E). No obvious difference in the appearance of MESA KO and 3D7 iRBCs was noted.

We have previously identified MESA in MAHRP2 co-immunoprecipitation experiments (unpublished). Therefore we performed an immunofluorescence assay with MESA KO cells to investigate MAHRP2 localization (Figure 4A). We found no aberrant localization of MAHRP2 in MESA KO compared to 3D7 wildtype.

RESA (ring infected erythrocyte surface antigen, PF3D7_0102200) localizes to the erythrocyte cytoskeleton in ring stage infected RBCs until approximately 24 hours post infection (Brown et al., 1985). MESA localizes to the erythrocyte cytoskeleton in the second half of the parasite lifecycle and interacts with band 4.1 (Bennett et al., 1997). We inquired whether MESA has a role in replacing RESA and therefore tested the (timed) presence of RESA in MESA KO iRBCs with an immunofluorescence assay (Figure 4B). By comparing RESA and MESA expression in ring and trophozoite stages of MESA KO and 3D7 wildtype respectively we found no difference.

Discussion

Many *P. falciparum* proteins are exported to the host erythrocyte and localize to the cytoskeleton. Their functions are diverse, e.g. stabilizing the cytoskeleton (RESA, Mills et al., 2007), contributing to the stability of the major virulence complex (PFE1605w, Oberli et al., 2016), or establishing NPPs (Nguitragool et al., 2011). However, many protein functions of exported *P. falciparum* proteins are not understood. We aimed at assigning a function to MESA, a long known protein residing at the erythrocyte cytoskeleton.

We successfully generated an endogenous C-terminally tagged MESA-GFP cell line by a combined CRISPR/Cas9-SLI approach. This gene editing strategy facilitates and accelerates genome manipulation greatly. On one hand, targeted DNA double strand breaks (with the help of a sequence-specific gRNAs) and customized sequence adjustments are introduced in the genome through the provided repair templates. On the other hand, the introduction of a resistance cassette separated from the gene of interest by a skip-peptide enables positive selection of transgenic parasites immediately after transfection thanks to the fast action of the CRISPR/Cas9 editing system.

MESA expression in trophozoite/schizont stages and MESA localization to the inner side of the iRBC membrane was confirmed in 3D7 wildtype and MESA-GFP transgenic parasite cell lines (Coppel et al., 1988). In cytoskeleton imaging iRBCs cannot be distinguished from uninfected RBCs by (parasite) nuclear staining. MESA is a suitable marker for this method as

it is strongly bound to the erythrocyte cytoskeleton and resistant to the harsh shearing conditions.

In order to identify interaction partners of MESA-GFP co-immunoprecipitation experiments were performed. From 4 independent replicates 8 PHIST family proteins were detected, from which 6 (PF3D7_0532400 PF3D7_1102500, PF3D7_0102200, PF3D7_0731300, PF3D7_1201000, and PF3D7_0424600) belong to the PHISTb subfamily. To our current knowledge, all members of this subfamily localize at the host cytoskeleton (Foley et al., 1991, Florens et al., 2004, Tarr et al., 2014, Proellocks et al., 2014, Warncke et al., 2016). PF3D7_0936800 localizes at the host cell membrane (Oberli et al., 2014). PF3D7_0501100 is a Hsp40 type II co-chaperone (Kulzer et al., 2010, Petersen et al., 2016) and Hsp70x is an *Plasmodium* exported chaperone (Kulzer et al., 2012). Hsp70/Hsp40 complexes are suggested to be involved in facilitating protein trafficking and targeting other proteins to their destination (Kampinga and Craig, 2010). MESA is a Triton X-100 insoluble protein (Coppel et al., 1988) that cannot simply diffuse through the RBC cytoskeleton as soluble proteins do. Thus it is conceivable that its transport is chaperone-assisted.

We also identified several human cytoskeleton or membrane associated proteins as expected regarding the localization of MESA-GFP. The previously reported MESA interaction partner band 4.1 (Bennett et al., 1997) as well as the MESA opponent p55 (55 kDa erythrocyte membrane protein) (Waller et al., 2003) were enriched in the MESA-GFP sample. Interestingly, MAHRP2 was not identified in our co-immunoprecipitation experiments, thus the MAHRP2 co-immunoprecipitation could not be complemented. MESA seems a very abundant protein which may contribute to the finding that we identify it almost in every immunoprecipitation experiment.

By immunofluorescence assays we sought to elucidate physical association of putative interaction partners and MESA. We observed some overlap of MESA with the 5 tested proteins PFE1605w, PFI1780w, PF3D7_0424600, band 4.1 and spectrin. However, co-labelling immunofluorescence assays are in principle not conclusive to show interaction of two proteins. For a better analysis of association of two proteins, colocalization analysis upon confocal microscopy would be appropriate. However, this is hardly possible as MESA figures as “surface” in fluorescence microscopy due to its localization at the erythrocyte membrane and a colocalization analysis of those is not possible. High resolution immunoelectron microscopy or biochemical interaction studies would help validating interaction partners.

A MESA KO cell line was successfully generated in order to study MESA function. MESA function had been investigated before but without assigning a specific function to the protein (Petersen et al., 1989, Magowan et al., 1995, Cooke et al., 2002, Waller et al., 2003). However, the studies form Petersen, Magowan, Cooke and colleagues used a spontaneously mutated cell line not expressing MESA. The exact extent of the deletion on chromosome 5, where the *mesa* gene is located, was not assessed. Thus it cannot be excluded that other genes besides the gene of interest were affected. In this study we have generated a new 5' MESA KO cell line by targeted single cross-over recombination disrupting *mesa* gene expression by insertion of a resistance marker.

We found no growth defect of MESA deficient cells according to findings from Magowan and colleagues (Magowan et al., 1995). By semi-static binding assay against CD36 and scanning electron microscopy we also found MESA is not required for the formation of knobs and cytoadherence as previously published (Petersen et al., 1989, Magowan et al., 1995, Cooke et al., 2002).

We found no difference in deformability of MESA KO and 3D7. We hypothesized that MESA would have an influence on the physical properties of the iRBC because of its localization at the host cell cytoskeleton. Similar observations were done with KAHRP and RESA. KAHRP is a constituent of knobs, KAHRP KO parasites have no knobs and are more deformable as wildtype parasites (Glenister et al., 2002). RESA localizes to the cytoskeleton and was suggested to have a role in temperature-dependent membrane stability as under heat stress RESA KO were found to be more deformable than wildtype iRBCs (Mills et al., 2007).

The microsphiltration method accurately reflects the physiological function of the spleen (Deplaine et al., 2011). There are other methods to assess deformability properties of an entire iRBC (e.g. microfluidics, Myrand-Lapierre et al., 2015) or of the iRBC membrane specifically (e.g micropipette aspiration, Glenister et al., 2002). Though, it is conceivable that the microsphiltration method used in this study is not able to detect the dynamic range of the deformability changes (if any) upon MESA deletion.

In conclusion we identified putative MESA interaction partners at the host cytoskeleton localization and exclude a function of MESA in knob formation, CD36 binding and deformability alteration.

Contribution and Acknowledgements

Esther Mundwiler-Pachlatko generated the MESA KO cell line. Jan Warncke provided the cell line episomally expressing PF3D7_0424600-GFP. Sebastian Rusch performed cytoskeleton imaging and Southern blot analysis. Falk Butter did mass spectrometry analysis. Françoise Brand did scanning electron microscopy experiments. We thank Henning Stahlberg and his team at the C-CINA, Biozentrum, University of Basel, for the access to the electron microscopy facility. We would like to thank the following colleagues for sharing antibodies: Claudia Daubenberger (α-GAPDH), Ross Coppel (α-MESA), and Robin Anders (α-RESA).

References

AEBERSOLD, R. H., TEPLOW, D. B., HOOD, L. E. & KENT, S. B. 1986. Electroblotting onto activated glass. High efficiency preparation of proteins from analytical sodium dodecyl sulfate-polyacrylamide gels for direct sequence analysis. *J Biol Chem,* 261**,** 4229-38.

BENNETT, B. J., MOHANDAS, N. & COPPEL, R. L. 1997. Defining the minimal domain of the Plasmodium falciparum protein MESA involved in the interaction with the red cell membrane skeletal protein 4.1. *J Biol Chem,* 272**,** 15299-306.

BERTIN, G. I., SABBAGH, A., ARGY, N., SALNOT, V., EZINMEGNON, S., AGBOTA, G., LADIPO, Y., ALAO, J. M., SAGBO, G., GUILLONNEAU, F. & DELORON, P. 2016. Proteomic analysis of Plasmodium falciparum parasites from patients with cerebral and uncomplicated malaria. *Sci Rep,* 6**,** 26773.

BIRNBAUM, J., FLEMMING, S., REICHARD, N., SOARES, A. B., MESEN-RAMIREZ, P., JONSCHER, E., BERGMANN, B. & SPIELMANN, T. 2017. A genetic system to study Plasmodium falciparum protein function. *Nat Methods,* 14**,** 450-456.

BLACK, C. G., PROELLOCKS, N. I., KATS, L. M., COOKE, B. M., MOHANDAS, N. & COPPEL, R. L. 2008. In vivo studies support the role of trafficking and cytoskeletal-binding motifs in the interaction of MESA with the membrane skeleton of Plasmodium falciparum-infected red blood cells. *Mol Biochem Parasitol,* 160**,** 143-7.

BLUHM, A., CASAS-VILA, N., SCHEIBE, M. & BUTTER, F. 2016. Reader interactome of epigenetic histone marks in birds. *Proteomics,* 16**,** 427-36.

BROWN, G. V., CULVENOR, J. G., CREWTHER, P. E., BIANCO, A. E., COPPEL, R. L., SAINT, R. B., STAHL, H. D., KEMP, D. J. & ANDERS, R. F. 1985. Localization of the ring-infected erythrocyte surface antigen (RESA) of Plasmodium falciparum in merozoites and ring-infected erythrocytes. *J Exp Med,* 162**,** 774-9.

CHISHTI, A. H. 1998. Function of p55 and its nonerythroid homologues. *Curr Opin Hematol,* 5**,** 116-21.

COLLINS, M. O., WRIGHT, J. C., JONES, M., RAYNER, J. C. & CHOUDHARY, J. S. 2014. Confident and sensitive phosphoproteomics using combinations of collision induced dissociation and electron transfer dissociation. *J Proteomics,* 103**,** 1-14.

COOKE, B. M., GLENISTER, F. K., MOHANDAS, N. & COPPEL, R. L. 2002. Assignment of functional roles to parasite proteins in malaria-infected red blood cells by competitive flow-based adhesion assay. *Br J Haematol,* 117**,** 203-11.

COPPEL, R. L., CULVENOR, J. G., BIANCO, A. E., CREWTHER, P. E., STAHL, H. D., BROWN, G. V., ANDERS, R. F. & KEMP, D. J. 1986. Variable antigen associated with the surface of erythrocytes infected with mature stages of Plasmodium falciparum. *Mol Biochem Parasitol,* 20**,** 265-77.

COPPEL, R. L., LUSTIGMAN, S., MURRAY, L. & ANDERS, R. F. 1988. MESA is a Plasmodium falciparum phosphoprotein associated with the erythrocyte membrane skeleton. *Mol Biochem Parasitol,* 31**,** 223-31.

COX, J. & MANN, M. 2008. MaxQuant enables high peptide identification rates, individualized p.p.b.-range mass accuracies and proteome-wide protein quantification. *Nat Biotechnol,* 26**,** 1367-72.

DEPLAINE, G., SAFEUKUI, I., JEDDI, F., LACOSTE, F., BROUSSE, V., PERROT, S., BILIGUI, S., GUILLOTTE, M., GUITTON, C., DOKMAK, S., AUSSILHOU, B., SAUVANET, A., CAZALS HATEM, D., PAYE, F., THELLIER, M., MAZIER, D., MILON, G., MOHANDAS, N., MERCEREAU-PUIJALON, O., DAVID, P. H. & BUFFET, P. A. 2011. The sensing of poorly deformable red blood cells by the human spleen can be mimicked in vitro. *Blood,* 117**,** e88-95.

DONNELLY, M. L., LUKE, G., MEHROTRA, A., LI, X., HUGHES, L. E., GANI, D. & RYAN, M. D. 2001. Analysis of the aphthovirus 2A/2B polyprotein 'cleavage' mechanism indicates not a proteolytic reaction, but a novel translational effect: a putative ribosomal 'skip'. *J Gen Virol,* 82**,** 1013-25.

FLORENS, L., LIU, X., WANG, Y., YANG, S., SCHWARTZ, O., PEGLAR, M., CARUCCI, D. J., YATES, J. R., 3RD & WU, Y. 2004. Proteomics approach reveals novel proteins on the surface of malaria-infected erythrocytes. *Mol Biochem Parasitol,* 135**,** 1-11.

FOLEY, M., TILLEY, L., SAWYER, W. H. & ANDERS, R. F. 1991. The ring-infected erythrocyte surface antigen of Plasmodium falciparum associates with spectrin in the erythrocyte membrane. *Mol Biochem Parasitol,* 46**,** 137-47.

GHORBAL, M., GORMAN, M., MACPHERSON, C. R., MARTINS, R. M., SCHERF, A. & LOPEZ-RUBIO, J. J. 2014. Genome editing in the human malaria parasite Plasmodium falciparum using the CRISPR-Cas9 system. *Nat Biotechnol,* 32**,** 819-21.

GLENISTER, F. K., COPPEL, R. L., COWMAN, A. F., MOHANDAS, N. & COOKE, B. M. 2002. Contribution of parasite proteins to altered mechanical properties of malaria-infected red blood cells. *Blood,* 99**,** 1060-3.

HOWARD, R. J., BARNWELL, J. W., ROCK, E. P., NEEQUAYE, J., OFORI-ADJEI, D., MALOY, W. L., LYON, J. A. & SAUL, A. 1988. Two approximately 300 kilodalton Plasmodium falciparum proteins at the surface membrane of infected erythrocytes. *Mol Biochem Parasitol,* 27**,** 207-23.

KAMPINGA, H. H. & CRAIG, E. A. 2010. The HSP70 chaperone machinery: J proteins as drivers of functional specificity. *Nat Rev Mol Cell Biol,* 11**,** 579-92.

KILILI, G. K. & LACOUNT, D. J. 2011. An erythrocyte cytoskeleton-binding motif in exported Plasmodium falciparum proteins. *Eukaryot Cell,* 10**,** 1439-47.

KULZER, S., CHARNAUD, S., DAGAN, T., RIEDEL, J., MANDAL, P., PESCE, E. R., BLATCH, G. L., CRABB, B. S., GILSON, P. R. & PRZYBORSKI, J. M. 2012. Plasmodium

falciparum-encoded exported hsp70/hsp40 chaperone/co-chaperone complexes within the host erythrocyte. *Cell Microbiol,* 14**,** 1784-95.

KULZER, S., RUG, M., BRINKMANN, K., CANNON, P., COWMAN, A., LINGELBACH, K., BLATCH, G. L., MAIER, A. G. & PRZYBORSKI, J. M. 2010. Parasite-encoded Hsp40 proteins define novel mobile structures in the cytosol of the P. falciparum-infected erythrocyte. *Cell Microbiol,* 12**,** 1398-420.

KUN, J. F., WALLER, K. L. & COPPEL, R. L. 1999. Plasmodium falciparum: structural and functional domains of the mature-parasite-infected erythrocyte surface antigen. *Exp Parasitol,* 91**,** 258-67.

LABUN, K., MONTAGUE, T. G., GAGNON, J. A., THYME, S. B. & VALEN, E. 2016. CHOPCHOP v2: a web tool for the next generation of CRISPR genome engineering. *Nucleic Acids Res,* 44**,** W272-6.

LAVAZEC, C., DEPLAINE, G., SAFEUKUI, I., PERROT, S., MILON, G., MERCEREAU-PUIJALON, O., DAVID, P. H. & BUFFET, P. 2013. Microsphiltration: a microsphere matrix to explore erythrocyte deformability. *Methods Mol Biol,* 923**,** 291-7.

LUSTIGMAN, S., ANDERS, R. F., BROWN, G. V. & COPPEL, R. L. 1990. The mature-parasite-infected erythrocyte surface antigen (MESA) of Plasmodium falciparum associates with the erythrocyte membrane skeletal protein, band 4.1. *Mol Biochem Parasitol,* 38**,** 261-70.

MAGOWAN, C., COPPEL, R. L., LAU, A. O., MORONNE, M. M., TCHERNIA, G. & MOHANDAS, N. 1995. Role of the Plasmodium falciparum mature-parasite-infected erythrocyte surface antigen (MESA/PfEMP-2) in malarial infection of erythrocytes. *Blood,* 86**,** 3196-204.

MAGOWAN, C., LIANG, J., YEUNG, J., TAKAKUWA, Y., COPPEL, R. L. & MOHANDAS, N. 1998. Plasmodium falciparum: influence of malarial and host erythrocyte skeletal protein interactions on phosphorylation in infected erythrocytes. *Exp Parasitol,* 89**,** 40-9.

MILLS, J. P., DIEZ-SILVA, M., QUINN, D. J., DAO, M., LANG, M. J., TAN, K. S., LIM, C. T., MILON, G., DAVID, P. H., MERCEREAU-PUIJALON, O., BONNEFOY, S. & SURESH, S. 2007. Effect of plasmodial RESA protein on deformability of human red blood cells harboring Plasmodium falciparum. *Proc Natl Acad Sci U S A,* 104**,** 9213-7.

MOLL, K., KANEKO, A., SCHERF, A. & WAHLGREN, M. 2013. Methods in Malaria Research (MR4/ATCC) 6th Edition.

MONTAGUE, T. G., CRUZ, J. M., GAGNON, J. A., CHURCH, G. M. & VALEN, E. 2014. CHOPCHOP: a CRISPR/Cas9 and TALEN web tool for genome editing. *Nucleic Acids Res,* 42**,** W401-7.

MYRAND-LAPIERRE, M. E., DENG, X., ANG, R. R., MATTHEWS, K., SANTOSO, A. T. & MA, H. 2015. Multiplexed fluidic plunger mechanism for the measurement of red blood cell deformability. *Lab Chip,* 15**,** 159-67.

NGUITRAGOOL, W., BOKHARI, A. A., PILLAI, A. D., RAYAVARA, K., SHARMA, P., TURPIN, B., ARAVIND, L. & DESAI, S. A. 2011. Malaria parasite clag3 genes determine channel-mediated nutrient uptake by infected red blood cells. *Cell,* 145**,** 665-77.

OBERLI, A., SLATER, L. M., CUTTS, E., BRAND, F., MUNDWILER-PACHLATKO, E., RUSCH, S., MASIK, M. F., ERAT, M. C., BECK, H. P. & VAKONAKIS, I. 2014. A Plasmodium falciparum PHIST protein binds the virulence factor PfEMP1 and comigrates to knobs on the host cell surface. *Faseb j,* 28**,** 4420-33.

OBERLI, A., ZURBRUGG, L., RUSCH, S., BRAND, F., BUTLER, M. E., DAY, J. L., CUTTS, E. E., LAVSTSEN, T., VAKONAKIS, I. & BECK, H. P. 2016. Plasmodium falciparum Plasmodium helical interspersed subtelomeric proteins contribute to cytoadherence and anchor P. falciparum erythrocyte membrane protein 1 to the host cell cytoskeleton. *Cell Microbiol,* 18**,** 1415-28.

PETERSEN, C., NELSON, R., MAGOWAN, C., WOLLISH, W., JENSEN, J. & LEECH, J. 1989. The mature erythrocyte surface antigen of Plasmodium falciparum is not required for knobs or cytoadherence. *Mol Biochem Parasitol,* 36**,** 61-5.

PETERSEN, W., KULZER, S., ENGELS, S., ZHANG, Q., INGMUNDSON, A., RUG, M., MAIER, A. G. & PRZYBORSKI, J. M. 2016. J-dot targeting of an exported HSP40 in Plasmodium falciparum-infected erythrocytes. *Int J Parasitol,* 46**,** 519-25.

PROELLOCKS, N. I., HERRMANN, S., BUCKINGHAM, D. W., HANSSEN, E., HODGES, E. K., ELSWORTH, B., MORAHAN, B. J., COPPEL, R. L. & COOKE, B. M. 2014. A lysine-rich membrane-associated PHISTb protein involved in alteration of the cytoadhesive properties of Plasmodium falciparum-infected red blood cells. *Faseb j,* 28**,** 3103-13.

RAPPSILBER, J., MANN, M. & ISHIHAMA, Y. 2007. Protocol for micro-purification, enrichment, pre-fractionation and storage of peptides for proteomics using StageTips. *Nat Protoc,* 2**,** 1896-906.

SCHINDELIN, J., ARGANDA-CARRERAS, I., FRISE, E., KAYNIG, V., LONGAIR, M., PIETZSCH, T., PREIBISCH, S., RUEDEN, C., SAALFELD, S., SCHMID, B., TINEVEZ, J. Y., WHITE, D. J., HARTENSTEIN, V., ELICEIRI, K., TOMANCAK, P. & CARDONA, A. 2012. Fiji: an open-source platform for biological-image analysis. *Nat Methods,* 9**,** 676-82.

SHI, H., LIU, Z., LI, A., YIN, J., CHONG, A. G., TAN, K. S., ZHANG, Y. & LIM, C. T. 2013. Life cycle-dependent cytoskeletal modifications in Plasmodium falciparum infected erythrocytes. *PLoS One,* 8**,** e61170.

SZYMCZAK, A. L., WORKMAN, C. J., WANG, Y., VIGNALI, K. M., DILIOGLOU, S., VANIN, E. F. & VIGNALI, D. A. 2004. Correction of multi-gene deficiency in vivo using a single 'self-cleaving' 2A peptide-based retroviral vector. *Nat Biotechnol,* 22**,** 589-94.

TARR, S. J., MOON, R. W., HARDEGE, I. & OSBORNE, A. R. 2014. A conserved domain targets exported PHISTb family proteins to the periphery of Plasmodium infected erythrocytes. *Mol Biochem Parasitol,* 196**,** 29-40.

WALLER, K. L., NUNOMURA, W., AN, X., COOKE, B. M., MOHANDAS, N. & COPPEL, R. L. 2003. Mature parasite-infected erythrocyte surface antigen (MESA) of Plasmodium falciparum binds to the 30-kDa domain of protein 4.1 in malaria-infected red blood cells. *Blood,* 102**,** 1911-4.

WARNCKE, J. D., VAKONAKIS, I. & BECK, H. P. 2016. Plasmodium Helical Interspersed Subtelomeric (PHIST) Proteins, at the Center of Host Cell Remodeling. *Microbiol Mol Biol Rev,* 80**,** 905-27.

ZAINUDIN, N. S., OTHMAN, N., MUHI, J., ABDU SANI, A. A. & NOORDIN, R. 2015. Mature Erythrocyte Surface Antigen Protein Identified in the Serum of Plasmodium falciparum-Infected Patients. *Am J Trop Med Hyg,* 93**,** 1268-73.

Table 1

Protein ID	Gene product	# peptides	Δ MesaGFP/ 3D7 Ctrl
PF3D7_0501100 (PFE0055c)	hsp40, J-dots	6	4.339163977
PF3D7_0532400 (PFE1605w)	PHISTb	12	4.299854761
PF3D7_0500800	*MESA*	*62*	*3.806428361*
PF3D7_1102500	PHISTb (GEXP02)	6	3.114333294
PF3D7_0832200	PHISTa-like	9	3.065429105
PF3D7_0102200	RESA	10	2.587767368
PF3D7_0731300	PHISTb	7	2.101269469
PF3D7_1201000	PHISTb	12	1.861195545
PF3D7_1001000	unknown function	6	1.794450405
PF3D7_0831700	Hsp70x	37	1.70581098
PF3D7_0936800 (PFI1780w)	PHISTc	14	1.629933309
PF3D7_0424600	PHISTb	11	1.484007808

Δvalue: the difference in the log10 p-value of the MESA-GFP samples versus the 3D7 control samples

Table 2

Protein name	localization	# peptides	Δ MesaGFP/ 3D7 Ctrl
55 kDa erythrocyte membrane protein	cytoskeleton	10	1.794494037
Tropomodulin-1	cytoskeleton	3	1.774023752
Spectrin beta chain, erythrocytic	cytoskeleton	123	1.634587147
Spectrin alpha chain, erythrocytic 1	cytoskeleton	137	1.620350511
Ankyrin-1	cytoskeleton	75	1.618289139
Beta-adducin	cytoskeleton	9	1.47738193
T-complex protein 1 subunit delta	chaperone complex	5	1.473385283
Protein 4.1	cytoskeleton	31	1.470327447
Flotillin-1	involved in vesicular trafficking and signal transduction	12	1.43552798
T-complex protein 1 subunit zeta	chaperone complex	4	1.419631315
Erythrocyte membrane protein band 4.2	cytoskeleton	32	1.369065576
Solute carrier family 2, facilitated glucose transporter member 1	membrane	7	1.368210461

Δvalue: the difference in the log10 p-value of the MESA-GFP samples versus the 3D7 control samples

Supplementary Table 1

Mesa-GFP 5HR fw	5'AGAAAGAGAAGTACAAGAAGAATC
Mesa-GFP 5HR rv	5'TTCATCAATAAACTTAAACATTGTATC
Mesa-GFP 3HR fw	5'ATTATGAAGAGAGAATACGCATG
Mesa-GFP 3HR rv	5'AATTAACCATCATTTGAGTATCC
Mesa-GFP gRNA	5'GAAATTTAGTGAAATGAATG
MESA KO fw	5'atatgaattcTGGAGGTAATTTGTAGAAATTTATG
MESA KO rv	5'atttggatccTTATTTCTTCAATATCCTTAGCATTC

Supplementary Table 2

Protein.IDs	difference_MesaGFP_3D7
PF3D7_0202400	5.703893372
PF3D7_1253400;PF3D7_1479000;PF3D7_0301000;PF3D7_0401900	4.384599308
PF3D7_0501100.2;PF3D7_0501100.1	4.339163977
PF3D7_0532400	4.299854761
PF3D7_0721100	4.117761326
P31948;G3XAD8;F5H0T1;F5H783;F5GXD8;H0YGI8	4.0359489
PF3D7_0500800	3.806428361
PF3D7_1102500	3.114333294
PF3D7_0832200.1;PF3D7_0832200.2	3.065429105
PF3D7_1132800	3.005714564
P07900;P07900-2;Q86U12;G3V2J8;Q14568;Q58FG0;Q58FF8;Q58FG1;Q58FF6	2.940623563
PF3D7_1001600	2.899632912
PF3D7_0102200	2.587767368
H0YG33;P08107;F8VZJ4;F5H1D3;F5GZ62;E7EP94;E7EQL7;Q5SP16;F8WEE3;Q53FA3;P34931;E7EP11;F8W1P1;B4DXY3;C9IYI3	2.443061337
P11142;E9PKE3;E7ET08;P11142-2;E9PNE6;E9PN89;E9PQQ4;E9PQK7;E9PK54;E9PLF4;A8K7Q2;E9PPY6;E9PN25;E9PI65;E9PS65;E9PM13;E9PSH5	2.418702995
PF3D7_1404900	2.326675749
PF3D7_1033200	2.305069863
PF3D7_0629200	2.162128158
PF3D7_0731300	2.101269469
F5H170;E9PDM9;Q8WW22;Q8WW22-2;F8WF76;C9JDE6	2.001154732
PF3D7_0731600;PF3D7_0215300	1.975885662
PF3D7_1201000	1.861195545
P08238;Q5T9W8;Q58FF7;H0Y6E4;E9PHI1	1.821263861

B4DZV5;Q00013;G3XAI1;C9J9J4;A8MTH1;A6NFY0;C9JB34	1.794494037
PF3D7_1001000	1.794450405
Q5T7W3;P28289	1.774023752
Q9Y230;B3KQ59	1.747226483
PF3D7_0831700	1.70581098
PF3D7_1239700	1.656230027
P11277;P11277-2;Q59FP5;P11277-3;E7EV95;H0YJE6;F8W6C1;Q01082-3;Q01082-2;Q01082;A4QPE4;O15020-2;O15020;C9JRP8;E9PDB1;Q9H254-2;Q9H254-4;Q9H254;E9PJZ2	1.634587147
PF3D7_0936800	1.629933309
P02549;P02549-2	1.620350511
E7EVE3;P16157-10;P16157-8;P16157-5;P16157-16;P16157-3;P16157;P16157-12;P16157-14;P16157-21;P16157-11;P16157-9;P16157-6;P16157-7;P16157-4;P16157-13;P16157-15;E7EVX7;P16157-2;H0YBS0;H0YAY8;D6RCB2;D6RHY3	1.618289139
PF3D7_1344200	1.585388759
P07384;E9PL37;E9PLX0;E9PJJ3;E9PLC9;E9PMC6;E9PJA6;E9PSA6;E9PLQ6;E9PQB3;E9PRM1;E9PIA9	1.5798803
PF3D7_0424600	1.484007808
P35612;P35612-2;B4DM17;P35612-4;P35612-3;E9PAV0;C9JTM0;C9J080;E9PAN1;G8JLN8;P35612-5;P35612-6	1.47738193
B7Z9L0;F5H5W3;P50991;B7Z2F4	1.473385283
P11171-4;P11171-3;P11171-2;P11171;E9PEX0;P11171-6;P11171-5;C9JTS2;P11171-7;E9PEW9;Q4VXN1;Q4VXN0;A8K968;B7Z653;Q9Y2J2-3;Q9H4G0-4;Q9H4G0-3;Q9H4G0-2;Q9Y2J2-2;Q9H4G0;F5GX05;Q9Y2J2	1.470327447
O75955;B0V109;B4DVY7;F8VSI6;B0S8A9;B0V111;A2AB09;A2AB10;B0V110;A2AB12;B0S8B0;B0V112;A2AB13;A2AB11;B0V2I8;H0Y4S3;B0V114;B0V113;B0V2J0;B0V108;A2ABJ5	1.43552798
A6NCD2;P40227;B4DPJ8	1.419631315
PF3D7_1222300;E9PEX3	1.415139964
PF3D7_0917900	1.395450896
Q4KKX0;P16452;P16452-2;F5H563;H0Y4W5;F5H080;P00488	1.369065576
P11166;F8WC15;C9JIM8;G8JLF4;A6NL68	1.368210461

Q5VU66;P06753-2;Q5VU59;Q5VU72;P06753-3;Q5VU58;Q5VU61;Q8NAG3;D6R904;P06753;Q5VU63;D6RFM2;P67936;P67936-2;H0YL80;H0YKP3;C9IZA2;Q5TCU3;CON__Q3SX28;Q5TCU8;P07951-3;P07951-2;P07951;A6NL28-2;A6NL28	1.367641169
P27105;B4E2V5;E7EQ93;B1AM77	1.353091965
PF3D7_0827900	1.318851364
E7EMK3;Q14254;E7EMK1	1.288668372
B4DUR8;E9PAQ6;P49368-2;P49368;Q5SZX6	1.282431094
G5E9B2;B4DEM7;P50990;B4DQH4	1.252159461
E7EV99;E7ENY0;P35611-2;A2A3N8;P35611;P35611-3;Q96D30;Q86XM2;D6RF25;H0Y9H2;D6RJE2;D6RAH3	1.244489597
P04040	1.23259985
PF3D7_1145400	-2.01201023
PF3D7_0401800	-2.504126429
PF3D7_0114100;PF3D7_0222100;PF3D7_0631400;PF3D7_0101300;PF3D7_0701600;PF3D7_0324100	-2.76139359

Figure legends

Figure 1: **Endogenous MESA-GFP expression.** A: Western blot analysis with α-GFP antibody shows expression of MESA-GFP in the MESAP-GFP and not in 3D7 parasite lysates. α-GAPDH antibody was used as loading control B: Immunofluorescence microscopy reveals MESA-GFP localization at the iRBC membrane of MESA-GFP parasites probed with α-MESA and α-GFP antibodies. Scale bar 2µm. C: Time course western blot with α-GFP antibody of MESA-GFP parasite lysates shows expression of MESA-GFP in trophozoite and schizont stages. α-GAPDH antibody staining was used as loading control. hpi: hours post infection D: Time course immunofluorescence assays of 3D7 parasites with α-MESA antibodies confirms MESA expression and localization at the iRBC membrane in trophozoite and schizont stages. Scale bar 2µm. hpi: hours post infection E: Cytoskeleton imaging with α-MESA and α-GlycophorinA/B antibodies shows MESA localization at the inner surface of the iRBC membrane. Scale bar 10µm.

Figure 2: **Localization of MESA-GFP potential protein interaction partners.** A: Immunofluorescence assay co-labelling MESA-GFP, 3D7, and PF3D7_0424600-GFP iRBCs with α-MESA, α-GFP, α-PFE1605w, and α-PFI1780w antibodies. Scale bar 2µm. B: Immunofluorescence assay co-labelling MESA-GFP iRBC with α-GFP, α-band 4.1. and α-spectrin. Scale bar 2µm.

Figure 3: **Phenotypical analysis of MESA KO infected red blood cells.** A: Southern blot confirming the replacement of MESA with a *hDHFR* cassette. Digested gDNA was run on an agarose gel and then probed with the 5' integration stretch. The expected band sizes are for 3D7 2529 bp, for MESA KO 3409bp and 3030 bp and for the plasmid 3910 bp. B: Growth assay of 3D7 and MESA KO iRBCs over 5 days, parasitemia was determined by FACS analysis, and an exponential curve was fitted. Shown are mean of triplicates with standard deviation. C: CD36 semi-static binding assay of 3D7 and MESA KO iRBCs. Shown are mean of triplicates with standard deviation. D: Time course deformability assay of 3D7 and MESA KO iRBCs of tightly synchronized cells. Shown are mean of biological duplicates with standard deviation. E: Scanning electron microscopy of uninfected red blood cell (RBC), wildtype 3D7 iRBC and MESA KO iRBC. Scale bar 2µm.

Figure 4: **Localization of MAHRP2 and RESA in MESA KO infected red blood cells.** A: Immunofluorescence assay labelling 3D7 and MESA KO iRBCs with α-MAHRP2 antibody. Scale bar 2µm. B: Immunofluorescence microscopy labelling of 3D7 and MESA KO ring and trophozoite iRBCs with α-MESA and α-RESA antibody. Scale bar 2µm.

Figure 1

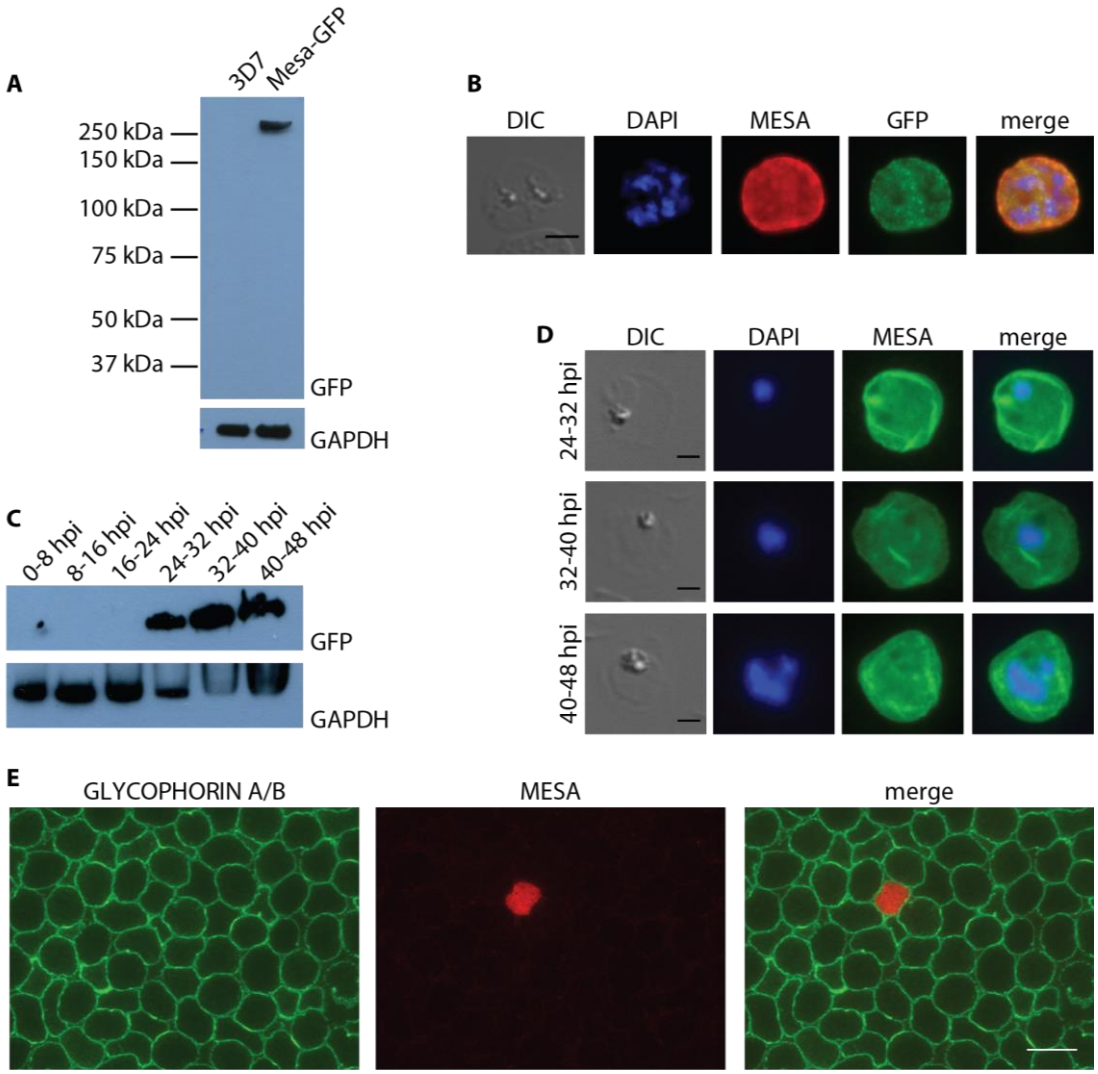
A
3D7
Mesa-GFP
250 kDa
150 kDa
100 kDa
75 kDa
50 kDa
37 kDa
GFP
GAPDH
B
DIC
DAPI
MESA
GFP
merge
C
0-8 hpi
8-16 hpi
16-24 hpi
24-32 hpi
32-40 hpi
40-48 hpi
GFP
GAPDH
D
DIC
DAPI
MESA
merge
24-32 hpi
32-40 hpi
40-48 hpi
E
GLYCOPHORIN A/B
MESA
merge

Figure 2

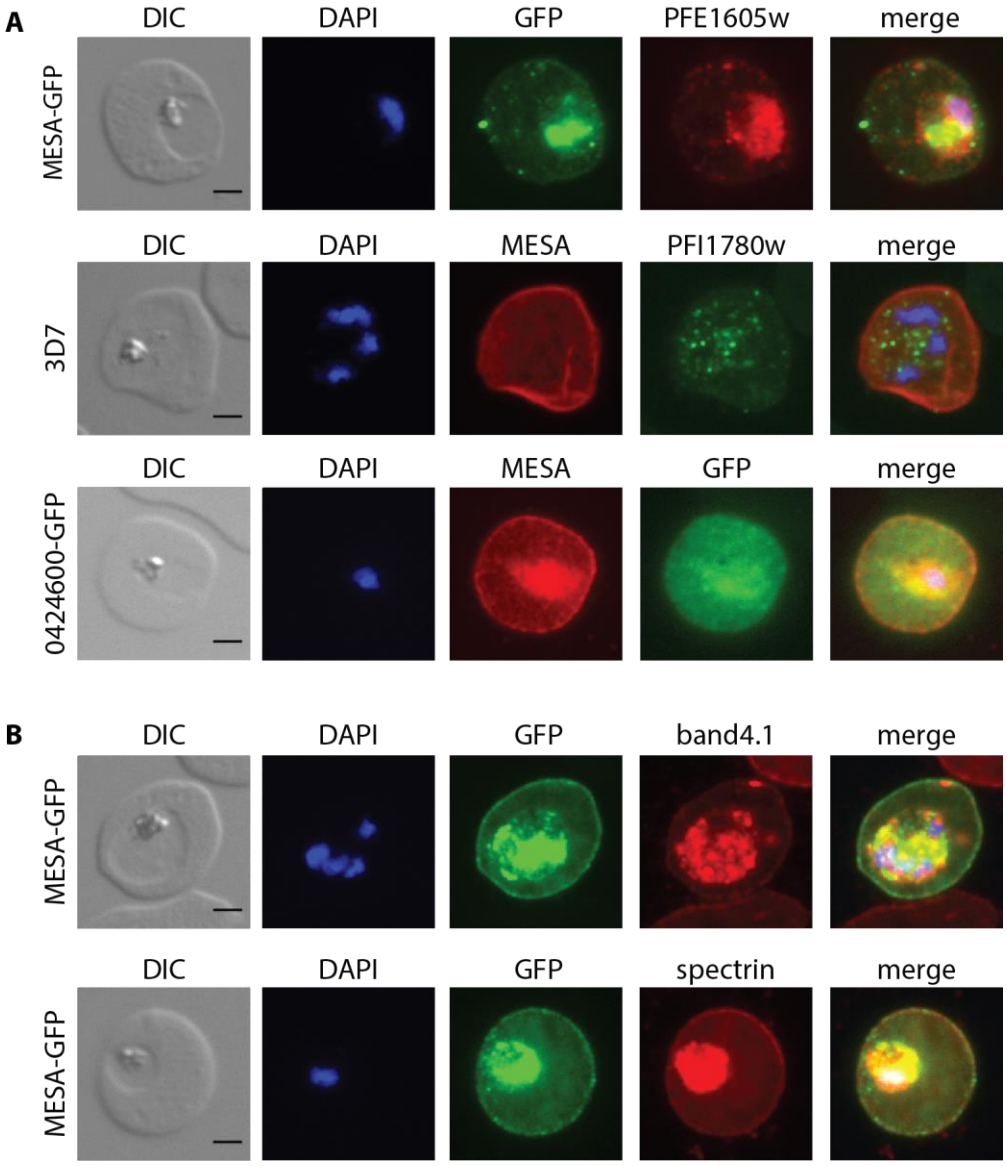
A
DIC
DAPI
GFP
PFE1605w
merge
MESA-GFP
DIC
DAPI
MESA
PFI1780w
merge
3D7
DIC
DAPI
MESA
GFP
merge
0424600-GFP
B
DIC
DAPI
GFP
band4.1
merge
MESA-GFP
DIC
DAPI
GFP
spectrin
merge
MESA-GFP

Figure 3

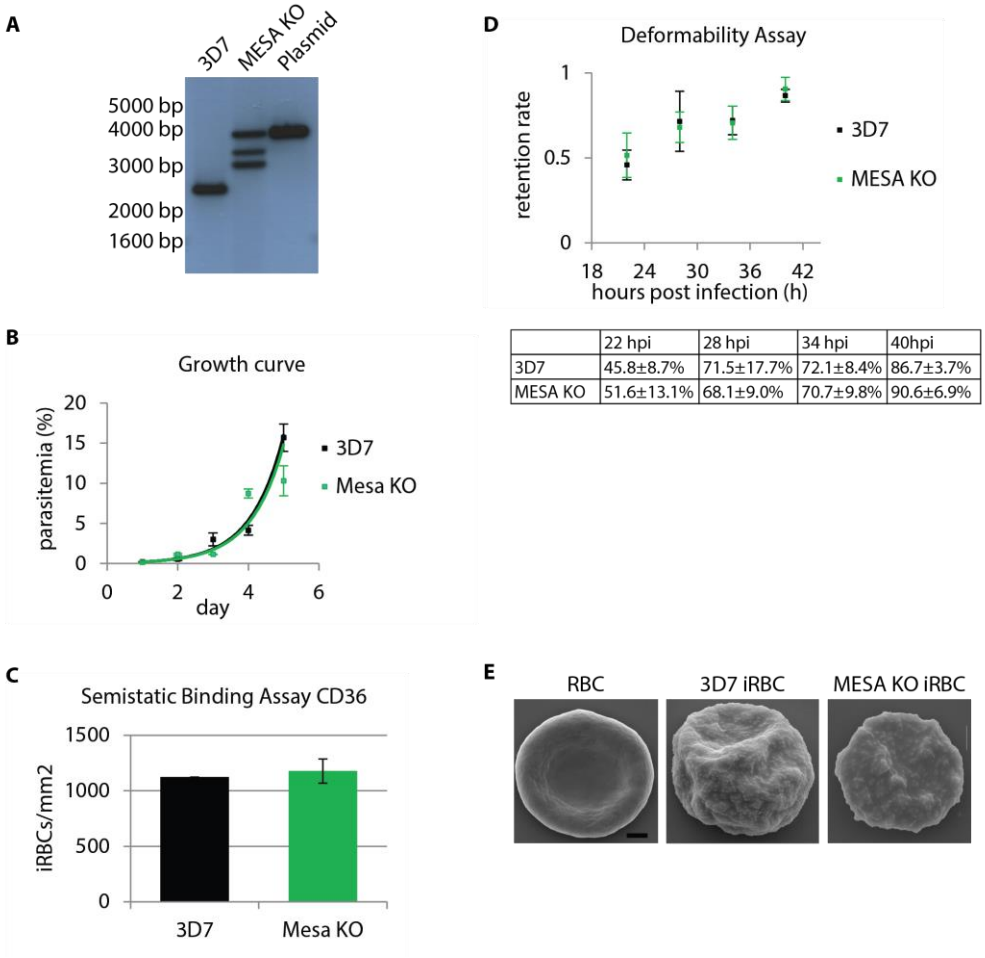

	22 hpi	28 hpi	34 hpi	40hpi
3D7	45.8±8.7%	71.5±17.7%	72.1±8.4%	86.7±3.7%
MESA KO	51.6±13.1%	68.1±9.0%	70.7±9.8%	90.6±6.9%

Figure 4

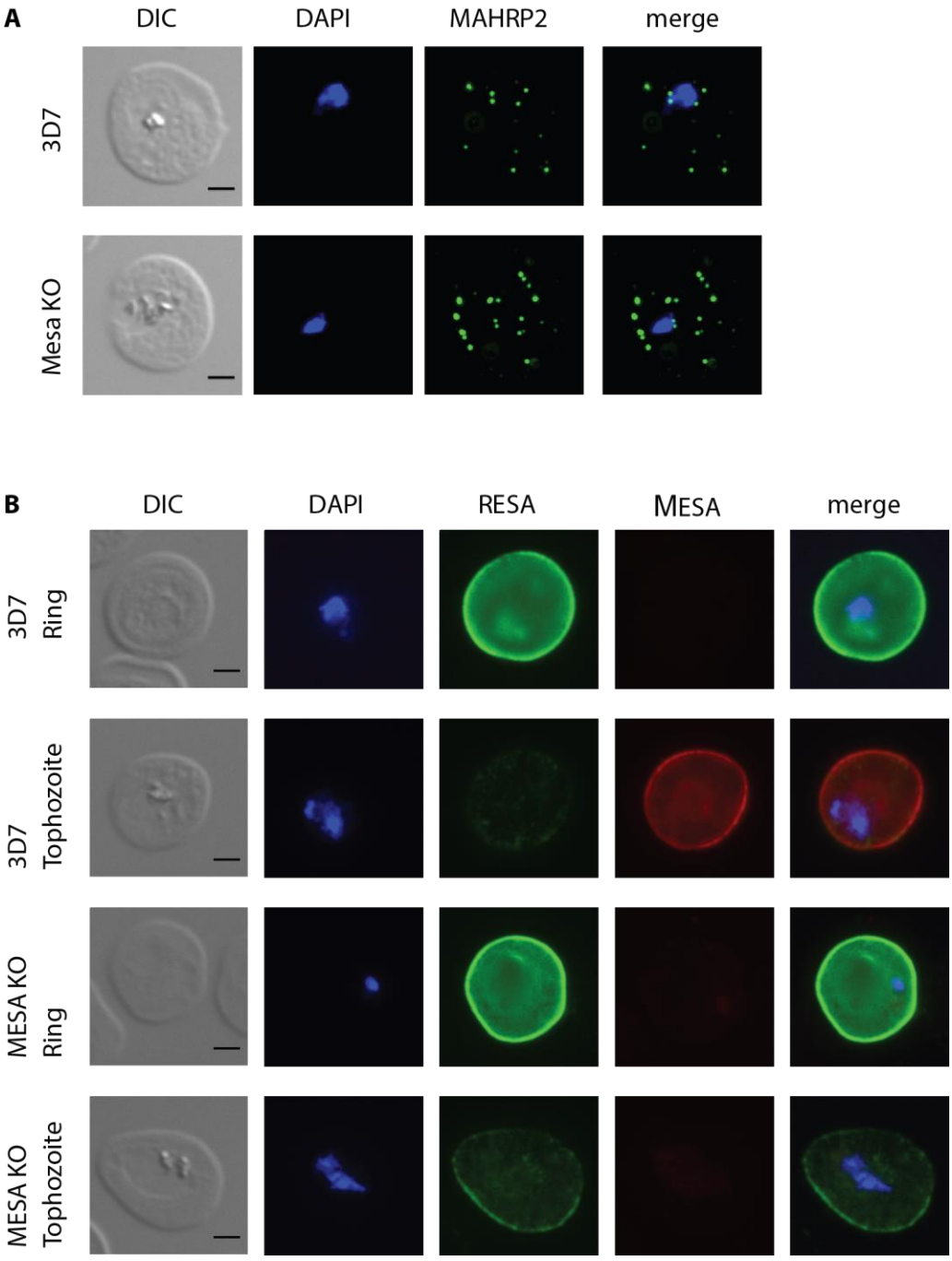
A
DIC
DAPI
MAHRP2
merge
3D7
Mesa KO
B
DIC
DAPI
RESA
MESA
merge
3D7 Ring
3D7 Tophozoite
MESA KO Ring
MESA KO Tophozoite

Chapter 4

Characterization of the *Plasmodium falciparum* Sporozoite Threonine and Asparagine-Rich Protein (STARP) in the intraerythrocytic cycle

Introduction

The Sporozoite Threonine and Asparagine-Rich Protein (STARP, PF3D7_0702300) was first described on the surface of *Plasmodium falciparum* sporozoites (Fidock et al., 1994a). Additionally, STARP was reported to be expressed in liver stages and early ring stages (Fidock et al., 1994a, Bozdech et al., 2003). STARP is also present in other *Plasmodium* species and has a highly conserved structure. The 78kDa protein contains 45-amino acid repeats which are highly enriched for asparagine and threonine being eponymous for it. These repeats are followed by multiple interspersed motifs of decapeptide repeats (Fidock et al., 1994b) and a C-terminal non-repetitive sequence. Several phosphorylation sites were predicted in the STARP protein (Treeck et al., 2011).

STARP is regarded as a potential pre-erythrocytic stage vaccine candidate due to its immunogenicity in various animal models and humans (Fidock et al., 1997, Lalvani et al., 1996, Perlaza et al., 1998). Further, STARP antibodies from malaria-exposed individuals were found to be efficient in blocking sporozoites from entering hepatocytes *in vitro* (Fidock et al., 1997, López et al., 2003).

We have identified STARP in intraerythrocytic stages by co-immunoprecipitation studies of tethers with antibodies directed against the exported protein MAHRP2. STARP contains a PEXEL motif and is thus putatively exported to the host cell. Episomal expression of STARP-GFP indeed showed that the protein is exported and localizes partially to Maurer's clefts. However, no specific localization to tethers was observed (unpublished).

In this study we aimed at the characterization of STARP in the intraerythrocytic life cycle by investigating the endogenous protein. To this end a GFP-tag was introduced at the C-terminal end of STARP by CRISPR/Cas9-selection-linked integration (SLI) (Ghorbal et al., 2014, Birnbaum et al., 2017) genome editing technology. In addition, a STARP knock out cell line was generated by single cross-over recombination and functional protein studies were performed.

Methods

Cell culture and transfections

P. falciparum 3D7 was cultured and transfected as described (Moll et al., 2013). Transfected parasites were positively selected with 10nM WR99210 (Jacobs Pharmaceuticals, Cologne, Germany).

Plasmid constructs

The STARP-GFP cell line was generated using a combined CRISPR/Cas9-SLI technology approach. Homology regions between 300-1000bp were designed, the gRNA was chosen with the CHOPCHOP software (Labun et al., 2016, Montague et al., 2014), and the gRNA recognition sequence in the 5' homology region was mutated to avoid (re)cleavage of successfully tagged endogenous protein. The homology regions and gRNA were PCR amplified using primers listed in Supplementary Table 1 and cloned into pCRISPR_GFP2ABSD using the In-Fusion® HD Cloning Kit (Clontech® Laboratories, Inc.). pCRISPR_GFP2ABSD contains the Cas9, the gRNA, and the integration cassette flanked by the 5' and 3' homology regions. The integration cassette consists of the GFP-tag and a *bsd* selection marker separated by a 2A skip peptide (Szymczak et al., 2004) and a terminator. The selectable marker lacks a promotor and can only be expressed after successful integration into the target locus. The skip peptide triggers a ribosomal skip mechanism and thus impairs normal peptide bond formation preventing the attachment of the selection marker to the target protein (Donnelly et al., 2001).

The STARP KO cell line was generated by single cross-over recombination. Thereby a *hDHFR* selection marker disrupting the *starp* gene was introduced into the parasite genome via a homologous targeting sequence. To this end a stretch of the *starp* gene was PCR amplified using primers listed below and cloned with *EcoRI* and *BamHI* into the pH-KO plasmid. After transfection, on/off drug selection cycling was performed to select for stably integrated constructs and remove residual episomal constructs.

Southern blot analysis

Southern blot analysis was performed to show *starp* disruption in the pH-KO-STARP plasmid transfected parasites. Genomic DNA was isolated by phenol/chloroform extraction of saponin lysed parasites. gDNA was digested with *AvaI* & *HincII* restriction enzymes, separated on a 0.8% agarose gel and transferred onto a Amersham Hybond-N+ membrane (GEHealthcare). Blots were probed with ^{32}P-dATP-labelled probe fragments. The probe was the *starp* homologous targeting sequence used for pH-KO plasmid contruction.

Western blot analysis

Parasite saponin lysates were obtained from 10ml culture (5% hematocrit, 5-10% parasitemia (Pachlatko et al., 2010) and run on 4-12% Bis/Tris precast gels (NuPAGE®, Life Technologies) according to the manufacturers' protocol (2017). Protein transfer was performed with the iBlot 2.0 onto a 0.2µm pore size nitrocellulose membrane (Life Technologies). Subsequently, the membrane was blocked with 10% skimmed milk/TNT (0.1% Tween in 100mM Tris, 150mM NaCl) and probed with the first antibody diluted in 3% skimmed milk/TNT at room temperature for 2h-O/N. After 6 washes for 5min with TNT the secondary antibody conjugated to HRP was incubated in the respective dilution in 3% skimmed milk/TNT for 2h at room temperature. After another 6 washes for 5min with TNT the signal was detected by Super Signal West Pico Chemiluminescent Substrate (Thermo Scientific) or LumiGlo Reserve Chemiluminescent Substrate (Seracare) according to the manufacturers protocol.

The antibodies used were: mouse α-GFP 1:250 (Roche), mouse α-GAPDH 1:20'000 (Daubenberger et al., 2003), goat α-mouse-HRP 1:20'000 (Pierce).

Fluorescence microscopy

Thin blood smears of infected parasite cultures were fixed in ice-cold 60% methanol/40% acetone for 2min. After air-drying of the smear, a small circle was drawn with a hydrophobic pen and the respective area was blocked with 3% BSA/PBS for 1h at room temperature in a humidified chamber. Then, the cells were incubated with mouse α-MAHRP1 (Spycher et al., 2003) (1:100), rabbit α-MAHRP2 (Pachlatko et al., 2010) (1:100), mouse α-ATS (1:50), mouse α-GFP (Roche, 1:100) in 3% BSA/PBS for minimum 2h at room temperature in a humidified chamber. After 3 washes with 3% BSA/PBS for 7min the secondary antibodies (goat α-mouse Alexa488, goat α-rabbit Alexa488, goat α-rabbit Alexa568, goat α-rat Alexa568; all Invitrogen, 1:200) were applied in the appropriate dilution in 3% BSA/PBS for minimum 1h at room temperature in a humidified chamber. After another 3 wash steps with 3% BSA/PBS for 7min each, a coverslip was mounted with 2µl VECTASHIELD® with DAPI (Vector Laboratories Inc.). For imaging a 63x oil-immersion lens (1.4 numerical aperture) on a Leica 5000 B microscope was used. The images were obtained and analyzed with Leica ApplicationSuite 4.4. and Fiji (Schindelin et al., 2012).

Growth assay

Asynchronous parasite infected cell cultures were set up at 0.2% parasitemia. Parasitemia was determined by flow cytometry and followed over 5 days. Parasites were stained with SYBR® Green I nucleic acid gel stain (Sigma-Aldrich) 1:5000 for 20min at 37°C in the dark, washed 3x with culture medium and 100'000 cells were assessed with a BD FACSCalibur. The experiment was performed in biological triplicates, standard deviations of parasitemias were calculated and exponential curves fitted to the data points.

Binding assay

Semi-static binding assays were performed as published before (Oberli et al., 2016). Human CD36 recombinant protein (Sino Biological, China) was spotted on wells of eight-chamber cell culture glass slides (Falcon, Big Flats, NY, USA) in 50µg/ml concentrations and incubated overnight at 4°C to allow proteins to absorb to the surface. The wells were blocked with 1% BSA/PBS for 1h at 37°C. Parasite cultures were washed twice with RPMI-HEPES and spotted onto immobilized CD36 and cultured for 2h under continuous and simultaneous shaking (140 rpm, proBlot 25 Rocker; Labnet International Inc., NY, USA) (105 rpm, Lab-Therm LT-W, Kühner, Switzerland) at 37°C. Non-bound erythrocytes were removed by six gentle washes with RPMI-HEPES with simultaneous shaking for 2min. Bound iRBCs were fixed with 2% glutaraldehyde in RPMI-HEPES overnight, stained with 10% Giemsa for 1h and microscopically counted. Results are shown as mean number of parasites bound per square millimetre and normalized to 1% parasitaemia. The experiment was performed in triplicates.

Results and Discussion

STARP is expressed in the intraerythrocytic lifecycle and exported to the host cytosol

In order to analyze STARP expression, a GFP-tag at the STARP C-terminus was introduced with a combined CRISPR/Cas9-SLI approach. Correct integration of the tag-cassette into the genome was assessed by PCR (Figure 1A). Then, Western blot analysis was performed to check protein expression (Figure 1B). STARP-GFP was detected at a much smaller size (approx. 45kDa) as the calculated molecular weight of 95kDa. We excluded protein degradation during sample preparation by handling all samples in presence of protease

inhibitor cocktail and at 4°C. Therefore, we suggest that the protein is processed by the parasite.

By fluorescence microscopy STARP-GFP was found to be exported to the iRBC cytosol and localizing in a dotted manner (Figure 1C). This confirms previous findings with episomally expressed STARP-GFP and indicates that the PEXEL motif is functional (unpublished).

Time course Western blot analysis showed STARP-GFP expression in the first half of the intraerythrocytic life cycle (Figure 1D). The protein expression therefore reflects nicely the transcriptome data from Bozdech et al. (2003).

STARP partially localizes to Maurer's clefts

By co-labeling immunofluorescence assays the localization of STARP-GFP was investigated. As very long exposure times were needed to detect the STARP-GFP signal, it might be speculated that either STARP-GFP is weakly expressed or the GFP-tag is not accessible to the antibody (due to cleavage or protein folding). For the latter case a change of tag could help to overcome the problem of weak signal. However, we found partial co-labeling of STARP-GFP with MAHRP1 indicating a transient or partial localization to Maurer's clefts (Figure 2A). No co-labeling of STARP-GFP and MAHRP2 was observed (Figure 2B), and therefore it can be excluded that STARP-GFP is a tether component or tether-associated protein. This is in accordance with previous observations with episomally expressed STARP-GFP (unpublished).

STARP functional analysis

To investigate the function of STARP, we generated a 5' single cross-over STARP knock out parasite line. Successful knock out (integration of a *hDHFR* cassette to disrupt the gene) was confirmed by Southern blot (Figure 3A). There is some residual plasmid in the knock out parasite cell line, which is usually lost over the course of several generations. The knock out was viable indicating that STARP is dispensable for the parasite in culture. We assessed growth of the STARP knock out cell line and no significant growth difference was observed compared to wildtype 3D7 parasites (Figure 3B).

A CD36 semi-static binding assay was performed to investigate whether STARP is involved in PfEMP1 transport or PfEMP1 anchoring to the iRBC surface. There was no significant difference in binding to CD36 between the STARP knock out strain and wildtype 3D7 iRBCs

(Figure 3C). The parasites were not preselected to express CD36 binding PfEMP1 variants. However, with previous binding assays with CD36 preselected parasites we have observed binding in the same range (Oberli et al., 2016). Thus we assume that both parasite lines express a CD36 binding PfEMP1 variant. By immunofluorescence assay we checked PfEMP1 localization in wildtype 3D7 and STARP knock out iRBC (Figure 3D). There is a stronger ATS signal observed within the parasite of STARP knock out iRBCs. Also the ATS signal at Maurer's clefts is more pronounced in wildtype 3D7 iRBCs compared to STARP KO iRBCs. With great care, this may indicate a PfEMP1 transport defect in STARP deficient iRBCs.
Further we analyzed the localization of MAHRP1 (Figure 4A) and MAHRP2 (Figure 4B) in STARP knock out cells by immunofluorescence microscopy. We didn't find a difference between knock out and wildtype parasites. This indicates that STARP absence is not affecting the localization of MAHRP1 and MAHRP2, and STARP probably has no role in their trafficking.

Summary and Conclusion

We have endogenously GFP-tagged STARP and found that STARP is (weakly) expressed and exported in the intraerythrocytic cycle, and partially localizing to Maurer's clefts. The Western blot results suggested that the protein is processed as we detected it at a significantly smaller size than anticipated by molecular weight calculations. By introducing the endogenous tag fused to a resistance cassette we apply a certain pressure on the parasite to express the protein in order to survive and are maybe looking at an artefact expression that is not reflecting the natural parasite situation. However, what holds against this argument is the presence of STARP transcripts in the intraerythrocytic life cycle (Bozdech et al., 2003) and the identification of STARP as a phosphoprotein in schizonts (Treeck et al., 2011). Still, we were not able to define the function of STARP in the *P. falciparum* intraerythrocytic life cycle. We assessed a putative function in PfEMP1 transport by performing a CD36 binding assay and ATS immunofluorescence assays with STARP knock out parasites. Nor in this neither in a localization study with MAHRP1 and MAHRP2 we found a distinct phenotype for the STARP knock out parasites.

Contribution and Acknowledgements

Esther Mundwiler-Pachlatko generated the 5' single cross-over STARP knock out parasite line. Sebastian Rusch performed Southern blot analysis. We are thankful to Brian Cooke for providing the α-ATS-antibody.

References

BIRNBAUM, J., FLEMMING, S., REICHARD, N., SOARES, A. B., MESEN-RAMIREZ, P., JONSCHER, E., BERGMANN, B. & SPIELMANN, T. 2017. A genetic system to study Plasmodium falciparum protein function. *Nat Methods,* 14**,** 450-456.

BOZDECH, Z., LLINAS, M., PULLIAM, B. L., WONG, E. D., ZHU, J. & DERISI, J. L. 2003. The transcriptome of the intraerythrocytic developmental cycle of Plasmodium falciparum. *PLoS Biol,* 1**,** E5.

DAUBENBERGER, C. A., DIAZ, D., CURCIC, M., MUELLER, M. S., SPIELMANN, T., CERTA, U., LIPP, J. & PLUSCHKE, G. 2003. Identification and characterization of a conserved, stage-specific gene product of Plasmodium falciparum recognized by parasite growth inhibitory antibodies. *Infect Immun,* 71**,** 2173-81.

DONNELLY, M. L., LUKE, G., MEHROTRA, A., LI, X., HUGHES, L. E., GANI, D. & RYAN, M. D. 2001. Analysis of the aphthovirus 2A/2B polyprotein 'cleavage' mechanism indicates not a proteolytic reaction, but a novel translational effect: a putative ribosomal 'skip'. *J Gen Virol,* 82**,** 1013-25.

FIDOCK, D. A., BOTTIUS, E., BRAHIMI, K., MOELANS, I. I. M. D., AIKAWA, M., KONINGS, R. N. H., CERTA, U., OLAFSSON, P., KAIDOH, T., ASAVANICH, A., GUERIN-MARCHAND, C. & DRUILHE, P. 1994a. Cloning and characterization of a novel *Plasmodium falciparum* sporozoite surface antigen, STARP. *Molecular and Biochemical Parasitology,* 64**,** 219-232.

FIDOCK, D. A., PASQUETTO, V., GRAS, H., BADELL, E., ELING, W., BALLOU, W. R., BELGHITI, J., TARTAR, A. & DRUILHE, P. 1997. Plasmodium falciparum sporozoite invasion is inhibited by naturally acquired or experimentally induced polyclonal antibodies to the STARP antigen. *Eur J Immunol,* 27**,** 2502-2513.

FIDOCK, D. A., SALLENAVE-SALES, S., SHERWOOD, J. A., GACHIHI, G. S., FERREIRA-DA-CRUZ, M. F., THOMAS, A. W. & DRUILHE, P. 1994b. Conservation of the Plasmodium falciparum sporozoite surface protein gene, STARP, in field isolates and distinct species of Plasmodium. *Mol Biochem Parasitol,* 67**,** 255-67.

GHORBAL, M., GORMAN, M., MACPHERSON, C. R., MARTINS, R. M., SCHERF, A. & LOPEZ-RUBIO, J. J. 2014. Genome editing in the human malaria parasite Plasmodium falciparum using the CRISPR-Cas9 system. *Nat Biotechnol,* 32**,** 819-21.

LABUN, K., MONTAGUE, T. G., GAGNON, J. A., THYME, S. B. & VALEN, E. 2016. CHOPCHOP v2: a web tool for the next generation of CRISPR genome engineering. *Nucleic Acids Res,* 44**,** W272-6.

LALVANI, A., AIDOO, M., KIBATALA, P., TANNER, M. & HILL, A. V. 1996. Cytotoxic T lymphocytes to Plasmodium falciparum epitopes in an area of intense and perennial transmission in Tanzania. *Eur J Immnol,* 26**,** 773-779.

LÓPEZ, R., GARCIA, J., PUENTES, A., CURTIDOR, H., OCAMPO, M., VERA, R., RODRIGUEZ, L. E., SUAREZ, J., URQUIZA, M., RODRíGUEZ, A. L., REYES, C. A., GRANADOS, C. G. & PATARROYO, M. E. 2003. Identification of specific Hep G2 cell binding regions in Plasmodium falciparum sporozoite–threonine–asparagine-rich protein (STARP). *Vaccine,* 21**,** 2404-2411.

MOLL, K., KANEKO, A., SCHERF, A. & WAHLGREN, M. 2013. Methods in Malaria Research (MR4/ATCC) 6th Edition.

MONTAGUE, T. G., CRUZ, J. M., GAGNON, J. A., CHURCH, G. M. & VALEN, E. 2014. CHOPCHOP: a CRISPR/Cas9 and TALEN web tool for genome editing. *Nucleic Acids Res,* 42**,** W401-7.

OBERLI, A., ZURBRUGG, L., RUSCH, S., BRAND, F., BUTLER, M. E., DAY, J. L., CUTTS, E. E., LAVSTSEN, T., VAKONAKIS, I. & BECK, H. P. 2016. Plasmodium falciparum Plasmodium helical interspersed subtelomeric proteins contribute to cytoadherence and anchor P. falciparum erythrocyte membrane protein 1 to the host cell cytoskeleton. *Cell Microbiol,* 18**,** 1415-28.

PACHLATKO, E., RUSCH, S., MULLER, A., HEMPHILL, A., TILLEY, L., HANSSEN, E. & BECK, H. P. 2010. MAHRP2, an exported protein of Plasmodium falciparum, is an essential component of Maurer's cleft tethers. *Mol Microbiol,* 77**,** 1136-52.

PERLAZA, B. L., AREVALO-HERRERA, M., BRAHIMI, K., QUINTERO, G., PALOMINO, J. C., GRAS-MASSE, H., TARTAR, A., DRUILHE, P. & HERRERA, S. 1998. Immunogenicity of four Plasmodium falciparum preerythrocytic antigens in Aotus lemurinus monkeys. *Infect Immun,* 66**,** 3423-3428.

SCHINDELIN, J., ARGANDA-CARRERAS, I., FRISE, E., KAYNIG, V., LONGAIR, M., PIETZSCH, T., PREIBISCH, S., RUEDEN, C., SAALFELD, S., SCHMID, B., TINEVEZ, J. Y., WHITE, D. J., HARTENSTEIN, V., ELICEIRI, K., TOMANCAK, P. & CARDONA, A. 2012. Fiji: an open-source platform for biological-image analysis. *Nat Methods,* 9**,** 676-82.

SPYCHER, C., KLONIS, N., SPIELMANN, T., KUMP, E., STEIGER, S., TILLEY, L. & BECK, H. P. 2003. MAHRP-1, a novel Plasmodium falciparum histidine-rich protein, binds ferriprotoporphyrin IX and localizes to the Maurer's clefts. *J Biol Chem,* 278**,** 35373-83.

SZYMCZAK, A. L., WORKMAN, C. J., WANG, Y., VIGNALI, K. M., DILIOGLOU, S., VANIN, E. F. & VIGNALI, D. A. 2004. Correction of multi-gene deficiency in vivo using a single 'self-cleaving' 2A peptide-based retroviral vector. *Nat Biotechnol,* 22**,** 589-94.

TREECK, M., SANDERS, J. L., ELIAS, J. E. & BOOTHROYD, J. C. 2011. The phosphoproteomes of Plasmodium falciparum and Toxoplasma gondii reveal unusual adaptations within and beyond the parasites' boundaries. *Cell Host Microbe,* 10**,** 410-9.

Supplementary Table 1

STARP-GFP 5HR fw	5'CAACAGATAATGATAATGCAGATAC
STARP-GFP 5HR rv (incl. mut)	5'ATTAATTAACATATATAAAGCAAAAGCTAAAATTAATTTTCGT
STARP-GFP 3HR fw	5'TAAATACTCTATGTAGTTTTTATGTACTA
STARP-GFP 3HR rv	5'GGTAATTATTATATGTATTTTTG
STARP-GFP gRNA	5'GAAGTAATATATAAATATGT
STARP KO fw	5'attagaattcATACATATTTTTTATAGGACAGCC
STARP KO rv	5' attaggatccCACTAGTATTTTCTGTTGAATTTG

Figure legends

Figure 1: **Endogenous STARP-GFP expression**. A: The GFP2ABSD cassette was successfully integrated into the genome of STARP-GFP as shown by PCR. Primers were chosen outside the homology regions. The expected band sizes in 3D7 are 1530bp and for STARP-GFP cell line 3364bp B: Western blot analysis with α-GFP antibody shows expression of STARP-GFP in the STARP-GFP and not in 3D7 parasite lysates. α-GAPDH antibody as loading control C: Immunofluorescence microscopy reveals punctuate STARP-GFP localization in the iRBC cytosol of STARP-GFP parasites probed with α-GFP antibody. Scale bar 2µm. D: Time course Western blot with α-GFP antibody of STARP-GFP parasite lysates shows expression of STARP-GFP in ring stages. α-GAPDH was used as loading control.

Figure 2: **Localization of endogenous STARP-GFP**. A: Immunofluorescence microscopy co-labeling STARP-GFP with α-GFP and α-MAHRP1 antibodies. B: Immunofluorescence microscopy co-labeling STARP-GFP with α-GFP and α-MAHRP2 antibody. Scale bar 2µm.

Figure 3: **Phenotypical analysis of STARP KO parasites**. A: Southern blot confirming the replacement of STARP with the *hDHFR* cassette. Digested gDNA was run on an agarose gel and then probed with the 3' integration stretch. The expected band sizes are for 3D7 1651bp, for STARP KO 3620bp and 2211bp and for the plasmid (P) 4180bp. B: Growth assay of 3D7 and STARP KO parasites over 5 days, parasitemia was determined by FACS analysis, exponential curve was fitted. Shown are mean of triplicates with standard deviation. C: CD36 semi-static binding assay of 3D7 and STARP KO. Shown are mean of triplicates with standard deviation. D: Immunofluorescence microscopy labeling of 3D7 and STARP KO parasites with α-ATS antibody. Scale bar 2µm.

Figure 4: **Localization of MAHRP1 and MAHRP2 in STARP KO parasites**. A: Immunofluorescence microscopy labeling of 3D7 and STARP KO parasites with α-MAHRP1 antibody. B: Immunofluorescence microscopy labelling of 3D7 and STARP KO parasites with α-MAHRP2 antibody. Scale bar 2µm.

Figure 1

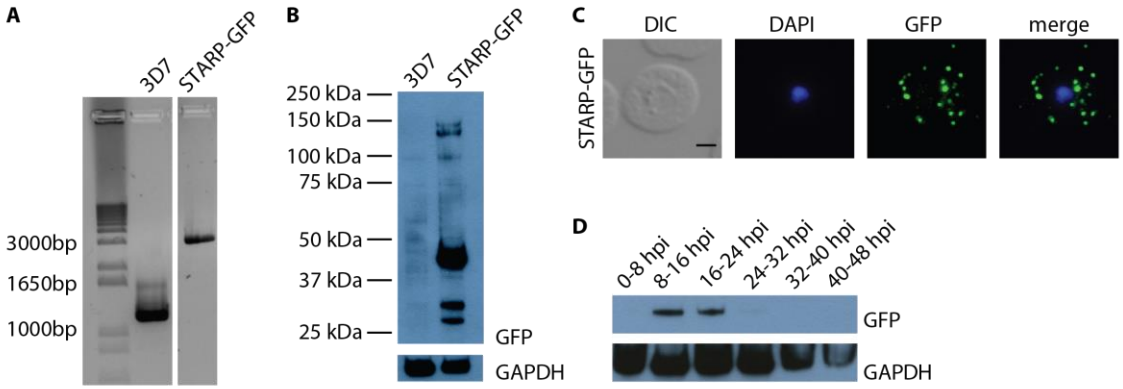

Figure 2

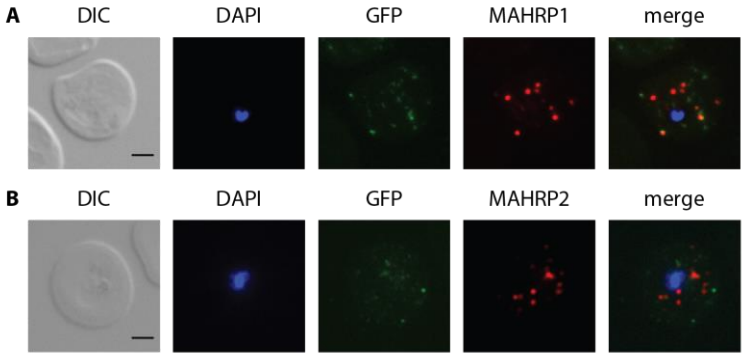

Figure 3

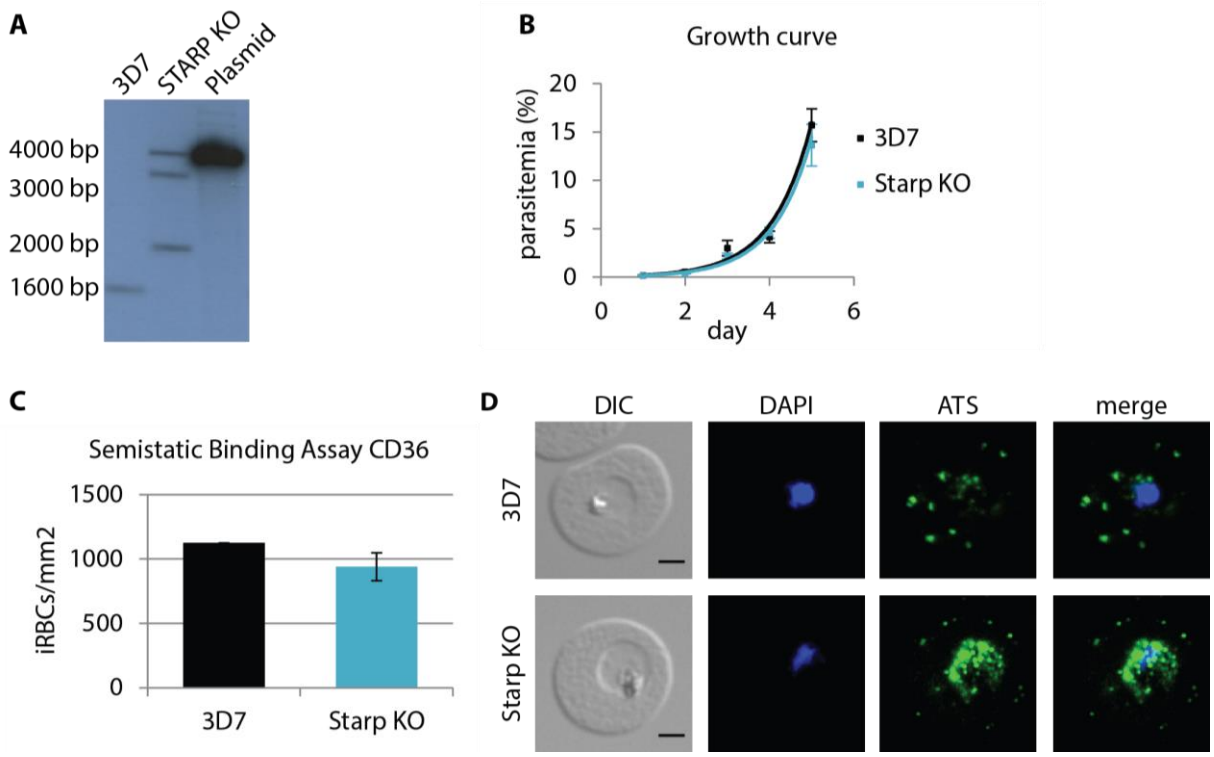

Figure 4

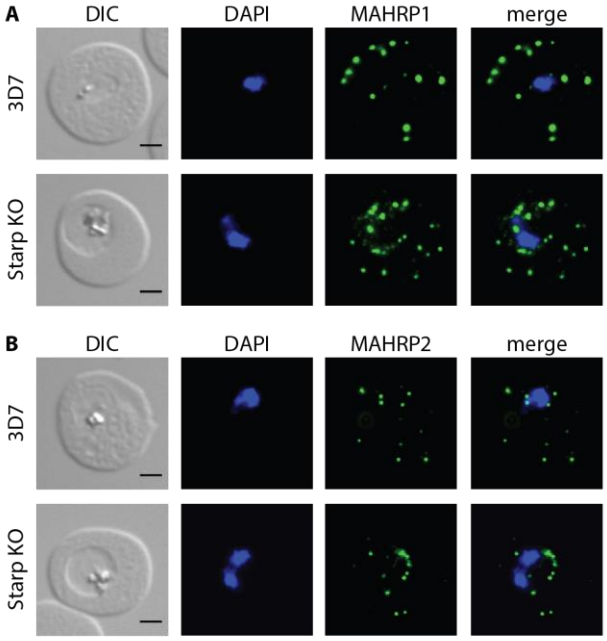

Chapter 5

Spiroindolone-enhanced rigidity in *Plasmodium* infected erythrocytes leads to rapid parasite removal by the spleen

Data in preparation for manuscript

Spiroindolone-enhanced rigidity in Plasmodium infected erythrocytes leads to rapid parasite removal by the spleen

---

Introduction

Malaria is a devastating disease affecting millions of people. In order to maintain the positive trend of decreasing disease burden during the last 20 years and to strive for elimination of malaria, continuous effort is needed. Particularly, a good development pipeline for new, effective drugs is essential to counter arising resistance against existing treatment. A promising new class of antimalarials are spiroindolones which have been shown to act rapidly and effectively against *Plasmodium falciparum and P. vivax* (Rottmann et al., 2010, White et al., 2014). Spiroindolones are active against the pathology-relevant asexual intraerythrocytic stages (Lakshminarayana et al., 2015) as well as against the transmission-relevant sexual stages (van Pelt-Koops et al., 2012). Spiroindolones target the cation pump ATPase PfATP4 localized in the parasite plasma membrane thereby disrupting the ion homeostasis inside the parasite (Spillman et al., 2013). The altered ion homeostasis not only has metabolic consequences on the parasite but also leads to altered biomechanical properties of the infected red blood cell (iRBC) (Zhang et al., 2016). The (uninfected) erythrocyte is a highly deformable cell as it needs to pass through the microvasculature. Erythrocytes are regularly passing the spleen where their deformability is assessed in the red pulp and abnormal e.g. *P. falciparum* iRBCs are removed from circulation. *P. falciparum* iRBC deformability decreases with progressing life cycle stages of the asexual parasite (Cranston et al., 1984). While *P. falciparum* trophozoite and schizont iRBCs avoid passage through the spleen by cytoadherence, *P. falciparum* ring iRBCs are transiting the spleen. Drugs that enhance the rigidification of iRBCs, especially in ring stages can enhance the filtering function of the spleen to remove iRBCs. The clinical spiroindolone compound cipargamin (KAE609) was reported to increase sphericity and reduce deformability of *P. falciparum* and *P. vivax* ring-infected RBC (Zhang et al., 2016).

Here we investigated changes in deformability of *P. falciparum* iRBC upon exposure to the spiroindolone KAF246, an analog of KAE609 (Yeung et al., 2010). For this we performed microsphiltration experiments, to assess *P. falciparum* iRBC deformability by mimicking the human spleen in vitro (Deplaine et al., 2011), and we further confirmed the in vitro findings with in vivo experiments using a *P. berghei* mouse model visualizing splenic clearance. By monitoring the pharmacodynamic effects of KAF246 on circulating *Plasmodium* iRBC we gain additional insight into the mechanism of the observed rapid parasite clearance upon spiroindolone treatment.

Methods

Plasmodium falciparum culture and reagents

P. falciparum 3D7 was cultured according to standard procedures (Moll et al., 2013). Parasite asexual stages were synchronized by MACS column (Miltenyi Biotec) (Ribaut et al., 2008) to a 4h time window. Gametocyte experiments were performed with the 3D7/pHcamGDV1-GFPDD cell line as described (Filarsky et al., 2018). Briefly, this cell line over-expresses the master regulator gene GDV1 in an inducible manner. Addition of 1.25mM Shield-1 (Viva Biotech (Shanghai) Ltd.) to a synchronously growing ring stage parasite culture for 48h stabilizes GDV1 and thus triggers gametocytogenesis. After reinvasion, the cultures were kept 5 days on medium containing 50mM N-Acetylglucosamine (Sigma) to kill remaining asexual blood stages and to obtain a pure gametocyte culture. Afterwards, cultures were maintained with regular medium until harvest.

Microsphiltration

Tightly synchronized parasite cultures were treated with 20nM KAF246 in ring stages (14-18 hpi), trophozoite stages (30-34 hpi), and schizont stages (38-42 hpi). Microsphiltration experiments were performed after 1h, 2h, 4h and 8h of drug addition as described in Lavazec et al. (2013). Parasitemia of the flow-through sample was determined by flow cytometry and compared to the similarly measured parasitemia of the input samples. Parasites were stained with SYBR® Green I nucleic acid gel stain (Sigma-Aldrich) 1:5000 for 20 minutes at 37°C in the dark, washed 3x with culture medium and 100'000 cells were assessed with a BD FACSCalibur. All experiments were performed in technical triplicates. Retention rates (in %) were calculated as 1−(parasitemia flow through sample/parasitemia input sample)×100. Microsphiltration of uninfected erythrocytes was performed as described above. Of the uninfected erythrocytes, a defined fraction of cells was labelled with the green fluorescent membrane stain PKH67 (Sigma-Aldrich) according to manufacturer's protocol. This enabled their monitoring by flow cytometry during the experiment.

Mice/Plasmodium berghei

Mice were infected with $2x10^7$ *P. berghei* PbmCherry$_{hsp70}$ + Luc$_{eef1\alpha}$ parasites (Prado et al., 2015) and treated after 24h with 1x50mg/kg or 1x10mg/kg KAF246 po respectively. Parasitaemia was monitored with the in vivo imaging system (IVIS II, PerkinElmer) to

monitor bioluminescence signal (100 mg/kg of D-luciferin was intravenously injected 3 min before imaging) at 1h, 2h, 4h, 6h, 8h, 24h, 48h, 72h, 144h, 240h post treatment. In addition blood smears were obtained from selected mice and viewed under a microscope after Giemsa staining. Animal experiments were carried out at the Swiss Tropical and Public Health Institute (Basel, Switzerland), adhering to local and national regulations of laboratory animal welfare in Switzerland (awarded permission no. 1731 and 2566).

Results

To evaluate the stage-specific effect of KAF246 on the deformability of *P. falciparum* iRBCs we performed microsphiltration experiments with highly synchronous asexual parasites. Parasites were treated with 20nM KAF246, which represents approximately 100 fold the IC50 (Lakshminarayana et al., 2015) for 1h, 2h, 4h, and 8h and increased retention rates upon KAF246 treatment were found for all incubation times and for all stages. The control ring stages had retention rates of 18.10%±5.58, 21.29%±6.31, 17.34%±5.92, and 23.08%±5.58 whereas KAF246 treated ring stages had 17.93%±6.70, 22.54%±11.07, 38.67%±9.02, and 44.03%±5.84 retention after 1h, 2h, 4h, and 8h treatment, respectively (Figure 1A). For control trophozoite stages retention rates of 51.80%±11.15, 72.14%±10.59, 68.98%±8.64, and 57.25%±24.72 and for KAF246 treated trophozoite stages retention rates of 69.00%±13.96, 80.04%±12.19, 87.64%±8.88, and 93.94%±4.10 were measured after 1h, 2h, 4h, and 8h, respectively (Figure 1B). Finally, the retention rates observed in control schizont stages were 54.21%±20.57, 61.97%±10.95, 55.41%±7.09, and 60.66%±15.08 versus 73.51%±10.72, 83.03%±7.39, 89.42%±4.71, and 95.64%±6.16 retention in KAF246 treated schizont stages after 1h, 2h, 4h, and 8h, respectively (Figure 1C). In summary, short treatment (1 and 2 hours) had no effect on the retention rate of ring stage parasites but the retention rate doubled after 4 hours KAF246 exposure. In trophozoite and schizont stages increased retention rates were observed already after 1h of KAF246 exposure. The stiffening effect on trophozoites increased steadily to a maximum after 8h drug exposure. In schizonts the stiffening effect increased more pronounced after 1h than in trophozoites but the maximum increase was slightly lower than in trophozoites.

In order to test the effect of KAF246 on the deformability of transmissible parasite stages we performed microsphiltration experiments with *P. falciparum* gametocytes treated with KAF246. No deformability differences between treated and untreated stage III gametocytes

were observed (data not shown), but reduced deformability in KAF246-treated stage V gametocytes was detected. For control stage V gametocytes retention rates of 39.82%±14.12, 36.53%±14.00, and 55.46%±3.48 and for KAF246 treated stage V gametocytes retention rates of 71.71%±5.71, 68.42%±9.10, and 70.34%±2.43 were measured after 1h, 2h, and 4h, respectively (Figure 1D).

Next, we addressed the question whether the observed in vitro rigidity changes upon KAF246 treatment are reflected in enhanced accumulation of iRBCs in the spleen in in vivo experiments. To this end, *P. berghei* PbmCherry$_{hsp70}$ + Luc$_{eef1\alpha}$ infected mice were treated with 50mg/kg or 10mg/kg KAF246 and parasitemia was monitored by bioluminescence (after luciferin injection) after 1h, 2h, 4h, 6h, 8h, 24h, 48h, 3d, 6d, and 10d (Figure 2A). After 2h treatment with KAF246 we observed an increased parasite load in the spleens of treated mice. A dose dependent accumulation was observed when comparing the parasite accumulation in the 50mg/kg and 10mg/kg group after 2h. After 4h and 8h of drug exposure the parasite load in the spleen further increased but was comparable between both dose groups. After 24h only a few parasites were found in the spleen and after 48h KAF246 exposure all treated mice were devoid of detectable parasites. The treated mice were monitored for 10 days after drug administration and recrudescence of parasites was observed after 6 days and 10 days in the 10mg/kg and 50mg/kg treatment group, respectively. Next, we evaluated the stage-specific effect of KAF246 on *P. berghei* by analyzing Giemsa-stained blood smears from the above mouse experiment (Figure 2B and 2C). The blood smears represented the circulating parasite population in the infected mice. In untreated control mice (Figure 2B) we found a parasite population composition of 42% rings/50% trophozoites/8% schizonts after 1h, 43% rings/47% trophozoites/9% schizonts after 2h, 22% rings/63% trophozoites/15% schizonts after 4h, and 26% rings/61% trophozoites/13% schizonts after 8h. In 50mg/kg KAF246 treated mice 48% rings/47% trophozoites /6% schizonts after 1h, 57% rings/43% trophozoites/0% schizonts after 2h, 75% rings/24% trophozoites/1% schizonts after 4h, and 68% rings/32% trophozoites/0% schizonts after 8h drug exposure were observed. In summary, KAF246-treated mice harbored fewer trophozoites and schizonts when compared to untreated control mice suggesting a rapid clearance of older stages.

Discussion

In order to address the hypothesis that the rapid parasite clearance upon KAF246 treatment is due to increased cell rigidity we performed microsphiltration experiments. Our data show that the spiroindolone KAF246 causes a rapid rigidity increase of both asexual and sexual stage *P. falciparum* iRBCs (Figure 1). The stage-specific retention rates we report for untreated ring and trophozoite control parasites are coherent with previously published observations (Sanyal et al., 2012). It is expected that retention rates of the control parasites increase during the experiment according to their progression in the lifecycle (Cranston et al., 1984). Instead, retention rates are not rising over time in all conditions. This may be explained by increased stress of the parasite cultures excerted by the experimental manipulations. Further, we found lower retention rates than expected in the control schizont fraction which might be explained by the early presence of ring stages already observed in Giemsa smears of this fraction perhaps due to the late addition of drug during the life cycle.

We observed that schizonts responded fastest to KAF246 treatment (after 1h) and with highest increase of retention rates. Ring and trophozoite stages reacted with a lower increase and ring stages responded even later (after 4h drug exposure) to KAF246 treatment. Gametocyte development has been reported to be impaired by spiroindolone KAE609 treatment (van Pelt-Koops et al., 2012), and all gametocyte stages have been shown to be susceptible to KAF246 (Plouffe et al., 2016).

Based on the in vitro results with *P. falciparum*, we propose that KAF246-induced rigidity changes of treated iRBCs would lead to an accumulation of iRBCs in the spleen followed by an effective removal from the circulation. This is supported by the observation of a rapid accumulation of *P. bergei* iRBCs in the spleen of mice treated with KAF246 (Figure 2A). We acknowledge that *P. falciparum* and *P. berghei* biology is quite distinct and that the physiology of the human and mouse spleen is slightly different. However, it was reported that metabolic stability of the spiroindolone KAE609 is comparable in humans and rodents (Rottmann et al., 2010). One difference is that *P. berghei* does not cytoadhere, hence all parasite stages pass the spleen regularly. This is reflected in the enumeration of different life cycle stages in the blood of the mice. Therefore it was possible to confirm in vitro pharmacodynamic stage specific differences in vivo where we observed a more rapid depletion of late stage parasites (Figure 2B and C). The in vivo pharmacodynamics (rapid

clearance in the spleen) correlates well with the observations made with microsphiltration experiments in *P. falciparum*.

Cell deformability is influenced by several factors, e.g internal viscosity, membrane and cytoskeleton dynamics, and cell geometry. Therefore it is not surprising that drugs with different mode of actions affect it, e.g. artesunate (Huang et al., 2013) and chloroquine (Huang et al., 2014). Nevertheless, spiroindolones seem to be unique in the way they kill the parasite with the combined effect of inhibiting essential biochemical processes and inducing altered deformability of iRBC with fatal consequences for the parasite leading to rapid clearance from the blood stream and relief for the patients. Notably, this is the first study to investigate the effect of the spiroindolone KAF246 on gametocyte deformability.

In conclusion, this study supports an explanation that the fast parasite clearance in vivo upon treatment with the new spiroindolone compound class might be due to increased rigidity of iRBCs leading to parasite accumulation in the spleen. Our results of stage V gametocyte rigidification upon KAF246 treatment indicate a possible additional effect (besides killing stage V gametocytes) on preventing transmission by fast removal of circulating mature gametocytes by the spleen.

References

CRANSTON, H. A., BOYLAN, C. W., CARROLL, G. L., SUTERA, S. P., WILLIAMSON, J. R., GLUZMAN, I. Y. & KROGSTAD, D. J. 1984. Plasmodium falciparum maturation abolishes physiologic red cell deformability. *Science,* 223**,** 400-3.

DEPLAINE, G., SAFEUKUI, I., JEDDI, F., LACOSTE, F., BROUSSE, V., PERROT, S., BILIGUI, S., GUILLOTTE, M., GUITTON, C., DOKMAK, S., AUSSILHOU, B., SAUVANET, A., CAZALS HATEM, D., PAYE, F., THELLIER, M., MAZIER, D., MILON, G., MOHANDAS, N., MERCEREAU-PUIJALON, O., DAVID, P. H. & BUFFET, P. A. 2011. The sensing of poorly deformable red blood cells by the human spleen can be mimicked in vitro. *Blood,* 117**,** e88-95.

FILARSKY, M., FRASCHKA, S. A., NIEDERWIESER, I., BRANCUCCI, N. M. B., CARRINGTON, E., CARRIO, E., MOES, S., JENOE, P., BARTFAI, R. & VOSS, T. S. 2018. GDV1 induces sexual commitment of malaria parasites by antagonizing HP1-dependent gene silencing. *Science,* 359**,** 1259-1263.

HUANG, S., AMALADOSS, A., LIU, M., CHEN, H., ZHANG, R., PREISER, P. R., DAO, M. & HAN, J. 2014. In vivo splenic clearance correlates with in vitro deformability of red blood cells from Plasmodium yoelii-infected mice. *Infect Immun,* 82**,** 2532-41.

HUANG, S., UNDISZ, A., DIEZ-SILVA, M., BOW, H., DAO, M. & HAN, J. 2013. Dynamic deformability of Plasmodium falciparum-infected erythrocytes exposed to artesunate in vitro. *Integr Biol (Camb),* 5**,** 414-22.

LAKSHMINARAYANA, S. B., FREYMOND, C., FISCHLI, C., YU, J., WEBER, S., GOH, A., YEUNG, B. K., HO, P. C., DARTOIS, V., DIAGANA, T. T., ROTTMANN, M. & BLASCO, F. 2015. Pharmacokinetic-pharmacodynamic analysis of spiroindolone analogs and KAE609 in a murine malaria model. *Antimicrob Agents Chemother,* 59**,** 1200-10.

LAVAZEC, C., DEPLAINE, G., SAFEUKUI, I., PERROT, S., MILON, G., MERCEREAU-PUIJALON, O., DAVID, P. H. & BUFFET, P. 2013. Microsphiltration: a microsphere matrix to explore erythrocyte deformability. *Methods Mol Biol,* 923**,** 291-7.

MOLL, K., KANEKO, A., SCHERF, A. & WAHLGREN, M. 2013. Methods in Malaria Research (MR4/ATCC) 6th Edition.

PLOUFFE, D. M., WREE, M., DU, A. Y., MEISTER, S., LI, F., PATRA, K., LUBAR, A., OKITSU, S. L., FLANNERY, E. L., KATO, N., TANASEICHUK, O., COMER, E., ZHOU, B., KUHEN, K., ZHOU, Y., LEROY, D., SCHREIBER, S. L., SCHERER, C. A., VINETZ, J. & WINZELER, E. A. 2016. High-Throughput Assay and Discovery of Small Molecules that Interrupt Malaria Transmission. *Cell Host Microbe,* 19**,** 114-26.

PRADO, M., EICKEL, N., DE NIZ, M., HEITMANN, A., AGOP-NERSESIAN, C., WACKER, R., SCHMUCKLI-MAURER, J., CALDELARI, R., JANSE, C. J., KHAN, S. M., MAY, J., MEYER, C. G. & HEUSSLER, V. T. 2015. Long-term live imaging reveals cytosolic immune responses of host hepatocytes against Plasmodium infection and parasite escape mechanisms. *Autophagy,* 11**,** 1561-79.

RIBAUT, C., BERRY, A., CHEVALLEY, S., REYBIER, K., MORLAIS, I., PARZY, D., NEPVEU, F., BENOIT-VICAL, F. & VALENTIN, A. 2008. Concentration and purification by magnetic separation of the erythrocytic stages of all human Plasmodium species. *Malar J,* 7**,** 45.

ROTTMANN, M., MCNAMARA, C., YEUNG, B. K., LEE, M. C., ZOU, B., RUSSELL, B., SEITZ, P., PLOUFFE, D. M., DHARIA, N. V., TAN, J., COHEN, S. B., SPENCER, K. R., GONZALEZ-PAEZ, G. E., LAKSHMINARAYANA, S. B., GOH, A., SUWANARUSK, R., JEGLA, T., SCHMITT, E. K., BECK, H. P., BRUN, R., NOSTEN, F., RENIA, L., DARTOIS, V., KELLER, T. H., FIDOCK, D. A., WINZELER, E. A. & DIAGANA, T. T. 2010. Spiroindolones, a potent compound class for the treatment of malaria. *Science,* 329**,** 1175-80.

SANYAL, S., EGEE, S., BOUYER, G., PERROT, S., SAFEUKUI, I., BISCHOFF, E., BUFFET, P., DEITSCH, K. W., MERCEREAU-PUIJALON, O., DAVID, P. H., TEMPLETON, T. J. & LAVAZEC, C. 2012. Plasmodium falciparum STEVOR proteins impact erythrocyte mechanical properties. *Blood,* 119**,** e1-8.

SPILLMAN, N. J., ALLEN, R. J., MCNAMARA, C. W., YEUNG, B. K., WINZELER, E. A., DIAGANA, T. T. & KIRK, K. 2013. Na(+) regulation in the malaria parasite Plasmodium falciparum involves the cation ATPase PfATP4 and is a target of the spiroindolone antimalarials. *Cell Host Microbe,* 13**,** 227-37.

VAN PELT-KOOPS, J. C., PETT, H. E., GRAUMANS, W., VAN DER VEGTE-BOLMER, M., VAN GEMERT, G. J., ROTTMANN, M., YEUNG, B. K., DIAGANA, T. T. & SAUERWEIN, R. W. 2012. The spiroindolone drug candidate NITD609 potently inhibits gametocytogenesis and blocks Plasmodium falciparum transmission to anopheles mosquito vector. *Antimicrob Agents Chemother,* 56**,** 3544-8.

WHITE, N. J., PUKRITTAYAKAMEE, S., PHYO, A. P., RUEANGWEERAYUT, R., NOSTEN, F., JITTAMALA, P., JEEYAPANT, A., JAIN, J. P., LEFEVRE, G., LI, R., MAGNUSSON, B., DIAGANA, T. T. & LEONG, F. J. 2014. Spiroindolone KAE609 for falciparum and vivax malaria. *N Engl J Med,* 371**,** 403-10.

YEUNG, B. K., ZOU, B., ROTTMANN, M., LAKSHMINARAYANA, S. B., ANG, S. H., LEONG, S. Y., TAN, J., WONG, J., KELLER-MAERKI, S., FISCHLI, C., GOH, A., SCHMITT, E. K., KRASTEL, P., FRANCOTTE, E., KUHEN, K., PLOUFFE, D., HENSON, K., WAGNER, T., WINZELER, E. A., PETERSEN, F., BRUN, R., DARTOIS, V., DIAGANA, T. T. & KELLER, T. H. 2010. Spirotetrahydro beta-carbolines (spiroindolones): a new class of potent and orally efficacious compounds for the treatment of malaria. *J Med Chem,* 53**,** 5155-64.

ZHANG, R., SUWANARUSK, R., MALLERET, B., COOKE, B. M., NOSTEN, F., LAU, Y. L., DAO, M., LIM, C. T., RENIA, L., TAN, K. S. & RUSSELL, B. 2016. A Basis for Rapid Clearance of Circulating Ring-Stage Malaria Parasites by the Spiroindolone KAE609. *J Infect Dis,* 213**,** 100-4.

Figure legends

Figure 1: **KAF246 exposure leads to an increase of iRBC deformability in all intraerythrocytic life stages.** Shown are microsphiltration retention rates of tightly synchronized *P. falciparum* ring (A), trophozoite (B), and schizont (C) and stage V gametocyte (D) cultures. Open squares represent untreated control *P. falciparum* iRBCs, filled squares 20nM KAF246 treated *P. falciparum* iRBC after 1h, 2h, 4h, and 8h drug exposure. All experiments were performed in biological triplicates, error bars represent standard deviation.

Figure 2: **KAF246 treatment of mice leads to parasites accumulation in the spleen.** *P. bergei* PbmCherry$_{hsp70}$ + Luce$_{efl\alpha}$ infected mice were treated with 50mg/kg or 10mg/kg KAF246 oral dose and parasitemia was monitored after 1h, 2h, 4h, 8h, 24h, and 48h drug exposure by IVIS bioluminescence (A). Bioluminescence signals were normalized between timepoints. Giemsa smears were prepared concomitant to bioluminescence measurements. They were microscopically analyzed and parasite stages were determined. Shown are ratios of ring (white), trophozoite (shaded), and schizont (black) parasites in control (B) and 50mg/kg KAF246 treated (C) mice. Minimum 100 parasites per smear were stage-assigned.

Figure 1

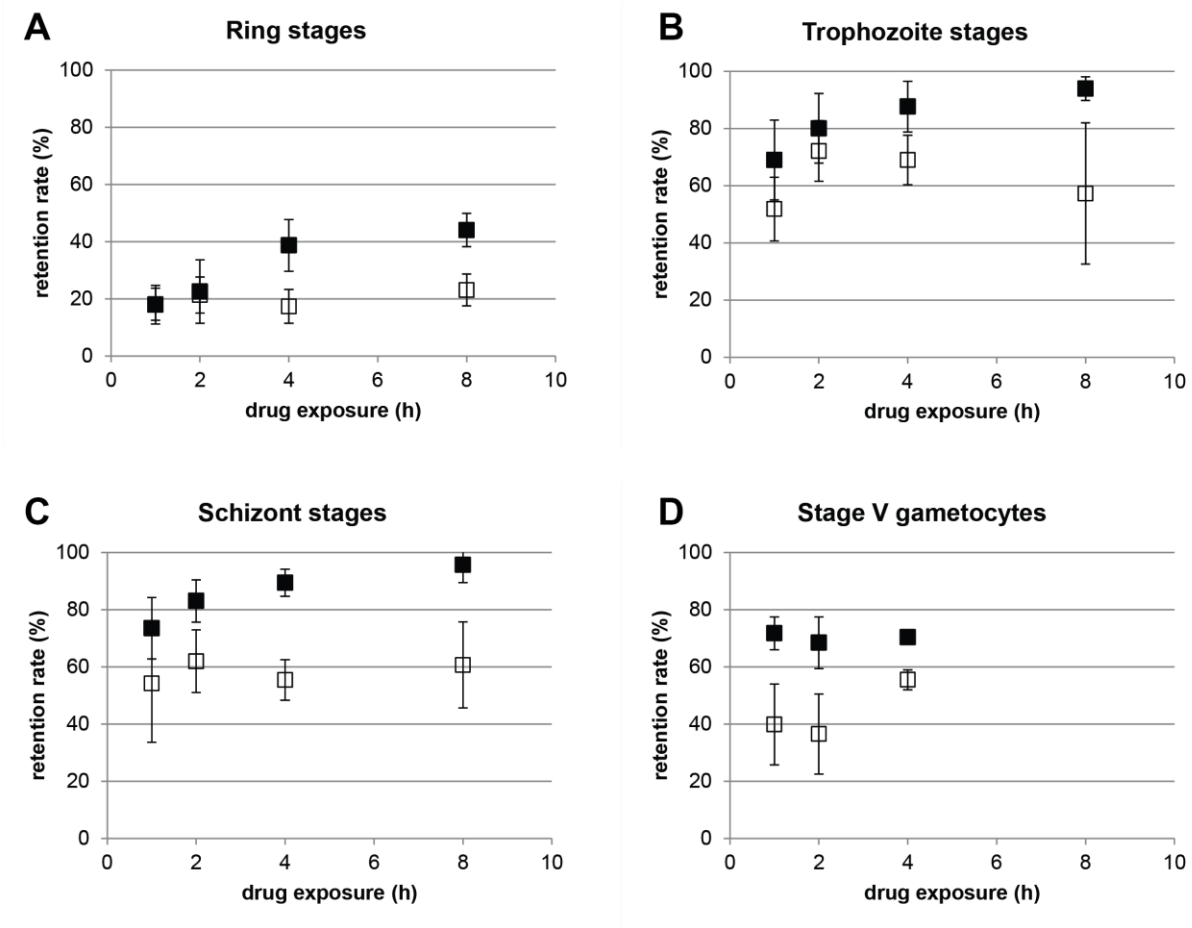
A
Ring stages
retention rate (%)
drug exposure (h)
B
Trophozoite stages
retention rate (%)
drug exposure (h)
C
Schizont stages
retention rate (%)
drug exposure (h)
D
Stage V gametocytes
retention rate (%)
drug exposure (h)

Figure 2

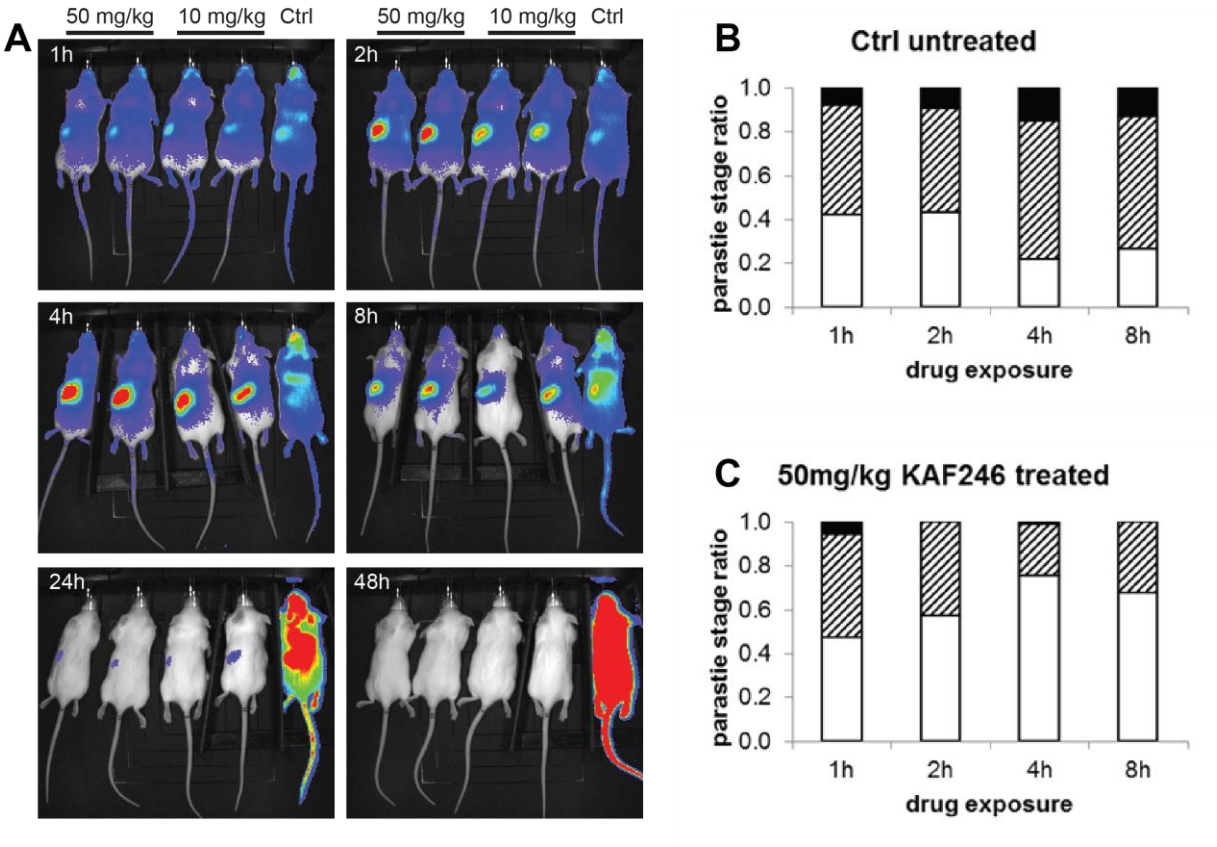
A
50 mg/kg
10 mg/kg
Ctrl
50 mg/kg
10 mg/kg
Ctrl
1h
2h
4h
8h
24h
48h
B
Ctrl untreated
parastie stage ratio
1.0
0.8
0.6
0.4
0.2
0.0
1h
2h
4h
8h
drug exposure
C
50mg/kg KAF246 treated
parastie stage ratio
1.0
0.8
0.6
0.4
0.2
0.0
1h
2h
4h
8h
drug exposure

Chapter 6
General Discussion

The malaria parasite *P. falciparum* triggers devastating pathology during its intraerythrocytic life cycle stage. In order to thrive, the parasite extensively remodels the terminally differentiated red blood cell to make it a favorable environment for massive replication. The refurbishment is mediated by a large number of parasite proteins that are exported to the host cell. The main pathways and processes installed by the parasite are 1) a protein trafficking network enabling the presentation of variant surface antigens that facilitate immune evasion and 2) the installation of nutrient uptake channels. In this study we set out to characterize three exported proteins initially identified in MAHRP1 and/or MAHRP2 co-immunoprecipitation experiments aiming at a better understanding of Maurer's clefts and Maurer's clefts tether function. These are PF3D7_0702500, MESA (PF3D7_0500800) and STARP (PF3D7_0702300). Apart from localization and expression studies, we performed protein interaction studies and protein functional analyses. Instrumental for the study were transgenic parasites and knock out cell lines were generated using the CRISPR/Cas9 system (Ghorbal et al., 2014). For gene tagging, a new approach combining the CRISPR/Cas9 system with selection linked integration (Birnbaum et al., 2017) was applied. The availability of these recent gene editing technologies accelerates the establishment of transgenic parasite cell lines to study specific proteins of interest.

All cellular processes are guided by proteins functioning in concert with other proteins. The understanding of protein-protein interactions is thus a substantial part of understanding biological processes. We were particularly interested in identifying protein networks of exported *P. falciarum* proteins around Maurer's clefts that are putatively involved in the establishment of a protein trafficking system. LaCount and colleagues predicted many *P. falciparum* asexual stage protein-protein interactions by a high-throughput yeast two hybrid system approach (LaCount et al., 2005). Among the different protein interaction clusters they also looked more specifically at exported proteins. They found 15 interactions among 19 exported proteins. One of these analyzed clusters involved MESA (PF3D7_0500800) interacting with SBP1 (PF3D7_0511300), PTP4 (PF3D7_0730900), PF3D7_0702100, and PF3D7_1401200. None of these predicted MESA interaction partners was confirmed in our MESA-GFP co-immunoprecipitation experiments (see chapter 4). The yeast two hybrid system used by LaCount and colleagues is an in vitro technique where protein domains are

expressed recombinantly, simultaneously and in the same cellular compartment. In contrast, co-immunoprecipitation experiments capture protein-protein interactions in the physiological environment. To confirm interaction between two proteins several different techniques should be applied, especially also biochemical interaction studies, e.g. fluorescence polarization binding assays, far Western blot, surface plasmon resonance, or NMR studies to validate direct physical interaction of two proteins. BioID is a relatively new method to identify proteins in close proximity of each other in vivo (Roux et al., 2013). A promiscuous biotin ligase fused to a protein of interest biotinylates proteins based on poximity and has been successfully applied in *Plasmodium* (Khosh-Naucke et al., 2017, Schnider et al., 2018). We have adapted this system in our experiments and successfully identified potential interaction partners for MESA and several PHIST family proteins.

The parasite-derived exported proteins do not only interact with other parasite-derived proteins but also with host red blood cell proteins. An example is the interaction of MESA with the erythrocyte skeletal protein 4.1 which is essential for parasite survival (Magowan et al., 1995). The investigation of protein-protein interactions from the host perspective is very challenging in the intraerythrocytic life cycle as the host cell cannot be easily genetically manipulated because it lacks a cell nucleus. However, the feasibility to use red blood cells derived from genetically manipulated hematopoietic stem cells to study host cell factors important for *P. falciparum* invasion was shown by Egan et al. (2015).

Over the last years, our laboratory has performed several co-immunoprecipitation protein interaction studies with various exported proteins. To get an impression of the interconnectedness of several exported proteins, a network with the co-immunoprecipitation data of SEMP1 (Dietz et al., 2014), MAHRP2 (unpublished), PF3D7_0702500-HA (chapter 3), and MESA-GFP (chapter 4) was assembled (Figure 1). These four proteins represent different structures in the iRBC cytosol: the iRBC cytoskeleton (MESA), electron-dense structures (PF3D7_0702500), Maurer's clefts tethers (MAHRP2) and Maurer's clefts (SEMP1).

The central node connected to MESA, PF3D7_0702500, MAHRP2 and SEMP1 contains REX1, PIESP2, Hsp70x and GBP130 (light green protein group). REX1 is a Maurer's clefts protein important for PfEMP1 delivery to the iRBC surface (Hawthorne et al., 2004, Dixon et al., 2011). PIESP2 also localizes to Maurer's clefts and is important for the formation of Maurer's clefts lamellar structure (Vincensini et al., 2005, Zhang et al., 2018). Their location in the center of the network underpins the central role of Maurer's clefts as protein trafficking

hubs. Hsp70x is an exported chaperone (Kulzer et al., 2012) and its interaction with many "client proteins" is comprehensible given that it assists protein folding. Interestingly, the co-chaperone Hsp40 (PFE55), which was previously found in complex with Hsp70x (Kulzer et al., 2010, Kulzer et al., 2012) was identified to interact with MESA and MAHRP2. GBP130 is an exported protein of unknown function. It was previously proposed to bind host cell glycophorin (Kochan et al., 1986, Ravetch et al., 1985), but this result was later questioned by van Schravendijk and colleagues (1987). Further, GBP130 was identified by Maier and colleagues to modulate host cell rigidity (Maier et al., 2008), however its exact localization and function is unclear.

Several proteins in the network belong to the PHIST protein family: PF3D7_0402000 (PHISTa), PF3D7_1201000 (PHISTb), PF3D7_0424600 (PHISTb), PF3D7_0731300 (PHISTb), PFE1605w (PHISTb), PF3D7_0801000 (PHISTc), and PFI1780w (PHISTc). This protein family has not been intensively studied but it seems that some PHIST proteins may function as "adaptor proteins" due to several occurring binding domains (reviewed in Warncke et al., 2016). Further studies on PHIST protein interactions will elucidate their role in host cell remodeling.

An intriguing protagonist of the network is CLAG3.1, a *Plasmodium* surface anion channel (PSAC) protein (Nguitragool et al., 2011). Little is known to date about the parasite-induced host cell changes enabling nutrient uptake, a crucial process for parasite survival (further detailed below).

In summary, this visualization of protein-protein interactions can be the basis for follow-up studies on exported proteins in consideration of the fact that many proteins are of unknown function. Elucidating the role of proteins located at intersection points may give new insights into processes established by the parasite.

These non-human parasite-specific pathways represent targets for new antimalarial drug development. Especially the unconventional protein trafficking pathways established in the host erythrocyte represent a unique opportunity to interfere with the mechanisms underlying the clinical symptoms of the disease. To this end, the functional characterization of exported parasite proteins is indispensable. However, the function of many exported proteins remains unclear. Actually, it even seems that many exported proteins are dispensable as a range of knock out cell lines shows no distinct phenotype.

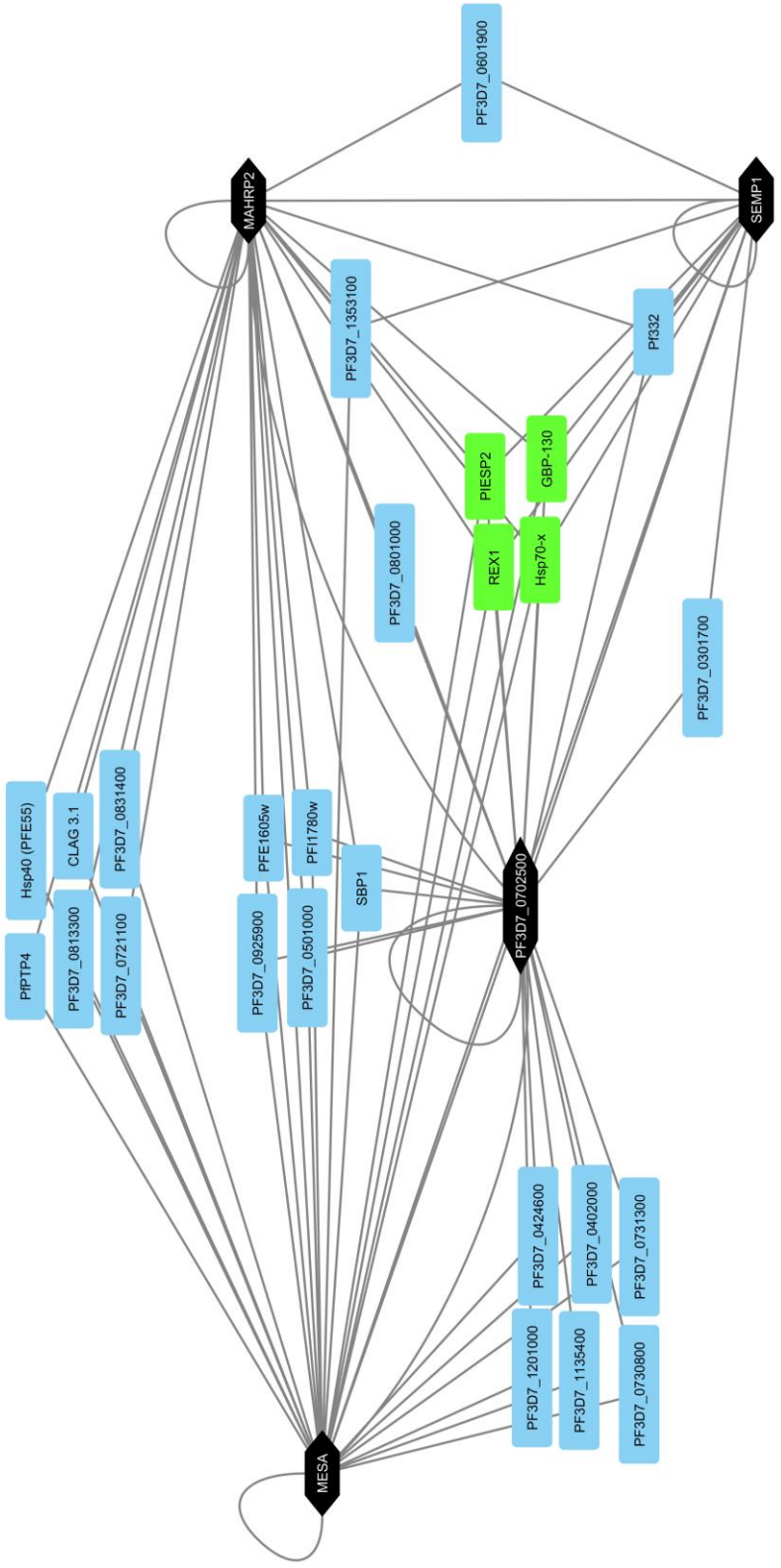

Figure 1: **Interaction network of exported *P. falciparum* proteins.** Shown are protein interactions identified by co-immunoprecipitation. The datasets of SEMP1-3xHA (Dietz et al., 2014), MAHRP2 (unpublished), PF3D7_0702500-3xHA (chapter 3) and MESA-GFP (chapter 4) were compared and all proteins that interact with a minimum of two of the bait proteins are shown. Light green are the proteins interacting with all four bait proteins.

On one hand this could be explained by a high redundancy of exported proteins due to their position at the interface to the host, enabling the parasite to respond to the unstable environment, for example the adaptive host immune system. This is shown by the findings of a systematic functional genome screen in *P.bergei* (Bushell et al., 2017) as well as in a large-scale gene knock out study of exported proteins (Maier et al., 2008) which reported that essentiality and phenotypical changes upon protein depletion were minor.

On the other hand it needs to be considered that the majority of the functional characterization data is from in vitro culture systems. Under cell culture conditions, the parasites have virtually unlimited supply of nutrients in very rich culture media and no host immune system is present. This may lead to an unintended miss of distinct phenotypes. An example is a study where the essentiality of the PSAC was only evident once the culture media composition was changed to contain lower concentrations of key nutrient components which notably were also closer to human plasma concentrations (Pillai et al., 2012). One can speculate that this is one of the reasons why so little is known about PSAC/NPPs. Recently, a model for PSAC assembly was proposed in which CLAG3, RhopH2 and RhopH3 form a complex and are trafficked to the rhoptries of the merozoite. Upon RBC invasion the complex is transferred to the iRBC parasitophorous vacuole. Then the proteins reach the iRBC cytosol via PTEX and finally reach the iRBC membrane via Maurer's clefts (Ito et al., 2017, Sherling et al., 2017). The interruption of the PSAC assembly process would putatively lead to a starving out of the parasite and thus could be an attractive intervention strategy.

Alteration of the biomechanical properties of *P. falciparum* iRBCs is another important factor for malaria pathogenesis: the hemodynamic properties of iRBCs are changed (Dasanna et al., 2017), their retention in the spleen is modified and cytoadherence (resulting in blockage of small capillaries) is facilitated (Dondorp et al., 2000, Lavazec, 2017). It is not clear whether altered iRBC biomechanical properties are a necessity for parasite survival or an unavoidable side effect of protein export. Nevertheless, the molecular mechanisms behind the parasite-induced changes in host cell deformability are more and more understood.

Generally, cell deformability is influenced by the internal viscosity of the cytoplasm, membrane and cytoskeleton dynamics, and cell geometry. The presence of the parasite inside the cell influences all these factors, either by its sole presence or by remodeling the host cell, e.g. the establishment of knob structures on the iRBC surface.

Alteration of host erythrocyte deformability starts during *P. falciparum* merozoite invasion (Sisquella et al., 2017, Koch et al., 2017): when the merozoite binds to the erythrocyte, the

viscoelastic properties of the host membrane change allowing the parasite to invade the cell. During the asexual stages, the iRBCs become increasingly rigid with progression of the parasite from young ring stages to late schizont stages (Cranston et al., 1984, Nash et al., 1989). The underlying mechanisms are manifold and include parasite growth and host cell remodeling.

During the asexual replication, the parasite refurbishes the host cell with exported proteins. In a large gene knock out screen, Maier and colleagues identified several proteins that are associated with the rigidification of the iRBCs (Maier et al., 2008): PF3D7_0730900 (PTP4), PF3D7_1002100 (PTP5), PF3D7_0102200 (RESA, Silva et al., 2005, Mills et al., 2007), PF3D7_0501300 (SBP1), PF3D7_0404600, PF3D7_0424400, PF3D7_0801900, and PF3D7_1401600. In other studies, PfEMP3 and STEVOR were shown to also contribute to increased iRBC membrane rigidity (Glenister et al., 2002, Sanyal et al., 2012). In this study we have assessed iRBC rigidity changes upon PF3D7_0702500 and MESA depletion and observed no effect. We expected MESA to have an influence on the deformability of iRBCs because of its position at the erythrocyte cytoskeleton (discussed in detail in chapter 4). For PF3D7_0702500 an indirect effect on iRBC deformability could be conceivable e.g. by interacting with or transporting of a protein directly involved in altering iRBC physical properties (PF3D7_1002100 (PTP5) and PF3D7_0501300 (SBP1) identified by Maier and colleagues (see above) are putative interaction partners of PF3D7_0702500 (chapter 2)).

iRBC rigidification seems dependent on the combined action of a number of exported proteins. In support of this hypothesis is the observation that the various proteins involved in the process have different gene expression profiles not all matching the onset of iRBC rigidity increase. A further observation is that knob structures introduced on the iRBC surface have a limited impact on iRBC deformability. KAHRP-deficient, knob-less iRBCs show only modest rigidity differences compared to wildtype iRBCs indicating a minor role of KAHRP/knobs in the rigidification of iRBCs (Sanyal et al., 2012).

Interestingly, also some “softeners” were identified in Maier’s study on exported proteins required for rigidity: PF3D7_1478600 (PTP3), PF3D7_0220100, PF3D7_1016300 (GBP130), and PF3D7_1301400 (Maier et al., 2008). We found PFE1605w knock down iRBCs to have higher retention rates in microsphiltration, thus also putatively contributing to iRBC deformability. The first protein identified involved in decreasing membrane rigidity was Pf332 (Glenister et al., 2009). Waller and colleagues studied the interaction of Pf332 with the RBC cytoskeleton and found Pf332 to interact with actin (Waller et al., 2010). In summary,

the finding of proteins involved in iRBC deformability increase may be an indication of "active" rigidity modulation by the parasite.

Direct and indirect interactions of parasite proteins with erythrocyte membrane cytoskeleton components lead to altered physical properties of the red blood cell. Further, iRBC deformability can be influenced by post-translational modifications of erythrocyte proteins. For instance, P. *falciparum* exported FIKK kinases were described to phosphorylate membrane skeleton proteins and thereby inducing alterations in biomechanical properties of the iRBCs (Nunes et al., 2010). In this project, post-translational modifications of the proteins of interest were not included in the characterization analysis. However, PF3D7_0702500, MESA and STARP have (predicted) phosphorylation sites (Treeck et al., 2011) and PF3D7_0702500 and MESA are putatively palmitoylated (Jones et al., 2012). A detailed study of the function of those post-translational modifications could give additional insights into the role and regulation of these proteins.

iRBC deformability has become a malaria drug-development target. Drug-induced rigidity increase of circulating *Plasmodium* stages can enhance their removal by the spleen. In our study on the effect of the spiroindolone KAF246 on iRBC rigidity (chapter 6) we have observed reduced deformability upon drug treatment in both asexual and sexual stages. In the light of eliminating malaria, sexual stages have recently obtained more attention as they are relevant for parasite transmission. Immature gametocyte iRBCs (stage I-IV) show high retention rates in microsphiltration experiments as do asexual late stage iRBC. Interestingly, stage V gametocyte iRBC are highly deformable. The rigidity switch linked to gametocyte maturation may allow the transmissible stages to leave the bone marrow and enter the circulation, pass the spleen and be transmitted to mosquitoes (Tiburcio et al., 2012). The molecular mechanisms underlying this rigidity switch are starting to be understood. The interaction of the STEVOR cytoplasmic domain with the ankyrin complex of the iRBC was reported to be important for iRBC deformability. In more detail, the STEVOR cytoplasmic domain is phosphorylated by PKA. PKA activity is controlled by cAMP signaling. During immature gametocyte stages I-IV, low levels of the plasmodial phosphodiesterase PDEδ lead to high cAMP levels in the cell. Phosphorylation of STEVOR is activated. Upon gametocyte maturation (stage V) the phosphodiesterase PDEδ is highly expressed and cAMP levels decrease. PKA is thus inactive and the STEVOR phosphorylation level subsequently decreases which may weaken or abolish the interaction with the cytoskeleton and lead to

increased deformability of the cell (Ramdani et al., 2015, Naissant et al., 2016, Lavazec, 2017).

We tested whether KAF246 induced rigidification relies on the same STEVOR phosphorylation pathway described above. This pathway is the only mechanism identified to date to be involved in the gametocyte rigidity switch. According to preliminary results, STEVOR doesn't seem to be involved in the KAF246-induced rigidification of stage V gametocytes. Elucidating the KAF246 mode of action on gametocyte deformability will contribute to our understanding of the underlying molecular processes.

References

BIRNBAUM, J., FLEMMING, S., REICHARD, N., SOARES, A. B., MESEN-RAMIREZ, P., JONSCHER, E., BERGMANN, B. & SPIELMANN, T. 2017. A genetic system to study Plasmodium falciparum protein function. *Nat Methods,* 14**,** 450-456.

BUSHELL, E., GOMES, A. R., SANDERSON, T., ANAR, B., GIRLING, G., HERD, C., METCALF, T., MODRZYNSKA, K., SCHWACH, F., MARTIN, R. E., MATHER, M. W., MCFADDEN, G. I., PARTS, L., RUTLEDGE, G. G., VAIDYA, A. B., WENGELNIK, K., RAYNER, J. C. & BILLKER, O. 2017. Functional Profiling of a Plasmodium Genome Reveals an Abundance of Essential Genes. *Cell,* 170**,** 260-272.e8.

CRANSTON, H. A., BOYLAN, C. W., CARROLL, G. L., SUTERA, S. P., WILLIAMSON, J. R., GLUZMAN, I. Y. & KROGSTAD, D. J. 1984. Plasmodium falciparum maturation abolishes physiologic red cell deformability. *Science,* 223**,** 400-3.

DASANNA, A. K., LANSCHE, C., LANZER, M. & SCHWARZ, U. S. 2017. Rolling Adhesion of Schizont Stage Malaria-Infected Red Blood Cells in Shear Flow. *Biophys J,* 112**,** 1908-1919.

DIETZ, O., RUSCH, S., BRAND, F., MUNDWILER-PACHLATKO, E., GAIDA, A., VOSS, T. & BECK, H. P. 2014. Characterization of the small exported Plasmodium falciparum membrane protein SEMP1. *PLoS One,* 9**,** e103272.

DIXON, M. W., KENNY, S., MCMILLAN, P. J., HANSSEN, E., TRENHOLME, K. R., GARDINER, D. L. & TILLEY, L. 2011. Genetic ablation of a Maurer's cleft protein prevents assembly of the Plasmodium falciparum virulence complex. *Mol Microbiol,* 81**,** 982-93.

DONDORP, A. M., KAGER, P. A., VREEKEN, J. & WHITE, N. J. 2000. Abnormal blood flow and red blood cell deformability in severe malaria. *Parasitol Today,* 16**,** 228-32.

EGAN, E. S., JIANG, R. H., MOECHTAR, M. A., BARTENEVA, N. S., WEEKES, M. P., NOBRE, L. V., GYGI, S. P., PAULO, J. A., FRANTZREB, C., TANI, Y., TAKAHASHI, J., WATANABE, S., GOLDBERG, J., PAUL, A. S., BRUGNARA, C., ROOT, D. E., WIEGAND, R. C., DOENCH, J. G. & DURAISINGH, M. T. 2015. A forward genetic screen identifies erythrocyte CD55 as essential for Plasmodium falciparum invasion. *Science,* 348**,** 711-4.

GHORBAL, M., GORMAN, M., MACPHERSON, C. R., MARTINS, R. M., SCHERF, A. & LOPEZ-RUBIO, J. J. 2014. Genome editing in the human malaria parasite Plasmodium falciparum using the CRISPR-Cas9 system. *Nat Biotechnol,* 32**,** 819-21.

GLENISTER, F. K., COPPEL, R. L., COWMAN, A. F., MOHANDAS, N. & COOKE, B. M. 2002. Contribution of parasite proteins to altered mechanical properties of malaria-infected red blood cells. *Blood,* 99**,** 1060-3.

GLENISTER, F. K., FERNANDEZ, K. M., KATS, L. M., HANSSEN, E., MOHANDAS, N., COPPEL, R. L. & COOKE, B. M. 2009. Functional alteration of red blood cells by a megadalton protein of Plasmodium falciparum. *Blood,* 113**,** 919-28.

HAWTHORNE, P. L., TRENHOLME, K. R., SKINNER-ADAMS, T. S., SPIELMANN, T., FISCHER, K., DIXON, M. W., ORTEGA, M. R., ANDERSON, K. L., KEMP, D. J. & GARDINER, D. L. 2004. A novel Plasmodium falciparum ring stage protein, REX, is located in Maurer's clefts. *Mol Biochem Parasitol,* 136**,** 181-9.

ITO, D., SCHURECK, M. A. & DESAI, S. A. 2017. An essential dual-function complex mediates erythrocyte invasion and channel-mediated nutrient uptake in malaria parasites. *Elife,* 6.

JONES, M. L., COLLINS, M. O., GOULDING, D., CHOUDHARY, J. S. & RAYNER, J. C. 2012. Analysis of protein palmitoylation reveals a pervasive role in Plasmodium development and pathogenesis. *Cell Host Microbe,* 12**,** 246-58.

KHOSH-NAUCKE, M., BECKER, J., MESEN-RAMIREZ, P., KIANI, P., BIRNBAUM, J., FROHLKE, U., JONSCHER, E., SCHLUTER, H. & SPIELMANN, T. 2017. Identification of novel parasitophorous vacuole proteins in P. falciparum parasites using BioID. *Int J Med Microbiol*.

KOCH, M., WRIGHT, K. E., OTTO, O., HERBIG, M., SALINAS, N. D., TOLIA, N. H., SATCHWELL, T. J., GUCK, J., BROOKS, N. J. & BAUM, J. 2017. Plasmodium falciparum erythrocyte-binding antigen 175 triggers a biophysical change in the red blood cell that facilitates invasion. *Proc Natl Acad Sci U S A,* 114**,** 4225-4230.

KOCHAN, J., PERKINS, M. & RAVETCH, J. V. 1986. A tandemly repeated sequence determines the binding domain for an erythrocyte receptor binding protein of P. falciparum. *Cell,* 44**,** 689-96.

KULZER, S., CHARNAUD, S., DAGAN, T., RIEDEL, J., MANDAL, P., PESCE, E. R., BLATCH, G. L., CRABB, B. S., GILSON, P. R. & PRZYBORSKI, J. M. 2012. Plasmodium falciparum-encoded exported hsp70/hsp40 chaperone/co-chaperone complexes within the host erythrocyte. *Cell Microbiol,* 14**,** 1784-95.

KULZER, S., RUG, M., BRINKMANN, K., CANNON, P., COWMAN, A., LINGELBACH, K., BLATCH, G. L., MAIER, A. G. & PRZYBORSKI, J. M. 2010. Parasite-encoded Hsp40 proteins define novel mobile structures in the cytosol of the P. falciparum-infected erythrocyte. *Cell Microbiol,* 12**,** 1398-420.

LACOUNT, D. J., VIGNALI, M., CHETTIER, R., PHANSALKAR, A., BELL, R., HESSELBERTH, J. R., SCHOENFELD, L. W., OTA, I., SAHASRABUDHE, S., KURSCHNER, C., FIELDS, S. & HUGHES, R. E. 2005. A protein interaction network of the malaria parasite Plasmodium falciparum. *Nature,* 438**,** 103-7.

LAVAZEC, C. 2017. Molecular mechanisms of deformability of Plasmodium-infected erythrocytes. *Curr Opin Microbiol,* 40**,** 138-144.

MAGOWAN, C., COPPEL, R. L., LAU, A. O., MORONNE, M. M., TCHERNIA, G. & MOHANDAS, N. 1995. Role of the Plasmodium falciparum mature-parasite-infected erythrocyte surface antigen (MESA/PfEMP-2) in malarial infection of erythrocytes. *Blood,* 86**,** 3196-204.

MAIER, A. G., RUG, M., O'NEILL, M. T., BROWN, M., CHAKRAVORTY, S., SZESTAK, T., CHESSON, J., WU, Y., HUGHES, K., COPPEL, R. L., NEWBOLD, C., BEESON, J. G., CRAIG, A., CRABB, B. S. & COWMAN, A. F. 2008. Exported proteins required for virulence and rigidity of Plasmodium falciparum-infected human erythrocytes. *Cell,* 134**,** 48-61.

MILLS, J. P., DIEZ-SILVA, M., QUINN, D. J., DAO, M., LANG, M. J., TAN, K. S., LIM, C. T., MILON, G., DAVID, P. H., MERCEREAU-PUIJALON, O., BONNEFOY, S. & SURESH, S. 2007. Effect of plasmodial RESA protein on deformability of human red blood cells harboring Plasmodium falciparum. *Proc Natl Acad Sci U S A,* 104**,** 9213-7.

NAISSANT, B., DUPUY, F., DUFFIER, Y., LORTHIOIS, A., DUEZ, J., SCHOLZ, J., BUFFET, P., MERCKX, A., BACHMANN, A. & LAVAZEC, C. 2016. Plasmodium falciparum STEVOR phosphorylation regulates host erythrocyte deformability enabling malaria parasite transmission. *Blood*.

NASH, G. B., O'BRIEN, E., GORDON-SMITH, E. C. & DORMANDY, J. A. 1989. Abnormalities in the mechanical properties of red blood cells caused by Plasmodium falciparum. *Blood,* 74**,** 855-61.

NGUITRAGOOL, W., BOKHARI, A. A., PILLAI, A. D., RAYAVARA, K., SHARMA, P., TURPIN, B., ARAVIND, L. & DESAI, S. A. 2011. Malaria parasite clag3 genes determine channel-mediated nutrient uptake by infected red blood cells. *Cell,* 145**,** 665-77.

NUNES, M. C., OKADA, M., SCHEIDIG-BENATAR, C., COOKE, B. M. & SCHERF, A. 2010. Plasmodium falciparum FIKK kinase members target distinct components of the erythrocyte membrane. *PLoS One,* 5**,** e11747.

PILLAI, A. D., NGUITRAGOOL, W., LYKO, B., DOLINTA, K., BUTLER, M. M., NGUYEN, S. T., PEET, N. P., BOWLIN, T. L. & DESAI, S. A. 2012. Solute restriction reveals an essential role for clag3-associated channels in malaria parasite nutrient acquisition. *Mol Pharmacol,* 82**,** 1104-14.

RAMDANI, G., NAISSANT, B., THOMPSON, E., BREIL, F., LORTHIOIS, A., DUPUY, F., CUMMINGS, R., DUFFIER, Y., CORBETT, Y., MERCEREAU-PUIJALON, O., VERNICK, K., TARAMELLI, D., BAKER, D. A., LANGSLEY, G. & LAVAZEC, C. 2015. cAMP-Signalling Regulates Gametocyte-Infected Erythrocyte Deformability Required for Malaria Parasite Transmission. *PLoS Pathog,* 11**,** e1004815.

RAVETCH, J. V., KOCHAN, J. & PERKINS, M. 1985. Isolation of the gene for a glycophorin-binding protein implicated in erythrocyte invasion by a malaria parasite. *Science,* 227**,** 1593-7.

ROUX, K. J., KIM, D. I. & BURKE, B. 2013. BioID: a screen for protein-protein interactions. *Curr Protoc Protein Sci,* 74**,** Unit 19.23.

SANYAL, S., EGEE, S., BOUYER, G., PERROT, S., SAFEUKUI, I., BISCHOFF, E., BUFFET, P., DEITSCH, K. W., MERCEREAU-PUIJALON, O., DAVID, P. H., TEMPLETON, T. J. & LAVAZEC, C. 2012. Plasmodium falciparum STEVOR proteins impact erythrocyte mechanical properties. *Blood,* 119**,** e1-8.

SCHNIDER, C. B., BAUSCH-FLUCK, D., BRUHLMANN, F., HEUSSLER, V. T. & BURDA, P. C. 2018. BioID Reveals Novel Proteins of the Plasmodium Parasitophorous Vacuole Membrane. *mSphere,* 3.

SHERLING, E. S., KNUEPFER, E., BRZOSTOWSKI, J. A., MILLER, L. H., BLACKMAN, M. J. & VAN OOIJ, C. 2017. The Plasmodium falciparum rhoptry protein RhopH3 plays essential roles in host cell invasion and nutrient uptake. *Elife,* 6.

SILVA, M. D., COOKE, B. M., GUILLOTTE, M., BUCKINGHAM, D. W., SAUZET, J. P., LE SCANF, C., CONTAMIN, H., DAVID, P., MERCEREAU-PUIJALON, O. & BONNEFOY, S. 2005. A role for the Plasmodium falciparum RESA protein in resistance against heat shock demonstrated using gene disruption. *Mol Microbiol,* 56**,** 990-1003.

SISQUELLA, X., NEBL, T., THOMPSON, J. K., WHITEHEAD, L., MALPEDE, B. M., SALINAS, N. D., ROGERS, K., TOLIA, N. H., FLEIG, A., O'NEILL, J., THAM, W. H., DAVID HORGEN, F. & COWMAN, A. F. 2017. Plasmodium falciparum ligand binding to erythrocytes induce alterations in deformability essential for invasion. *Elife,* 6.

TREECK, M., SANDERS, J. L., ELIAS, J. E. & BOOTHROYD, J. C. 2011. The phosphoproteomes of Plasmodium falciparum and Toxoplasma gondii reveal unusual adaptations within and beyond the parasites' boundaries. *Cell Host Microbe,* 10**,** 410-9.

VAN SCHRAVENDIJK, M. R., WILSON, R. J. & NEWBOLD, C. I. 1987. Possible pitfalls in the identification of glycophorin-binding proteins of Plasmodium falciparum. *J Exp Med,* 166**,** 376-90.

VINCENSINI, L., RICHERT, S., BLISNICK, T., VAN DORSSELAER, A., LEIZE-WAGNER, E., RABILLOUD, T. & BRAUN BRETON, C. 2005. Proteomic analysis identifies novel proteins of the Maurer's clefts, a secretory compartment delivering Plasmodium falciparum proteins to the surface of its host cell. *Mol Cell Proteomics,* 4**,** 582-93.

WALLER, K. L., STUBBERFIELD, L. M., DUBLJEVIC, V., BUCKINGHAM, D. W., MOHANDAS, N., COPPEL, R. L. & COOKE, B. M. 2010. Interaction of the exported malaria protein Pf332 with the red blood cell membrane skeleton. *Biochim Biophys Acta,* 1798**,** 861-71.

WARNCKE, J. D., VAKONAKIS, I. & BECK, H. P. 2016. Plasmodium Helical Interspersed Subtelomeric (PHIST) Proteins, at the Center of Host Cell Remodeling. *Microbiol Mol Biol Rev,* 80**,** 905-27.

ZHANG, M., FAOU, P., MAIER, A. G. & RUG, M. 2018. Plasmodium falciparum exported protein PFE60 influences Maurer's clefts architecture and virulence complex composition. *Int J Parasitol,* 48**,** 83-95.

Conclusion and Outlook

This thesis contributes to a better understanding of *P. falciparum* exported proteins during the intraerythrocytic life cycle. Three selected exported proteins expressed during the intraerythrocytic life cycle, namely PF3D7_0702500, MESA and STARP were characterized. Functional analysis suggested a role of PF3D7_0702500 in PfEMP1 transport efficiency between Maurer's clefts and the erythrocyte membrane or the anchoring of PfEMP1 at the cytoskeleton. Future experiments should detail the nature of the electron-dense structures to which PF3D7_0702500 localizes to, and thereby give more insights into the underlying mechanism of the PF3D7_0702500 KO phenotype of reduced binding to CD36 endothelial receptors. The roles of MESA and STARP remain elusive. It is conceivable that they function in a different life cycle stage or in a different process than analyzed. The functional readouts used in this thesis focused on the surface presentation of PfEMP1 and biomechanical changes of the iRBC. Additional future experiments should include the analysis of an involvement of the proteins of interest in nutrient uptake or differentiation into other life stages (e.g. sexual commitment). The characterization of exported proteins and the understanding of their interplay will ultimately help to identify new intervention strategies against malaria and its transmission.

During the work described in this thesis, I have established a useful tool for endogenous tagging of parasite genes by combining CRISPR/Cas9 and SLI genome editing technologies. A set of plasmids with different tags (3xHA, GFP, BirA*3xHA) and multiple cloning sites was generated and is available for sharing. This tagging-approach allows a reliable and time-efficient generation of transgenic parasite cell lines. Further, the microsphiltration method for assessing iRBC deformability was successfully established at the Swiss TPH and has proven to work reliably. This method is not only useful to assess asexual stage iRBC deformability but also gametocyte deformability and expands the toolbox of available assays at the institute.

Finally, I have shown during this thesis that the increase of spiroindolone-induced rigidity of circulating *Plasmodium* stages can enhance their removal by the spleen. It will be interesting to look more into the mechanism of the induced rigidity changes, especially in gametocyte stages that are transmission-relevant.

Appendix

Maurer's clefts movement

Introduction

Maurer's clefts are formed early in the intraerythrocytic lifecycle (approximately 2-6 hours post infection (hpi)) and are highly mobile in the first half of the lifecycle until they are immobilized around 22hpi (McMillan et al., 2013, Gruring et al., 2011).

The mechanism and function of Maurer's clefts immobilization is unclear. Interestingly, it coincides with surface presentation of PfEMP1 (Gruring et al., 2011). Thus it is conceivable that there is a functional relationship between Maurer's clefts immobilization and PfEMP1 surface presentation.

Three main observations have been made that led to (different) hypothesis for the mechanism of Maurer's clefts arrest. First, Maurer's clefts change their morphology during the lifecycle from globular to disk-shaped. This may influence their motion properties (Kilian et al., 2013). Second, actin-like filaments have been observed that connect Maurer's clefts with the erythrocyte membrane/knobs (Taraschi et al., 2003, Cyrklaff et al., 2011). They were not only suggested to be important for structural integrity of Maurer's clefts (Cyrklaff et al., 2011) but also to be trafficking routes of vesicles (Taraschi et al., 2003). However, actin depolymerization by cytochalsin D did not abolish Maurer's clefts arrest completely indicating that actin alone is not accountable for Maurer's clefts immobilization (Kilian et al., 2013). Third, tether-like structures associated with Maurer's clefts were observed in electron microscopy (Hanssen et al., 2008, Hanssen et al., 2010, Pachlatko et al., 2010). To date, MAHRP2 is the only known resident tether protein (Pachlatko et al., 2010). Its location in very close proximity to Maurer's clefts and that expression coincides with the arrest of Maurer's clefts could indicate an involvement of MAHRP2 in the fixation of Maurer's clefts.

In a hypothesis-driven approach we set out to investigate the role of MAHRP2 in Maurer's clefts movement arrest. To this end, MAHRP1 was endogenously GFP–tagged at the C-terminus in 3D7 wildtype and MAHRP2 deficient cell lines. This allowed tracking of Maurer's clefts movement and arrest in life cell imaging.

Methods

Cell culture and transfections

P. falciparum 3D7 was cultured and transfected as described (Moll et al., 2013). Transfected parasites were positively selected with 10nM WR99210 (Jacobs Pharmaceuticals, Cologne, Germany), or 5mg ml^{-1} blasticidin (Sigma-Aldrich, Inc.)

Transfection constructs

For endogenous tagging the plasmid pCRISPR_GFP2ABSD was used. 300-600bp long homology regions were designed and the gRNA was chosen with the CHOPCHOP software (Montague et al., 2014, Labun et al., 2016). gRNA recognition sequence mutations were introduced with the 5'homology region reverse primer to avoid re-cleavage of successfully tagged endogenous protein. The homology regions and gRNA were PCR amplified using primers listed in Supplementary Table 1 and cloned into pCRISPR_GFP2ABSD using the In-Fusion® HD Cloning Kit (Clontech® Laboratories, Inc.).

A MAHRP2 knock out cell line was obtained by double crossover homologous recombination. To increase homologous recombination efficiency, a longer DNA segment, namely the *mahrp2* gene (PF3D7_1353200/PF13_0276) and its neighboring gene (PF3D7_1353100/PF13_0276) coding for an exported protein of unknown function, were replaced with a *hDHFR* resistance cassette. 275-276 KO was generated by cloning PCR amplified 5'UTR and 3'UTR (using primers listed in Supplementary Table 1) with *AflII/SacII* and *NcoI/AvrII*, respectively into the pCC1 plasmid (pCC1_PF13_0275-PF13_0276). After transfection, on/off drug selection cycling was performed to select for stably integrated constructs and remove residual episomal constructs.

Western blot analysis

Parasite saponin lysates were run on 4-12% Bis/Tris precast gels (NuPAGE®, Life Technologies) according to the manufacturer's protocol. Protein transfer was performed with the iBlot 2.0 (Life Technologies). Subsequently, the membrane was blocked with 10% skimmed milk/TNT (100mM Tris, 150mM NaCl, 0.1% Tween) and probed with the first antibody in 3% skimmed milk/TNT at room temperature for 2h-O/N. After 6 washes for 5min with TNT the secondary antibody conjugated to HRP was incubated in the respective dilution in 3% skimmed milk/TNT for 2h at room temperature. After another 6 washes for 5min with TNT the signal was detected by Super Signal West Pico Chemiluminescent Substrate (Thermo Scientific) or LumiGlo Reserve Chemiluminescent Substrate (Seracare) according to the manufacturer's protocol. The antibodies used were: mouse α-GFP (Roche, 1:250), mouse α-GAPDH (1:20'000), rabbit α-MAHRP1 (1:5000), rabbit α-MAHRP2 (1:1000), goat α-mouse-HRP (Pierce, 1:5000), and goat α-rabbit-HRP (Pierce, 1:10'000).

Immunofluorescence Assay

Thin blood smears of parasite cultures were fixed in ice-cold 60% methanol/40% acetone for 2min. After air-drying of the smear, a small circle was drawn with a hydrophobic pen and the respective area was blocked with 3% BSA/PBS for 1h at room temperature in a humidified chamber. Then, the cells were incubated with mouse α-GFP (Roche, 1:100), rabbit α-SBP1 (1:400) in 3% BSA/PBS for minimum 2h at room temperature in a humidified chamber. After 3 washes with 3% BSA/PBS for 7min the secondary antibody (goat α-mouse Alexa488, goat α-rabbit Alexa568; all Invitrogen, 1:200) was applied in the appropriate dilution in 3% BSA/PBS for minimum 1h at room temperature in a humidified chamber. After another 3 wash steps with 3% BSA/PBS for 7min each, a coverslip was mounted with 2µl VECTASHIELD® with DAPI (Vector Laboratories Inc.). For imaging a 63x oil-immersion lens (1.4 numerical aperture) on a Leica 5000 B microscope was used. The images were obtained by using the software Leica ApplicationSuite 4.4. and analyzed using Fiji (Schindelin et al., 2012).

Life imaging

For live imaging 1ml of a synchronously growing culture was pelleted and washed in 1ml PBS. Then, the pellet was resuspended in 100µl PBS and 2.5µl sample was mixed with 2.5µl VECTASHIELD® with DAPI (Vector Laboratories Inc.) on a glass slide and covered with a coverslip. The coverslip was sealed with nail polish and the sample was immediately imaged with a 63x oil-immersion lens on a Leica 5000 B microscope. The images were obtained and analyzed with Leica ApplicationSuite 4.4. and Fiji (Schindelin et al., 2012).

For high content life imaging highly synchronous parasite cultures were stained with SiRHoechst (Spirochrome) for 20min in the dark at 37°C. After washing the cells in PBS, the hematocrit was adjusted to 0.05% in PBS and 200µl cell suspension was seeded in 96-well poly-D-lysine coated imaging plates (Greiner) and allowed to settle for 30min. Time series of 40s with an image taken every 2s of one position/well of 12 wells/timepoint/cell line were taken at 14-18hpi/18-22hpi/22-26hpi/26-30hpi with the 60x Plan Apo objective. Images were acquired with the ImageXpress Micro XLS Widefield High-Content Imaging System (Molecular Devices) and the MetaXpress Analysis Software.

Results and Discussion

Generation of endogenous MAHRP1-GFP expressing cell lines

In order to follow Maurer's clefts movement, MAHRP1, a resident Maurer's cleft protein, was GFP-tagged at the C-terminus. We have introduced the tag in 3D7 parasites and MAHRP2 knock out parasites (275-276 KO) to investigate the function of MAHRP2 in Maurer's clefts movement arrest (tethering). Successful integration of the tag in 2 independent transfections (sp and dp) was confirmed by PCR (Figure 1A). Absence of MAHRP2 protein expression in the 275-276 KO/MAHRP1-GFP cell lines and MAHRP1-GFP fusion protein expression was confirmed by Western blot (Figure 1B). Untagged MAHRP1 runs at around 30kDa whilst, MAHRP1-GFP runs at around 55kDa. We observed an additional band around 70kDa which could be the fused and uncleaved *bsd* cassette (bsd Western blot not shown). Immunofluorescent co-labeling of GFP and SBP1, a resident Maurer's cleft protein, confirmed the correct localization of the MAHRP1-GFP fusion protein at Maurer's clefts (Figure 1D).

Life imaging of MAHRP1-GFP cell lines

Life imaging of 3D7/MAHRP1-GFP and 275-276 KO/MAHRP1-GFP was performed in ring stages (14-18hpi) to verify that there is enough GFP fluorescence for time-lapse life imaging and that movement of Maurer's clefts is visible. Figure 1E shows a time lapse over 20s with images taken every 5 seconds. The position of Maurer's clefts is different between every picture reflecting the rapid movement of the organelles.

In a next step we monitored Maurer's clefts movement arrest by life imaging of tightly synchronized 3D7/MAHRP1-GFP and 275-276 KO/MAHRP1-GFP at 14-18hpi, 18-22hpi, 22-26hpi, and 26-30hpi with a high content microscope. At the first time point (14-18hpi), all Maurer's clefts were moving rapidly whereas at the last time point (26-30hpi) Maurer's clefts movement stopped. We observed no significant difference in Maurer's clefts motion behavior between the two cell lines.

Conclusion

In conclusion, we successfully generated the 3D7/MAHRP1-GFP and 275-276 KO/MAHRP1-GFP cell lines which were suitable for life imaging of Maurer's clefts movement. Unexpectedly, MAHRP2 does not seem sufficient to trigger Maurer's clefts movement arrest although no tether-like structures could be retrieved in absence of MAHRP2

from ultracentrifugation experiments (Pachlatko et al., 2010). Therefore, the function of these structures and of MAHRP2, their only identified constituent, remains elusive. Repetition of the high content imaging experiment including more detailed analysis of Maurer's clefts motion may give more insight in the contribution of MAHRP2 and tethers to Maurer's clefts arrest.

Contribution and Acknowledgements

Esther Mundwiler-Pachlatko and Sebastian Rusch generated and validated the 275-276 KO cell line. We would like to thank Claudia Daubenberger for α-GAPDH antibodies and Catherine Braun-Breton for α-SBP1 antibodies.

References

CYRKLAFF, M., SANCHEZ, C. P., KILIAN, N., BISSEYE, C., SIMPORE, J., FRISCHKNECHT, F. & LANZER, M. 2011. Hemoglobins S and C interfere with actin remodeling in Plasmodium falciparum-infected erythrocytes. *Science,* 334**,** 1283-6.

GRURING, C., HEIBER, A., KRUSE, F., UNGEFEHR, J., GILBERGER, T. W. & SPIELMANN, T. 2011. Development and host cell modifications of Plasmodium falciparum blood stages in four dimensions. *Nat Commun,* 2**,** 165.

HANSSEN, E., CARLTON, P., DEED, S., KLONIS, N., SEDAT, J., DERISI, J. & TILLEY, L. 2010. Whole cell imaging reveals novel modular features of the exomembrane system of the malaria parasite, Plasmodium falciparum. *Int J Parasitol,* 40**,** 123-34.

HANSSEN, E., SOUGRAT, R., FRANKLAND, S., DEED, S., KLONIS, N., LIPPINCOTT-SCHWARTZ, J. & TILLEY, L. 2008. Electron tomography of the Maurer's cleft organelles of Plasmodium falciparum-infected erythrocytes reveals novel structural features. *Mol Microbiol,* 67**,** 703-18.

KILIAN, N., DITTMER, M., CYRKLAFF, M., OUERMI, D., BISSEYE, C., SIMPORE, J., FRISCHKNECHT, F., SANCHEZ, C. P. & LANZER, M. 2013. Haemoglobin S and C affect the motion of Maurer's clefts in Plasmodium falciparum-infected erythrocytes. *Cell Microbiol,* 15**,** 1111-26.

LABUN, K., MONTAGUE, T. G., GAGNON, J. A., THYME, S. B. & VALEN, E. 2016. CHOPCHOP v2: a web tool for the next generation of CRISPR genome engineering. *Nucleic Acids Res,* 44**,** W272-6.

MCMILLAN, P. J., MILLET, C., BATINOVIC, S., MAIORCA, M., HANSSEN, E., KENNY, S., MUHLE, R. A., MELCHER, M., FIDOCK, D. A., SMITH, J. D., DIXON, M. W. & TILLEY, L. 2013. Spatial and temporal mapping of the PfEMP1 export pathway in Plasmodium falciparum. *Cell Microbiol,* 15**,** 1401-18.

MONTAGUE, T. G., CRUZ, J. M., GAGNON, J. A., CHURCH, G. M. & VALEN, E. 2014. CHOPCHOP: a CRISPR/Cas9 and TALEN web tool for genome editing. *Nucleic Acids Res,* 42**,** W401-7.

PACHLATKO, E., RUSCH, S., MULLER, A., HEMPHILL, A., TILLEY, L., HANSSEN, E. & BECK, H. P. 2010. MAHRP2, an exported protein of Plasmodium falciparum, is an essential component of Maurer's cleft tethers. *Mol Microbiol,* 77**,** 1136-52.

SCHINDELIN, J., ARGANDA-CARRERAS, I., FRISE, E., KAYNIG, V., LONGAIR, M., PIETZSCH, T., PREIBISCH, S., RUEDEN, C., SAALFELD, S., SCHMID, B., TINEVEZ, J. Y., WHITE, D. J., HARTENSTEIN, V., ELICEIRI, K., TOMANCAK, P. & CARDONA, A. 2012. Fiji: an open-source platform for biological-image analysis. *Nat Methods,* 9**,** 676-82.

TARASCHI, T. F., O'DONNELL, M., MARTINEZ, S., SCHNEIDER, T., TRELKA, D., FOWLER, V. M., TILLEY, L. & MORIYAMA, Y. 2003. Generation of an erythrocyte vesicle transport system by Plasmodium falciparum malaria parasites. *Blood,* 102**,** 3420-6.

Supplementary Table 1

MAHRP1 5HR fw	5'ACAGATCAAGAGTGAACATAAAGC
MAHRP1 5HR rv (incl. mut)	5'ATTATCTTTTTTTCCTGTTCCAATTTAGCTTTTTGACAATCGC ATGGCTCACCGGGTTTC
MAHRP1 3HR fw	5'AAATGAGGAGAGGAAAGGAAAG
MARHP1 3HR rv	5'AGTATTGGAGTCATAATAAG
MAHRP1 gRNA	5'TGGCAATCACATGGTTCTCC
PF13_0275-PF13_0276 KO 5' UTR fw	5'AATCCGCGGtatgaaagttcgtaaatcgttatatg
PF13_0275-PF13_0276 KO 5'UTR rv	5'ATTTCTTAAGtttatattcgtattatatttgtgcaag
PF13_0275-PF13_0276 KO 3'UTR fw	5'ATTTCCATGGgtatatgtaattttccgaacaatttg
PF13_0275-PF13_0276 KO 3'UTR rv	5'ATATCCTAGGtttaaagagtccacaattgagac

Figure legends

Figure 1: **Generation of MAHRP1-GFP expressing cell lines**. A: The GFP2ABSD cassette was successfully integrated into the genome of 3D7 and 275-276 KO as shown by PCR. Primers were chosen outside the homology regions. The expected band sizes are for 3D7 1840bp and for MAHRP1-GFP 3558bp B: Western blot analysis with α-MAHRP2 antibody to confirm the absence of MAHRP2 in 275-276 KO cell lines. GAPDH was used as loading control. C: Western blot analysis with α-MAHRP1 and α-GFP antibodies shows expression of MAHRP1-GFP in the 3D7/MAHRP1-GFP and 275-276 KO/MAHRP1-GFP parasite lysates. α-GAPDH antibody was used as loading control. D: Immunofluorescence microscopy shows correct MAHRP1-GFP localization at Maurer's clefts of 3D7/MAHRP1-GFP and 275-276 KO/MAHRP1-GFP parasites probed with α-GFP and α-SBP1 antibodies. Scale bar 2µm. E: Life cell microscopy of 14-18hpi ring stage 3D7/MAHRP1-GFP and 275-276 KO/MAHRP1-GFP parasites. Pictures are taken every 5s, scale bar 2µm.

Figure 1

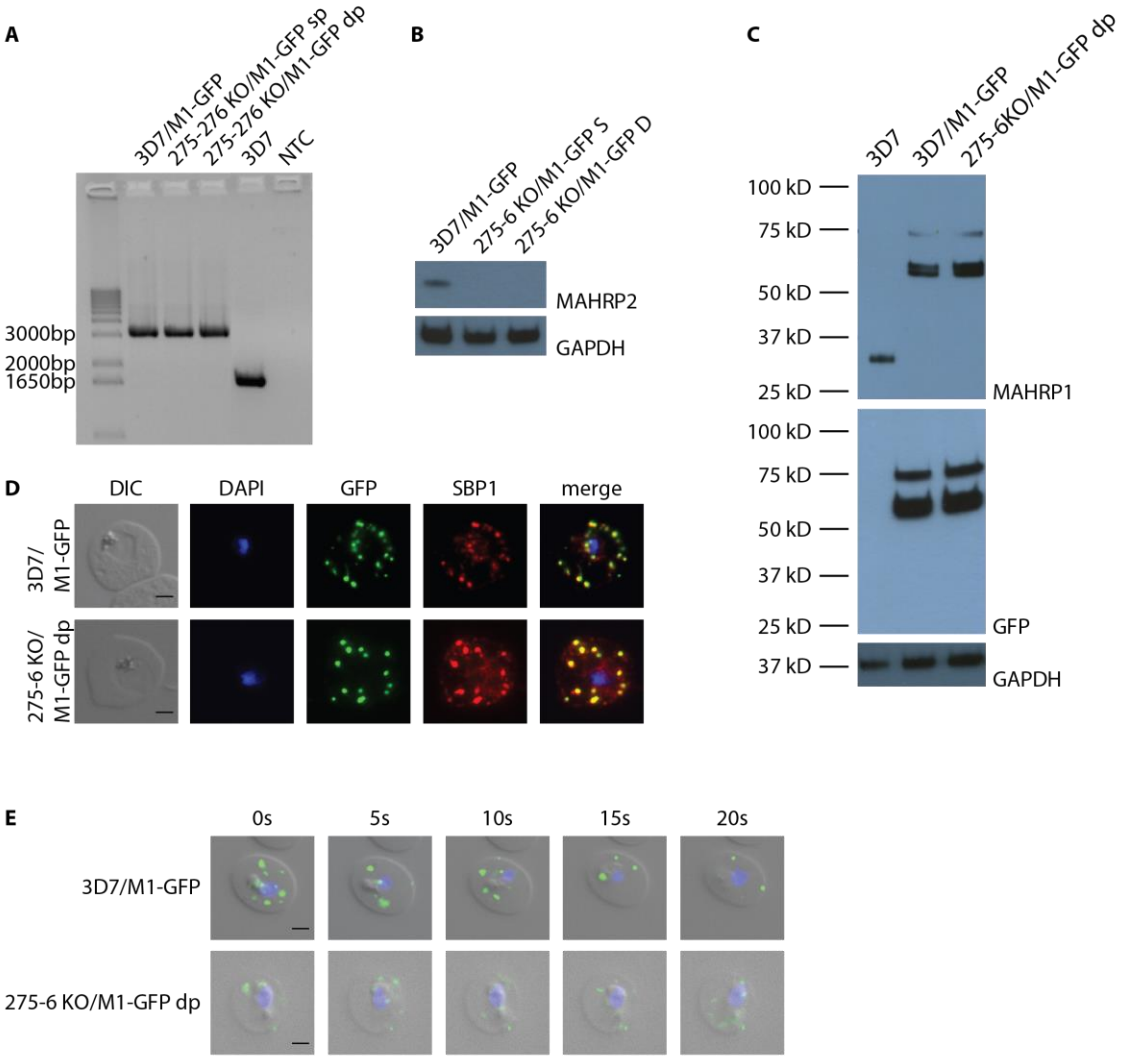
A
3D7/M1-GFP
275-276 KO/M1-GFP sp
275-276 KO/M1-GFP dp
3D7
NTC
3000bp
2000bp
1650bp
B
3D7/M1-GFP
275-6 KO/M1-GFP S
275-6 KO/M1-GFP D
MAHRP2
GAPDH
C
3D7
3D7/M1-GFP
275-6KO/M1-GFP dp
100 kD
75 kD
50 kD
37 kD
25 kD
MAHRP1
GFP
GAPDH
D
DIC
DAPI
GFP
SBP1
merge
3D7/ M1-GFP
275-6 KO/ M1-GFP dp
E
0s
5s
10s
15s
20s
3D7/M1-GFP
275-6 KO/M1-GFP dp

Functional characterization of MAHRP1 domains

The described study summarizes the findings of the Master students Eva Hitz, Stephan Wichers, and Eron Rushiti under the supervision of Beatrice Schibler and Sebastian Rusch.

Introduction

The membrane-associated histidine-rich protein 1 (MAHRP1) is a Maurer's clefts resident protein. Its 249 amino acids (aa) code for a 29 kDa protein that is expressed in early ring stages and present throughout the intraerythrocytic life cycle. The protein contains a transmembrane domain and a histidine rich domain at the C-terminus (Figure 2A, Spycher et al., 2003).

MAHRP1 has no specific export signal and thus belongs to the PNEPs. In order to identify MAHRP1 regions needed for export, Spycher and colleagues generated several cell lines episomally expressing MAHRP1 subdomain-GFP chimeras. The main findings of their study were: 1) the transmembrane domain is needed for MAHRP1 entry in to the ER, 2) aa 52-130 are sufficient for correct MAHRP1 export to the Maurer's clefts, 3) aa 131-169 may facilitate MAHRP1 delivery to Maurer's clefts, and 4) the histidine repeats (aa 169-215) are not needed for correct MAHRP1 trafficking (Spycher et al., 2008).

MAHRP1 is essential for PfEMP1 export to the erythrocyte surface. In MAHRP1 deficient cells, PfEMP1 remains inside the parasite and is not exported to the host cytosol (Spycher et al., 2006). We hypothesize that MAHRP1 interacts directly or indirectly with PfEMP1 in order to facilitate its export into the PV or through the PVM.

The previously described MAHRP1 knock out (Spycher et al., 2008) was achieved by an unintended 5′ UTR single cross-over recombination that lead to the integration of the entire transfection plasmid into the parasite genome (instead of a double cross-over recombination event). This cell line was observed to revert to wildtype. Therefore, in this study we have generated a novel MAHRP1 knock out cell line by CRISPR/Cas9 genome editing that could be complemented episomally with different 5'-end GFP-tagged MAHRP1 fragments in order to identify MAHRP1 domains involved in PfEMP1 export.

Methods

Cell culture and transfections

P. falciparum 3D7 was cultured and transfected as described (Moll et al**.**, 2013). Transfected parasites were positively selected with 10nM WR99210 (Jacobs Pharmaceuticals, Cologne, Germany), 5mg ml^{-1} blasticidin (Sigma-Aldrich, Inc.), negative selection was done with 1µM 5-Fluorocytosine (Valeant Pharmaceuticals, Laval, CA).

Transfection constructs

To generate the MAHRP1 knock out cell line KOMIC #3, parasites were transfected with the pB-CC plasmid. The pB-CC plasmid contains the MAHRP1 specific gRNA under a U6 promoter and sequence-specific 5' and 3' HRs flanking the positive selection cassette *hDHFR*. Further, the endonuclease Cas9 followed by a 2A skip peptide and the negative selection cassette y*fcu* followed by the 2A skip peptide and then by the positive selection cassette *bsd* are encoded on the plasmid. 300-700bp long homology regions flanking *mahrp1* were designed and a gRNA recognition site inside *mahrp1* was chosen with the CHOPCHOP software (Montague et al., 2014, Labun et al., 2016). The homology regions were PCR amplified with primers M1_5HR fw 5'CATTATATAGAGATTATCCACAAATCCG, M1_5HR rv 5'CTCTATAATACAACAGAATAATGTTAC, M1_3HR fw 5'ACCAGGAGAACC ATGTGATTGC, and M1_3HR rv 5'GAAGTAACATTATTATGCGTG, and cloned into pB-CC by using the restriction sites *SacII/AflII* (5HR) and *EcoRI/AvrII* (3HR). The complementary gRNA oligos were annealed and cloned into pB-CC using the *BtgZI* restriction site (M1 KO gRNA fw 5'GATCACGGACATGGACATGG and M1 KO gRNA rv 5'CCATGTCCA TGTCCGTGATC).

To complement KOMIC#3 with different MAHRP1 domains, parasites were transfected with a pARL_GFP(bsd) plasmid. For this, *mahrp1* fragments were PCR-amplified using primers M1_1-130 fw 5'ATGGCAGAGCAAGCAGCAGT, M1_1-130 rv 5'TGAGTGGTATA AGAAGGCGTG, M1_1-169 fw 5'ATGGCAGAGCAAGCAGCAGT, M1_1-169 rv 5'CATATATTCTGG ATCAAA, M1_52-130 fw 5'ATGGATAACTATGCTAGGAA TTGG, M1_52-130 rv 5'TGAGTGGTATAAGAAGGCGTG, M1_52-249 fw 5'ATGGA TAACTATGCTAGGAATTGG, M1_52-249 rv 5'TTATCTTTTTTTTCTTGTTCTAATT TTGC, M1_1-169 fw 5'ATGGCAGAGCAAGCAGCAGT, M1_1-169 rv 5'CATATAT TCTGGATCAAAAAATGGGT, M1_1-215 fw 5'ATGGCAGAGCAAGCAGCAGT, M1_1-

215 rv 5'TCCATGTCCGTGATCGTGTC, M1ΔTM fw 5'- ATGGCAGAGCAAGCAGTAC, M1ΔTM rv 5'ATTATCTTTTTTTTCTTGTTCTAAT and cloned upstream of the GFP-tag into pARL_GFP(bsd) using the restriction sites *AflII* and *ClaI*.

Western blot analysis

Parasite saponin lysates were run on 4-12% Bis/Tris precast gels (NuPAGE®, Life Technologies) according to the manufacturer's protocol. Protein transfer was performed with the iBlot 2.0 (Life Technologies). Subsequently, the membrane was blocked with 10% skimmed milk/TNT (100mM Tris, 150mM NaCl, 0.1% Tween) and probed with the first antibody in 3% skimmed milk/TNT at room temperature for 2h-O/N. After 6 washes for 5min with TNT the secondary antibody conjugated to HRP was incubated in the respective dilution in 3% skimmed milk/TNT for 2h at room temperature. After another 6 washes for 5min with TNT the signal was detected by Super Signal West Pico Chemiluminescent Substrate (Thermo Scientific) or LumiGlo Reserve Chemiluminescent Substrate (Seracare) according to the manufacturer's protocol. The antibodies used were: mouse α-GFP (Roche, 1:250), mouse α-ATS (1:100), rabbit α-MAHRP1 (1:5'000), mouse α-GAPDH (1:20'000), goat α-mouse-HRP (Pierce, 1:5000), goat α-rabbit-HRP (Pierce, 1:10'000).

Immunofluorescence microscopy

Thin blood smears of parasite cultures were fixed in ice-cold 60% methanol/40% acetone for 2min. After air-drying of the smear, a small circle was drawn with a hydrophobic pen and the respective area was blocked with 3% BSA/PBS for 1h at room temperature in a humidified chamber. Then, the cells were incubated with mouse α-GFP (Roche, 1:100), rabbit α-MAHRP1 (1:500), mouse α-ATS (1:50) in 3% BSA/PBS for minimum 2h at room temperature in a humidified chamber. After 3 washes with 3% BSA/PBS for 7min the secondary antibody (goat α-mouse Alexa488, goat α-rabbit Alexa488; all Invitrogen, 1:200) was applied in the appropriate dilution in 3% BSA/PBS for minimum 1h at room temperature in a humidified chamber. After another 3 wash steps with 3% BSA/PBS for 7min each, a coverslip was mounted with 2µl VECTASHIELD® with DAPI (Vector Laboratories Inc.). For imaging a 63x oil-immersion lens (1.4 numerical aperture) on a Leica 5000 B microscope was used. The images were obtained by using the software Leica ApplicationSuite 4.4. and analyzed using Fiji (Schindelin et al., 2012).

Scanning electron microscopy

For scanning electron microscopy mature parasites were knob-selected, purified by Percoll density gradient and fixed in 2.5% PBS for 1h at room temperature. After transfer to coverslips preliminary coated with Poly-L-lysine, the samples were dehydrated in increasing concentration of ethanol (10% v/v, 25% v/v, 50% v/v, 75% v/v, 90% v/v and 2 x 100% v/v, 10min each), critical point dried and finally sputtered with 5nm Platinum (LEICA EM ACE600). The micrographs were taken with a SEM Versa 3D (FEI) at 5kV.

Results and Discussion

MAHRP1 knock out cell line generation, characterization and complementation with MAHRP1 fragments

A MAHRP1 knock out cell line called knock out MAHRP1 complete #3 (KOMIC #3) was generated by CRISPR/Cas9-mediated double cross-over recombination. Based on the plasmid system from Ghorbal et al. (2014), we have designed a single plasmid approach, where Cas9, the gRNA and the repair template are provided on the same plasmid. Successful *mahrp1* disruption by replacement of the gene with a *hDHFR* resistance cassette was verified by Western blot (Figure 1A) and immunofluorescence assay (Figure 1B). In both assays a MAHRP1 signal was present in 3D7 control samples but absent in the KOMIC #3 samples indicating that MAHRP1 is not expressed in the KOMIC #3.

We found chromosome 2 breaks occurring frequently in our lab culture strains and this chromosome break involves the loss of the *kahrp* gene resulting in knob deficient iRBCs (Lanzer et al., 1994). Since knobs are an important part of the *P. falciparum* virulence complex where the major virulence factor PfEMP1 is presented on the iRBC surface, we regularly selected our culture strains for presence of knobs by gelatin floatation (Malaria Methods and Protocols, Sixth Edition, 2013). Presence of knobs in the KOMIC #3 cell line was confirmed by scanning electron microscopy (Figure 1C).

Maurer's clefts morphology analyzed by immunoelectron microscopy seemed aberrant in KOMIC #3 compared to 3D7 wildtype infected red blood cells as previously described (Spycher et al., 2008). Further, we confirmed the finding that MAHRP1 deficient cells do not present PfEMP1 on the iRBC surface. In a trypsin cleavage assay KOMIC #3 samples contained only full-length, intracellular PfEMP1 as compared to 3D7 control where we detected the cleaved intracellular part of surface-exposed PfEMP1 (Figure 1D).

In order to get new insights into the function of the different MAHRP1 domains in MAHRP1 trafficking and PfEMP1 export, the KOMIC #3 cell line was complemented with different MAHRP1 fragments (Figure 2A) fused to GFP. MAHRP1 full length (aa 1-249) was used as control. Previously, Spycher and colleagues concluded that the MAHRP1 aa 52-130 are sufficient to promote MAHRP1 export (Spycher et al., 2006) hence we wanted to confirm this by complementing KOMIC #3 with this fragment (MAHRP1 aa 52-130). We also wanted to confirm that the transmembrane domain is needed for MAHRP1 entry into the ER (Spycher et al., 2006) by transfecting a MAHRP1ΔTM construct into KOMIC #3. Further, we aimed to clarify the role of aa 130-169 in facilitating MAHRP1 export by analyzing KOMIC #3 expressing a MAHRP1 aa 1-130 and a MAHRP1 aa 1-169 construct. The function of the C-terminal histidine-rich domain of MAHRP1 had not been elucidated yet. Therefore, we compared the cell lines either expressing a MAHRP1 fragment truncated before the histidine-rich domain (MAHRP1 aa 1-169) or expressing a fragment expressing MAHRP1 including the histidine repeats (MAHRP1 aa 1-215). Since MAHRP1 is a PNEP which needs an internal hydrophobic signal for efficient export (Spielmann and Gilberger, 2010) we wanted to test whether MAHRP1 aa 52-249 in the KOMIC #3 would be exported since Grüring et al. had shown that the first 20 aa of MAHRP1 mediated export of a reporter construct (Gruring et al., 2012).

Expression of all MAHRP1-GFP fragments was confirmed by Western blot (Figure 2B). The calculated molecular weight of the different MAHRP1-GFP fragments were 56 kDa, 37 kDa, 51 kDa, 43 kDa, and 47 kDa for MAHRP1 full length, MAHRP1 aa 52-130, MAHRP1 aa 52-249, MAHRP1 aa 1-130, and MAHRP1 aa 1-169, respectively. All fragments ran at the expected sizes.

Transfections of KOMIC #3 with constructs MAHRP1 1-215, and MAHRP1ΔTM came up but expression of the GFP-fusion protein yet needs to be confirmed by Western blot.

MAHRP1 export does not depend on its N-terminus (aa 1-52)

Trafficking of all MAHRP1 fragments to Maurer's clefts was monitored by immunofluorescence (Figure 3). KOMIC #3 as expected showed no GFP signal (Figure 3, first panel) whilst MAHRP1 full length was observed at Maurer's clefts (Figure 3, second panel). MAHRP1 aa 52-130 GFP signal was only detected inside the parasite, thus this fragment was not exported (Figure 3, third panel). This finding is in contrast to previously published data showing MAHRP1 aa 52-130 being the minimal construct needed for export

(Spycher et al. 2006). As previously observed MAHRP1 aa 1-130 was not found in all iRBC at Maurer's clefts, in a proportion of cells it was not exported (Figure 3, fourth panel). This supports the hypothesis of Spycher and colleagues that aa 130-169 maybe required for export of MAHRP1 (Spycher et al., 2006). The construct MAHRP1 aa 1-169 has not yet been analyzed but may clarify the role of aa 130-169. MAHRP1 aa 52-249 (MAHRP1, fifth panel) was correctly transported to Maurer's clefts indicating that the N-terminal region of MAHRP1 is dispensable for export. The finding that aa 1-52 are dispensable for MAHRP1 export (shown with the construct MAHRP1 aa 52-249) indicates that MAHRP1 is an exception of the general PNEP export pathway requiring an N-terminal signal sequence (Heiber et al., 2013). The finding also stands in contrast to the finding that MAHRP1 aa 1-20 are able to drive export of a reporter construct (Gruring et al., 2012). In summary, it seems that the MAHRP1 N-terminus is sufficient but not essential for protein export.

Additionally, the export of the MAHRP1ΔTM and MAHRP aa 1-215 constructs in the respective cell lines will be analyzed which may allow to draw conclusions on the importance of the transmembrane domain and the histidine-rich domain in MAHRP1 trafficking to Maurer's clefts.

Contrasting results to the previous study of Spycher and colleagues (Spycher et al., 2006) may be explained by the fact that their assays were done in a 3D7 background with endogenous full length MAHRP1 still expressed whilst our assays were done in a complete MAHRP1 knock out cell line. The presence of MAHRP1 may facilitate export of the truncated constructs (e.g. MAHRP1 aa 52-130) by an unknown co-transport mechanism.

The MAHRP1 C-terminus (aa 130-249) is important for PfEMP1 export

To identify MAHRP1 domains that enable PfEMP1 transport, immunofluorescence assays were performed with all complemented cell lines described above (Figure 2A). We used the α-ATS antibody to monitor PfEMP1 export to Maurer's clefts but this antibody does not label PfEMP1 on the iRBC surface. We observed similar ATS signal at Maurer's clefts in 3D7 and MAHRP1 full length complemented KOMIC #3 as expected (Figure 4, first and third panel). It was previously shown that MAHRP1 is needed for PfEMP1 export (Spycher et al., 2008) and we also confirmed the absence of surface exposed PfEMP1 in KOMIC #3 by trypsin cleavage assay (Figure 1D). Accordingly, we found no ATS signal at Maurer's clefts in the KOMIC #3 cell line by immunofluorescence microscopy (Figure 4, second panel). The constructs MAHRP1 aa 52-130 (Figure 4, fourth panel) and MAHRP1 aa 1-130 (Figure 4,

fifth panel) were not able to restore PfEMP1 delivery to Maurer's clefts, whereas MAHRP1 aa 52-249 complemented KOMIC #3 showed PfEMP1 localization at Maurer's clefts (Figure 4, sixth panel). This suggests that the C-terminal part of MAHRP1 (aa 130-249) is important for the export of PfEMP1. Especially the analysis of the KOMIC #3 cell lines expressing MAHRP1 aa 1-169 and MAHRP1 aa 1-215 respectively will give insights whether the histidine-rich domain is important for direct or indirect interaction with PfEMP1.

In a next step, cell lines expressing fragments that restore PfEMP1 transport to Maurer's clefts should be analyzed on PfEMP1 presentation on the iRBC surface, either by trypsin cleavage or CD36 binding assays.

Provided that a certain fragment/domain can be assigned to restore PfEMP1 export, additional experiments investigating the putative interaction between MAHRP1 and PfEMP1 should be performed.

Summary and Outlook

A new MAHRP1 knock out cell line called KOMIC #3 was generated and complemented with different GFP-tagged MAHRP1 fragments. Immunofluorescence assays were performed to investigate the role of different MAHRP1 domains in the export of MAHRP1 and PfEMP1. From the current results we conclude that 1) aa 130-169 seemed to be important for efficient MAHRP1 export and 2) the MAHRP1 C-terminus is important for PfEMP1 export. Analysis of the remaining cell lines will lead to more specific conclusions.

Acknowledgements

Françoise Brand did scanning electron microscopy experiments. We thank Henning Stahlberg and his team at the C-CINA, Biozentrum, University of Basel, for the access to the electron microscopy facility. We would like to thank the following colleagues for sharing antibodies: Claudia Daubenberger (α-GAPDH) and Brian Cooke (α-ATS).

References

GHORBAL, M., GORMAN, M., MACPHERSON, C. R., MARTINS, R. M., SCHERF, A. & LOPEZ-RUBIO, J. J. 2014. Genome editing in the human malaria parasite Plasmodium falciparum using the CRISPR-Cas9 system. *Nat Biotechnol,* 32**,** 819-21.

GRURING, C., HEIBER, A., KRUSE, F., FLEMMING, S., FRANCI, G., COLOMBO, S. F., FASANA, E., SCHOELER, H., BORGESE, N., STUNNENBERG, H. G., PRZYBORSKI, J. M., GILBERGER, T. W. & SPIELMANN, T. 2012. Uncovering common principles in protein export of malaria parasites. *Cell Host Microbe,* 12**,** 717-29.

HEIBER, A., KRUSE, F., PICK, C., GRURING, C., FLEMMING, S., OBERLI, A., SCHOELER, H., RETZLAFF, S., MESEN-RAMIREZ, P., HISS, J. A., KADEKOPPALA, M., HECHT, L., HOLDER, A. A., GILBERGER, T. W. & SPIELMANN, T. 2013. Identification of new PNEPs indicates a substantial non-PEXEL exportome and underpins common features in Plasmodium falciparum protein export. *PLoS Pathog,* 9**,** e1003546.

LABUN, K., MONTAGUE, T. G., GAGNON, J. A., THYME, S. B. & VALEN, E. 2016. CHOPCHOP v2: a web tool for the next generation of CRISPR genome engineering. *Nucleic Acids Res,* 44**,** W272-6.

LANZER, M., WERTHEIMER, S. P., DE BRUIN, D. & RAVETCH, J. V. 1994. Chromatin structure determines the sites of chromosome breakages in Plasmodium falciparum. *Nucleic Acids Res,* 22**,** 3099-103.

MONTAGUE, T. G., CRUZ, J. M., GAGNON, J. A., CHURCH, G. M. & VALEN, E. 2014. CHOPCHOP: a CRISPR/Cas9 and TALEN web tool for genome editing. *Nucleic Acids Res,* 42**,** W401-7.

SPIELMANN, T. & GILBERGER, T. W. 2010. Protein export in malaria parasites: do multiple export motifs add up to multiple export pathways? *Trends Parasitol,* 26**,** 6-10.

SPYCHER, C., KLONIS, N., SPIELMANN, T., KUMP, E., STEIGER, S., TILLEY, L. & BECK, H. P. 2003. MAHRP-1, a novel Plasmodium falciparum histidine-rich protein, binds ferriprotoporphyrin IX and localizes to the Maurer's clefts. *J Biol Chem,* 278**,** 35373-83.

SPYCHER, C., RUG, M., KLONIS, N., FERGUSON, D. J., COWMAN, A. F., BECK, H. P. & TILLEY, L. 2006. Genesis of and trafficking to the Maurer's clefts of Plasmodium falciparum-infected erythrocytes. *Mol Cell Biol,* 26**,** 4074-85.

SPYCHER, C., RUG, M., PACHLATKO, E., HANSSEN, E., FERGUSON, D., COWMAN, A. F., TILLEY, L. & BECK, H. P. 2008. The Maurer's cleft protein MAHRP1 is essential for trafficking of PfEMP1 to the surface of Plasmodium falciparum-infected erythrocytes. *Mol Microbiol,* 68**,** 1300-14.

Figure legends

Figure 1: **Generation and characterization of MAHRP1 knock out cell line KOMIC #3.** A: Western blot analysis of 3D7 and KOMIC #3 saponin lysates. The membrane was probed with α-MAHRP1 antibodies, GAPDH was used as loading control. B: Immunofluorescence analysis of thin smears of 3D7 and KOMIC #3 with α-MAHRP1 antibodies. C: Scanning electron microscopy of uninfected, 3D7 and KOMIC #3 infected red blood cells (iRBCs). Scale bar 1µm. D: Western blot analysis of trypsin cleavage assay with 3D7 and KOMIC #3 samples. +T: trypsin treated, -T: control, not trypsin treated, RBC: red blood cells. The membrane was probed with the α-ATS antibody.

Figure 2: **Complementation of KOMIC #3.** A: Schematic representation of MAHRP1 and the different complementation constructs. Indicated numbers are amino acid positions, TM: transmembrane domain, HHH: histidine-rich domain. B: Western blot analysis of complemented KOMIC #3 saponin lysates MAHRP1 full length (M1 FL), MAHRP1 aa 52-130 (M1 52-130), MAHRP1 aa 52-249 (M1 52-249), MAHRP1 aa 1-130 (M1 1-130), and MAHRP1 aa 1-169 (M1 1-169). HP1-GFP was used as positive control. Membranes were probed with α-GFP antibody; GAPDH was used as loading control.

Figure 3: **Localization of MAHRP1 fragments in complemented KOMIC #3 cell lines.** Immunofluorescence assay of thin smears of KOMIC #3, MAHRP1 full length (M1 FL), MAHRP1 aa 52-130 (M1 52-130), MAHRP1 aa 1-130 (M1 1-130), and MAHRP1 aa 52-249 (M1 52-249) probed with α-MAHRP1 antibody.

Figure 4: **Localization of PfEMP1 in complemented KOMIC #3 cell lines.** Immunofluorescence asssay of thin smears of 3D7, KOMIC #3, MAHRP1 full length (M1 FL), MAHRP1 aa 52-130 (M1 52-130), MAHRP1 aa 1-130 (M1 1-130), and MAHRP1 aa 52-249 (M1 52-249) probed with α-ATS antibody.

Figure 1

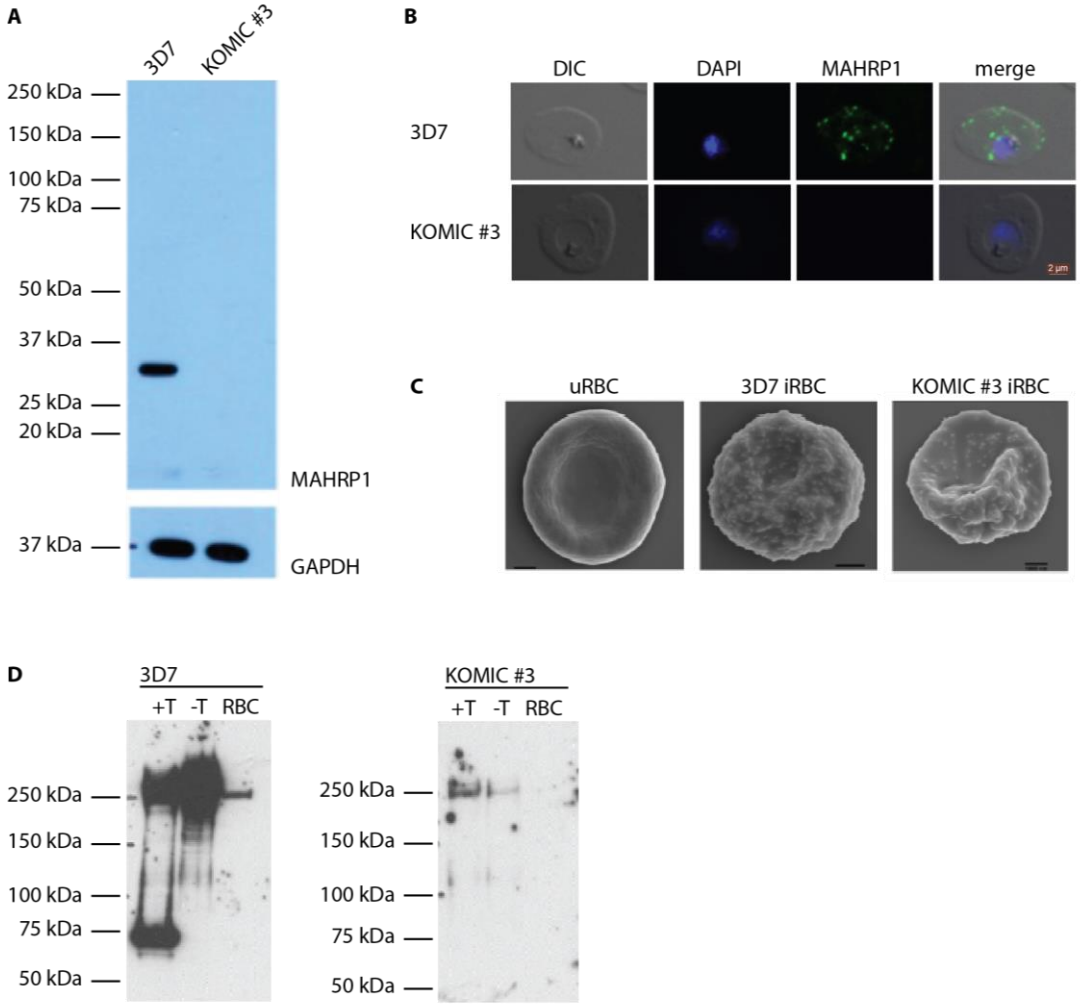
A
3D7
KOMIC #3
250 kDa
150 kDa
100 kDa
75 kDa
50 kDa
37 kDa
25 kDa
20 kDa
MAHRP1
37 kDa
GAPDH
B
DIC
DAPI
MAHRP1
merge
3D7
KOMIC #3
C
uRBC
3D7 iRBC
KOMIC #3 iRBC
D
3D7
+T -T RBC
250 kDa
150 kDa
100 kDa
75 kDa
50 kDa
KOMIC #3
+T -T RBC
250 kDa
150 kDa
100 kDa
75 kDa
50 kDa

Figure 2

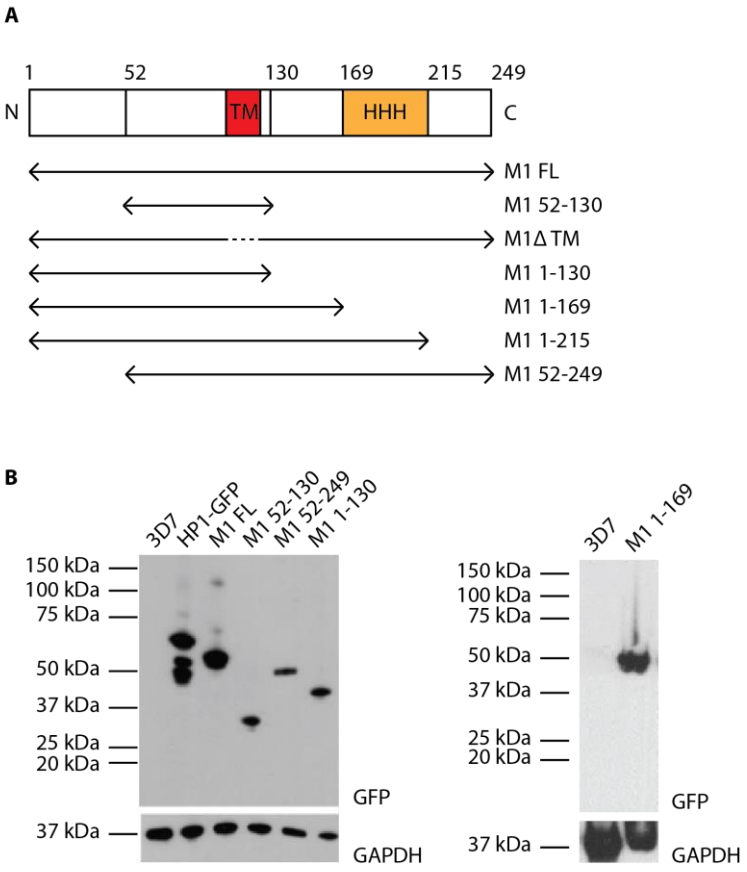
A
1
52
130
169
215
249
N
TM
HHH
C
M1 FL
M1 52-130
M1ΔTM
M1 1-130
M1 1-169
M1 1-215
M1 52-249
B
3D7
HP1-GFP
M1 FL
M1 52-130
M1 52-249
M1 1-130
150 kDa
100 kDa
75 kDa
50 kDa
37 kDa
25 kDa
20 kDa
GFP
37 kDa
GAPDH
3D7
M1 1-169
150 kDa
100 kDa
75 kDa
50 kDa
37 kDa
25 kDa
20 kDa
GFP
37 kDa
GAPDH

Figure 3

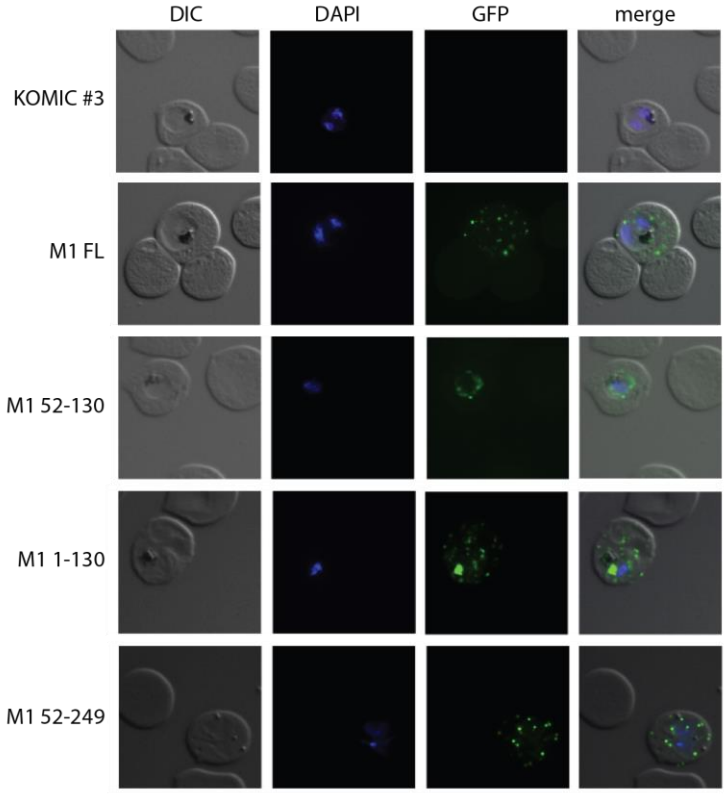

Figure 4